AD-A255 226

ACTIVE CONTROL OF COMBUSTION INSTABILITY IN A RAMJET USING LARGE-EDDY SIMULATIONS

S. Menon

DTIC
ELECTE
SEP 18 1992
S   A   D

September 1992

Prepared for
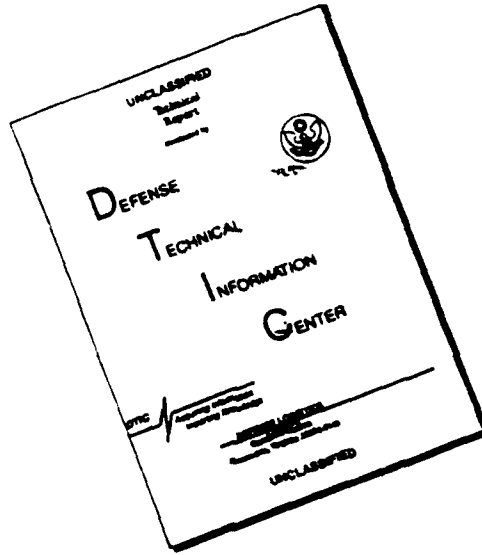
OFFICE OF NAVAL RESEARCH

92-25157

92   9   14   053

QUEST INTEGRATED, INC.
21414 - 68th Avenue South
Kent, Washington 98032
(206) 872-9500

DISCLAIMER NOTICE

THIS DOCUMENT IS BEST QUALITY AVAILABLE. THE COPY FURNISHED TO DTIC CONTAINED A SIGNIFICANT NUMBER OF PAGES WHICH DO NOT REPRODUCE LEGIBLY.

QUEST Technical Report No. 575

ACTIVE CONTROL OF COMBUSTION INSTABILITY IN A RAMJET USING LARGE-EDDY SIMULATIONS

S. Menon

September 1992

Prepared for

OFFICE OF NAVAL RESEARCH

Under Contract No. N00014-90-C-0089

Accesion For		
NTIS CRA&I		☑
DTIC TAB		☐
Unannounced		☐
Justification		
By		
Distribution /		
Availability Codes		
Dist	Avail and / or Special	
A-1	23	

DTIC QUALITY INSPECTED 3

1. INTRODUCTION

Combustion instability in a ramjet engine is an extremely complex phenomenon involving nonlinear interactions among acoustic waves, vortex motion and unsteady heat release. Typically, the instability manifests itself as a large-amplitude pressure oscillation in the low-frequency range (100-800 Hz) and is very difficult to control. When the amplitude of the pressure oscillation reaches some critical limit, it can cause structural damage due to fatigue or can cause an engine "unstart," which occurs when the shock in the inlet duct is expelled to form a bow shock ahead of the inlet. This phenomenon of engine unstart is one of the most serious technical problems encountered in developing an operational ramjet engine.

In recent years, both experimental (e.g., Schadow et al., 1989; Smith and Zukoski, 1985; Hedge et al., 1987) and numerical (e.g., Menon and Jou, 1990, 1991; Jou and Menon, 1990) investigations have been conducted to determine the mechanism of the combustion instability. Attempts to control combustion instability using both passive and active control techniques have also been carried out in the past (Culick, 1989). Passive control methods that typically involve structural (i.e., geometrical) modifications have proven insufficient for controlling the low-frequency instability. Recent experimental studies (e.g., Langhorne and Hooper, 1989; Schadow et al., 1990; Gutmark et al., 1990) suggest that active control techniques may be more effective in controlling the combustion instability in a ramjet. In parallel to the experimental studies, a numerical study of active control methods was carried out in this project. Earlier, the result of numerical studies of active control using acoustic feedback techniques was reported (Menon, 1990, 1991) and it was shown that combustion instability can be successfully controlled using such techniques provided certain feedback criteria are satisfied. Although, the results are in good agreement with experimental observations, it is well known that in realistic ramjet combustors, acoustic feedback control using loudspeakers as the controller may not be practical due to the prevailant hostile (hot) environment in the combustor. A numerical study of another type of active control technique which uses secondary injection of the premixed fuel as the controller was also carried out. Such a technique has been shown experimentally to be a more practical and effective control system (e.g., Langhorne and Hooper, 1989).

In this report, the results of the simulations carried out over the two-year period (May 1990 - May 1992) are summarized. For completeness, the papers that were written using the results of the study (Menon, 1990, 1991, 1992a, 1992b) are included in Appendix A.

2. THE SIMULATION MODEL

The simulation model used in this study was developed through a series of numerical experiments starting with cold flow studies (Menon and Jou, 1987, 1990; Jou and Menon, 1987, 1990) and culminating in the simulation of combustion instability (Menon and Jou, 1991). The equations are the full compressible Navier-Stokes equations formulated in the axisymmetric coordinate system. The original numerical technique is an unsplit second-order-accurate, finite-volume scheme based on MacCormack's method; it has been described elsewhere (Menon and Jou, 1987, 1990). In the present study, a fourth-order-accurate spatial differencing scheme has been used for most of the simulations. The modeled ramjet combustor consists of an axisymmetric inlet duct connected to an axisymmetric dump combustor by a sudden expansion. A convergent-divergent nozzle is attached downstream of the combustor. This configuration is similar to an experimental test rig currently being used for active control studies at the Naval Weapons Center, China Lake, except that, in the simulations, a convergent-divergent nozzle is attached downstream of the combustor. This is more representative of a real operating ramjet configuration. The flow through this nozzle is choked, and the outflow at the downstream computational boundary is supersonic.

2.1. The Combustion Model

In premixed combustion, the amount of heat release per unit area of flame is determined by the local flame speed and by the specific chemical energy available in the fuel. If a finite-rate chemical mechanism for premixed combustion is employed in an LES, the numerical simulation must implicitly compute the local flame speed. Unfortunately, this is difficult to achieve in practice. The flame speed depends upon the dissipation mechanism and therefore, the internal structure of the flame sheet. Because the number of grid points are limited in LES, the flame sheet cannot be resolved adequately. Also, all numerical schemes involve some form of artificial dissipation, either explicitly added to stabilize the computations or implicitly present due to the differencing algorithm. As a result, the computed flame structure will be numerically diffused and the temporal-spatial distribution of the heat release could be overwhelmed by numerical diffusion.

The problems associated with employing a classical finite-rate model can be circumvented by using a thin flame model. In this approach, the flame thickness is considered small compared to the smallest turbulent length scale (i.e., the Kolmogorov scale), and if the changes in the reaction-diffusion structure due to turbulent straining are also small, then the reaction zone can be considered to be asymptotically thin. Within the thin flame approximation, a model equation for premixed combustion is considered in which the local flame speed explicitly appears. If the local flame speed u_F is known, a progress variable G can be defined that is governed by the equation (Kerstein et al., 1988; Menon and Jou, 1991):

$$\frac{\partial \rho G}{\partial t} + \frac{\partial}{\partial x_i} \rho u_i G = -\rho\, u_F \left| \nabla G \right| \tag{1}$$

where ρ is the density and u_i is the fluid velocity. Equation (1) describes the convection of the flame by the local fluid velocity and the flame propagation into the unburnt mixture through a Huygens type mechanism, $u_F | \nabla G |$. Here, by definition, $G = 1$ corresponds to the premixed fuel state, $G = 0$ corresponds to the fully burnt state and the flame is located at a prescribed $G = G_o$ level surface, where, $0 < G_o < 1$. For laminar premixed combustion, the local flame speed u_F is the laminar flame speed S_L which contains the information on the chemical kinetics and the molecular dissipation. When Equation (1) is applied to turbulent flows, the local flame speed u_F is taken to be the local turbulent flame speed u_T, where u_T is a prescribed function of local turbulence intensity u' and the laminar flame speed S_L (here treated as a constant chemical property, though in reality it is sensitive to the strain field affecting the flame). The implementation of the thin flame model as a part of the LES transport equations therefore explicitly requires the specification of the subgrid turbulent kinetic energy to determine the turbulent flame speed. This is accomplished in the present study by explicitly computing the subgrid turbulent kinetic energy as described in Section 2.2. The next issue that must be addressed is the determination of the functional relation: $u_T = u_T(S_L, u')$. It appears that a general functional relationship between the turbulent flame speed, the laminar flame speed and the turbulence intensity which is valid for all types of fuel and flow conditions is difficult to develop. Yakhot (1988) used renormalization theory to develop a relation of the form $u_T/S_L = \exp(u'^2/u_T^2)$ which reduces to the linear scaling, $u_T/S_L \approx (1 + u'/S_L)$ when $u'/S_L \gg 1$ limit, and to the Clavin-Williams relation $u_T/S_L \approx (1 + (u'/S_L)^p)$, where $p = 2$ when $u'/S_L <$ limit. He also showed that, at least for high u'/S_L cases, this expression shows good agreement with experimental data. However, recently, Kerstein and Ashurst (1992) showed that for low u'/S_L, the Clavin-Williams expression maybe incorrect and proposed a scaling with $p = 4/3$. In the present study, both Yakhot's expression and the more simplified approximations (linear scaling, i.e., $p = 1$ for $u'/S_L > 1$ and the modified Clavin-Williams relation, i.e., $p = 4/3$ for $u'/S_L < 1$) were investigated. Yakhot's relation is a nonlinear equation that requires iteration at every grid point and at every time step to determine the turbulent flame speed. This is computationally very expensive and therefore, to reduce computational effort, an approach is being implemented in which a look-up table of $u_T = u_T(S_L, u')$ is first generated and then the turbulent flame speed is determined by using interpolation routines. However, since this approach is still under development, so far, the more simpler

relations described above have been used to determine the turbulent flame speed.

In addition to the specification of the turbulent flame speed, the effect of heat release must be included to couple the effect of combustion with the large-scale transport. The chemical energy of the mixture is included in the formulation by specifying the specific enthalpy h of the mixture in the energy equation as $h = C_p T + h_f G$. Here, h_f is the heat of formation of the premixed fuel, C_p is the specific heat of the mixture at constant pressure, and T is the temperature. The heat of formation of the fuel determines the amount of heat released during combustion and thus is a function of the equivalence ratio for a given fuel. The product temperature T_p can be estimated for a given heat of formation by the relation $h_f = C_p (T_p - T_{fu})$, where T_{fu} is the fuel temperature at the inlet. In the simulations, the combustion product temperature is initially specified, and the heat of formation is determined from the above noted expression for h_f.

2.2. The Subgrid Model

In a practical ramjet device, the Reynolds number of the flow is extremely high. A LES of such a flow requires a validated subgrid model. Subgrid models for compressible flows have just begun to be investigated (e.g., Speziale et al., 1987, Squires and Zeeman 1990). At present, it is not clear what is an appropriate subgrid model for flows such as those in a ramjet combustor. The earlier simulations (Menon and Jou, 1991) with the short inlet duct length were carried out using a constant eddy viscosity model and a constant turbulent flame speed for flows in a moderate Reynolds number range. Some important physical properties, such as the spatial nonuniformity of subgrid turbulence and its effect on the local flame speed and the amount of heat release, were not included in this approach. However, as shown earlier (Menon and Jou, 1991), the major qualitative interactions between the large-scale vortex structures and the combustion heat release could be captured by the constant flame speed model. In the present study, the effect of nonuniform subgrid turbulence on the turbulent flame speed and on combustion instability has been included by using a subgrid model for turbulent kinetic energy and then determining the turbulent flame speed based on the scaling relationships described in Secfion 2.1. The subgrid model used for this study is described in this section.

Recently, Zeeman (1990) has proposed a model for the subgrid eddy viscosity which requires the determination of the subgrid turbulent kinetic energy. He employed concepts from the traditional Reynolds-averaged second-order closure approach to derive this model and showed that this eddy viscosity model reduces to the Smagorinsky's model in the incompressible limit. Although this model has been tested only for simple problems, such as decaying, compressible homogeneous turbulence (Squires and Zeeman, 1990), the relevant feature of this model is that the subgrid kinetic energy is computed in terms of the resolved fields to determine the subgrid eddy viscosity. Since, the subgrid kinetic energy distribution is essential for the specification of the turbulent flame speed, this model has been implemented to determine its applicability for LES of reacting flow fields.

The formulation begins by considering a one-equation model for the subgrid turbulent kinetic energy, and then neglecting the convective term Dk/Dt by using inertial range scaling to show that the convective term is much smaller than the source terms of this k-transport equation. Without going into the details of this formulation (Squires and Zeeman, 1990) a final expression for the subgrid kinetic energy is obtained as:

$$ k = 2C\Delta^2 |\bar{S}_{ij}|^2 + C\Delta^2 \frac{\overline{\nabla p} \cdot \nabla T}{\rho T Pr_t} - \frac{\sqrt{2C}}{3}\Delta^2 |\bar{S}_{ij}| \frac{\partial u_i}{\partial x_i} \tag{2} $$

Here, Δ is the characteristic filter size, u_i, ρ, $\bar{p}$ and T are, respectively, the Favre-filtered (Erlebacher et al., 1988) large-scale (resolved) velocity, density, pressure and temperature, and $k = \frac{1}{2}(u_i''^2)$ is the subgrid turbulent kinetic energy. Also, $\bar{S}_{ij} = \frac{1}{2}(\frac{\partial u_i}{\partial x_j} + \frac{\partial u_j}{\partial x_i})$ is the strain tensor in terms of the resolved velocity field. The constants C and Pr_t are chosen for the

present study to be 0.05 and 0.8, respectively.

The subgrid eddy viscosity ν_t is related to the subgrid kinetic energy by the expression: $\nu_t = C\,k^{\frac{1}{2}}\Delta$ Once k is known, the subgrid turbulence intensity u' ($u' = \sqrt{2k}$) and the turbulent flame speed u_F can be determined. This model is also used to determine the turbulent subgrid fluxes appearing in the momentum equations. Thus, the subgrid stresses in the momentum transport, $\tau_{ij}{}' = \rho(u_i u_j - u_j u_i) \approx \rho u_i\, u_j$ is given as

$$\tau_{ij}{}' - \frac{1}{3}\tau_{kk}{}'\delta_{ij} = -2\bar{\rho}\nu_t\,\bar{S}_{ij} \tag{3}$$

Closure of the subgrid terms appearing in the energy transport is also accomplished using the eddy viscosity model. The typical term that needs to be modeled is: $q_i{}' = \rho c_v (T u_i - T u_i) \approx \rho c_v\, T\, u_i$. This term is modeled as

$$\bar{\rho}C_v\, T\, u_i = -\sigma_{ij}\frac{\partial T}{\partial x_i} \tag{4}$$

where, σ_{ij} is determined from the relation:

$$\sigma_{ij} = \bar{\rho}c_v\left[\frac{\nu_t}{Pr_t}\delta_{ij} - \frac{\nu_t}{3}\frac{\Delta}{\sqrt{k}}\bar{S}_{ij}\right] \tag{5}$$

Some modifications are required to implement this model in axisymmetric flows and in flows with complex geometries. To include the effect of walls, an additional correction has been used to ensure that the subgrid stress variation is modeled correctly near the wall. Here, the wall damping model of Piomelli et al. (1988) is used to redefine the filter width as $\Delta = \Delta_g[1 - \exp(-y^{+3}/A^{+3})]$ where Δ_g is the characteristic grid size, $y^+ = yu_*/\nu$ is the distance from the wall in wall units and $A^+ = 25$. With this definition, the subgrid stress $\tau_{xy}{}'$ varies as y^{+3} near the wall.

A major issue for LES of complex flows is whether the primary assumption that the subgrid scales are primarily dissipative (and contain negligible kinetic energy) is valid. Past direct numerical simulations of relatively simpler flows (e.g., Piomelli et al., 1990) have demonstrated that the unresolved scales can contain significant kinetic energy and thus the phenomena of backscatter (transfer of energy from the small scales to the large scales) will have to be take into account. Thus, in general, equation (4) will not correctly reflect the process of energy transfer at the filter cutoff. A stochastic backscatter model was recently developed by Chasnov (1991) for application as a subgrid model. However, this model was developed in the spectral space and, as such, is not practical for application to complex flows and to complex geometries. Here, we consider an approach in the physical space that contains the elements of the model developed by Chasnov in the spectral space. A backscatter model was also recently shown by Leith (1990). By carrying out a simple phenomenological analysis, a similar model has been developed that uses the results of the study by Chasnov. The basic properties that are used to derive the backscatter model are: (1) forward scatter and backscatter are modeled by two distinctly different mechanisms, (2) forward scatter is modeled by an eddy damping term as in the spectral formulation (results in an expression similar to equation 3), (3) backscatter is modeled by a random force (as in the spectral formulation) which satisfies certain constraints (it is uncorrelated in time with a zero mean, and, to ensure that it adds a finite amount of energy to the turbulence, the force is proportional to $\Delta t^{-1/2}$). These properties are discussed in more details by Chasnov (1991).

Thus, the total subgrid eddy viscosity is a sum of two terms: an eddy damping term ν_e and a random "diffusion" term such that: $\nu_T(\bar{x}, t) = \nu_e(\bar{x}, t) - F_r(\bar{x}, t)$, where ν_T is the total subgrid eddy viscosity and $F_r(\bar{x}, t)$ is the random diffusion term. The model of the anisotropic part of the subgrid Reynolds-stress term is then written as

$$\tau_{ij}{}' - \frac{1}{3}\tau_{kk}{}'\delta_{ij} \;=\; -2\bar{\rho}\nu_e \bar{S}_{ij} + \bar{\rho}F_r \bar{S}_{ij} \tag{6}$$

The eddy damping term ν_e is chosen to be the same as the original forward scatter eddy viscosity, ν_t, given above. The backscatter contribution to the subgrid stress is determined by using the points noted above and by using simple dimensional analysis. Without going into details (Menon, 1991b) the random diffusion term is given as:

$$F_r \bar{S}_{ij} \;=\; C_{BS}\; rand\; \frac{\Delta^2}{\sqrt{\Delta t}}\; |\,\bar{S}\,|\; \bar{S}_{ij}{}^{1/2} \tag{7}$$

where $|\,\bar{S}\,| = |\,\bar{S}_{ij}\bar{S}_{ij}\,|^{1/2}$, $rand$ is a random number with zero mean and unit variance and C_{BS} is a constant of $O(1)$ taken here to be 0.1. On using equations (3) and (7) in equation (6), the final expression for the two-term subgrid model is

$$\tau_{ij}{}' - \frac{1}{3}\tau_{kk}{}'\delta_{ij} \;=\; -2\bar{\rho}\nu_t \bar{S}_{ij} + C_{BS}\; \bar{\rho}\; rand\; \frac{\bar{\Delta}^2}{\sqrt{\Delta t}}\; |\,\bar{S}\,|\; \bar{S}_{ij}{}^{1/2} \tag{8}$$

3. RESULTS OF THE STUDY

This research program has made significant advances towards accomplishing the research goals and objectives. The simulation model has been further extended for general applications, the axisymmetric code has been implemented on a massively parallel processor and studies of two active control techniques have been carried out. In the following, the various accomplishments so far in this research study are briefly described in separate subsections.

3.1. Further Development of the Simulation Model

The simplifying assumptions used for the earlier combustion instability simulations have now been removed. For example, the earlier model employed a second-order-accurate numerical scheme with a constant eddy-viscosity subgrid model. The turbulent flame speed used for the combustion simulations was also assumed to be a constant. The numerical scheme is now fourth-order-accurate in space and a new subgrid model that explicitly computes the subgrid kinetic energy has been successfully implemented (see section 2.0 and Menon, 1992b, for more details). The inclusion of a more general subgrid model allows simulations with coarser grids and at higher Reynolds number. Simulations of flows at high Reynolds number are essential to model realistic combustor flows. The new subgrid model also allows the proper closure of the subgrid Reynolds stresses and heat flux terms (which were assumed to be constants earlier). The spatial accuracy has been increased to ensure that the reduction of the grid resolution does not effect the computed physics of the flow field. Preliminary validation of the new simulation model has been completed (Menon, 1992b) and the results show that the current approach is capturing features of combustion instability seen in recent NWC experiments. Further validation studies are currently being carried out.

With the subgrid kinetic energy known, a more general expression of the turbulent flame speed (in terms of the laminar flame speed and subgrid turbulence intensity) is now being used for all simulations. Thus, the current simulation model allows the inclusion of the effects of nonuniform turbulent flame speed on combustion instability and control. Some of these simulations are discussed in Menon (1992a). It was found that for a long inlet duct configuration (this is a configuration similar to a NWC test-rig), the inlet duct acoustics controls the dominant mode of the pressure oscillation. It was also shown that when the inlet flow speed was changed the frequency of the pressure oscillation is effected indicating that in some cases, in addition to the inlet duct acoustics, a convective mode (i.e. a coupled acoustic-vortex mode) may play a role in exciting combustion instability. This is exactly what has been observed in many experiments, at NWC and at UC Berkeley.

3.2. Development of a Massively Parallel LES Code

Another major development task accomplished during this research year was the implementation of the simulation code on a massively parallel processor (the iPSC/860) at NASA Ames. This task was not in the original work plan; however, it was considered worthwhile since processing capability of supercomputers such as the Cray is not increasing and thus, full 3D LES on these machines will be very expensive. On the other hand, the scalable nature of the massively parallel processors provides a capability that may be more efficient for detailed 3D LES in the near future. To evaluate these types of machines, the axisymmetric LES code was successfully implemented on the iPSC/860 and preliminary simulations have been completed. The results of these tests suggests that the current code executes with nearly the same speed on a 32-processor iPSC/860 as on a single Cray-YMP processor. We are currently carrying out combustion instability simulations to evaluate the performance of the new code and to obtain data for analysis. Some results of this study will be reported soon (Menon and Weeratunga, 1992; Weeratunga and Menon, 1992).

3.3. Acoustic Feedback Control of Combustion Instability

Simulations of combustion instability in the ramjet were carried out earlier using the simplified subgrid and combustion models (Menon and Jou, 1991). These simulations showed that two types of instability processes can occur. The first type (Type I) is characterized by a small-amplitude high-frequency pressure oscillation, and the second type (Type II) involves a large-amplitude low-frequency pressure oscillation. Both types of combustion instabilities have been experimentally observed at NWC and CalTech. Furthermore, many of the numerically computed features, such as the levels of pressure fluctuation, the phase relation between velocity and pressure fluctuations, and the structure of the flame, were qualitatively similar to experimental observations.

Using the stored data for these simulations, an investigation of acoustic feedback control technique was carried out. The experimental control system, which consists of a sensor (microphone), a phase shifter, an amplifier and a control driver (loudspeaker), was numerically modeled. A time-delay controller which is a more general implementation of the phase-shift controller was used for the simulations. It was shown that the control of both Type I and Type II instabilities in the ramjet can be successfully accomplished using this closed-loop system. A significant decrease in the pressure fluctuation levels occurs when the control is used. It was shown that with active acoustic feedback control, the pressure oscillation level can be brought down to the level seen in cold flows. It was also shown that the instability returns to its original form when the control is turned off.

The control also appeared to be effective for different values of time-delays between the sensor and the control signals, indicating that this is not an "anti-sound" approach (which would require a specific phase relation between the sensor and control signals). The success of different time-delays in suppressing the instability was similar to the observations made at NWC using different phase shifts. The results also showed that not all time-delays will provide control. This is again similar to the observations made in the experiments. By careful parametric analysis of the numerical simulations, a criterion for achieving control using acoustic feedback was determined. It was shown that as long as the cross-correlation between the sensor (microphone) and driver (loudspeaker) signals remained negative, the control technique will succeed and when the cross-correlation becomes positive, the control will fail. The results of the acoustic feedback control studies were described in a series of papers (Menon, 1990; Menon, 1991 and Menon, 1992a) which are included in Appendix A.

3.4. Secondary Fuel Injection Control of Combustion Instability

Another active control strategy that is being studied is the introduction of additional premixed fuel at some chosen location. Earlier experiments have shown that this approach is quite effective in suppressing combustion instability and may in fact result in an increase in thrust. Also, such a controller is probably more practical for realistic combustors since,

acoustic drivers may not survive in hot environments. Only simplified control systems have been investigated so far to first understand the behavior of the instability when additional heat release occurs. These controllers employed steady injection, pulsed injection or injection with a fixed time-delay. These controllers can be considered simplification of a general controller (which employs a dynamically varying time-delay) that is now being investigated.

The location used for injecting the secondary fuel is in the inlet upstream of the dump plane. This is similar to the approach taken in earlier experiments at Cambridge University. It is also somewhat similar to the NWC fuel modulation approach since one of the effects of secondary fuel injection in the inlet is a modification of the inlet duct boundary layer. The net effect of this approach is a modification of the total mass flow rate of the fuel into the combustor and thus a modification of the associated heat release. The results of these studies are described in a series of papers (Menon, 1991, 1992b, 1992c).

The secondary fuel injection control technique resulted in some interesting behavior that gives a physical insight into the mechanism of the instability and the effect of secondary heat release. In the short inlet configuration studied earlier (using the constant flame speed model), it was found that when the control is only partially effective, although the amplitude is reduced, the source of the oscillation is uneffected but when the control is very effective, not only the amplitude is reduced drastically, the source of the oscillation also is changed.

When secondary fuel injection control technique was used in the long inlet configuration, two important behavior was uncovered. In the case when the inlet duct acoustics was controlling the instability, the control results in reduction of the pressure fluctuation level from the original 30 percent to around 15 percent, but the frequency remained uneffected. This showed that inlet acoustics is still driving the instability. In the case when a convective mode of oscillation was occuring, the injection control again reduced the pressure level from the original 30 percent to 15 percent, but now, two new low frequencies appears in the oscillation. It appears from the preliminary analysis that the lower new frequency is related to the convective component while the higher one was again the inlet duct acoustic mode.

The behavior of the instability seen in these simulations are in remarkable agreement with recent observations at NWC. For example, in their recent study, when one mode was controlled additional modes of oscillation was excited. Control of both modes of oscillation appears to require a dual-mode controller. We are also now investigating a dual-mode, dynamically adjusting controller for our simulations so that when a new mode of oscillation appears the controller will automatically adjust for the change. The results of these studies will be reported in the future.

4. SIGNIFICANCE OF THE ACCOMPLISHMENTS

The development of a numerical simulation tool to study complex and realistic phenomena such as combustion instability in a ramjet is a major accomplishment in computational research. The development of a massively parallel LES code is also a major development in CFD since, so far, no one has yet addressed the potential of parallel computing for unsteady combustion. Results obtained so far indicate that active control techniques can be studied using such a simulation code. The study of acoustic feedback control has resulted in the determination of a criterion that can be used to judge whether control will work or not. If further experiments of acoustic feedback control are planned it would be worthwhile to find out if this criteria can be used to develop an automatic controller that would work for a wide range of operating conditions. The secondary fuel injection control approach will be the major focus of the next year study. The results obtained so far has clearly shown that many of the important features of the instability seen in the experiments have been captured in the simulation. The effect of control is also quite similar to that seen in the experiments. Further research using theoretical considerations are planned to provide some insight into the details of the instability process and its control that cannot be determined experimentally.

5. WORK PLAN FOR THE NEXT TWO YEARS

The research will be continued for the next two years at Georgia Tech, where the principal investigator is becoming an Associate Professor. There are three major objectives for the rest of this program:

[1]   Use theoretical considerations to analyse the simulation data to determine a fuel injection controller

[2]   Simulation and Active Control Studies on the iPSC/860

[3]   Full Three-Dimensional Simulations of Combustion Instability and Active Control

[1] Use theoretical considerations to analyse the simulation data to determine a fuel injection controller

Since it is computationally expensive to carry out a series of simulations to train a controller (as done experimentally), it is planned to address the active control techniques from a theoretical standpoint. Some work in that direction has already started (Menon and Yang, 1993). In this approach, the simulated instability signals will be used in a theoretical model for combustion instability developed by Vigor Yang to determine the stability margin required for controller. The theoretically derived controller will then be used in the simulation. Since the theory neglects some important nonlinear features, further finetuning will be required; however, it is hoped that only a few training simulations will be required to develop a robust controller. If this approach succeeds, then a strong theoretical/numerical capability would become available that could be used for active control studies.

(2) Simulation and Active Control Studies on the iPSC/860

Since the current code is operational on the iPSC/860, most of the next two years axisymmetric simulations are planned on the parallel machine. Further development of the LES model to account for flame curvature and local extinction will be incorporated and tested on the Cray, and then ported on to the iPSC/860.

(3) Full Three-Dimensional Simulations of Combustion Instability and Active Control The full 3D code is now ready and we have received sufficient time on the Cray-YMP to carry out a limited number for full 3D simulations. The goal of this study is to evaluate the importance of three- dimensionality on the evolution of the coherent structures and on the combustion instability. Since the computational cost of 3D LES is quite extensive, active control studies will be considered only after the controller has been successfuly demonstrated on the axisymmetric code and only if sufficient computer time is available. From practical standpoint, full 3D LES may be more economically feasible on the iPSC/860; however, porting the 3D code on to the parallel machine will require a major effort and will have to wait availability of further resources.

6. PUBLICATIONS/PRESENTATIONS

Menon, S. (1990) "Numerical Simulation and Active Control of Combustion Instability in a Ramjet Combustor," AIAA Paper No. 90-3930, presented at the 13th Aeroacoustics Conference, Tallahassee, FL, October 22-24.

Menon, S. (1991) "Active Control of Combustion Instability in a Ramjet using Large-Eddy Simulations," AIAA Paper No. 91-0411, presented at the 29th Aerospace Sciences Meeting, Reno, NV, January 7-11.

Menon, S. (1992a) "Active Combustion Control in a Ramjet using Large-Eddy Simulations", *Combustion, Science and Technology*, VOl 84, pp 53-72.

Menon, S. (1992b) "A Numerical Study of Secondary Fuel Injection Techniques for Active Control of Combustion Instability in a Ramjet," AIAA Paper No. 92-0777, presented at the

30th Aerospace Sciences Meeting, Reno, NV, January 6-10.

Menon, S. (1992c) "Secondary Fuel Injection Control of Combustion Instability in a Ramjet," under preparation, to be submitted to *J. of Propulsion and Power*.

Menon, S. and Yang V. (1993) "Some Issues Concerning Active Control of Combustion Instability in Ramjets", AIAA Paper No. 92-   , to be presented at the 31st Aerospace Sciences Meeting, Reno, NV, January 7-11.

Menon, S., and Weeratunga, S. (1992) "Large-Eddy Simulations of Combustion Instability in a Ramjet using the iPSC/860", under preparation.

Weeratunga, S. and Menon, S. (1992) "Implementation of a Large-Eddy Simulation Code on the iPSC/860," under preparation.

REFERENCES

Chasnov, J. R. (1991) "Simulation of the Kolmogorov Inertial Subrange using an Improved Subgrid Model," *Phy. Fluids A.*, Vol. 3, pp. 188-200.

Culick, F. E. C. (1989) "Combustion Instabilities in Liquid-Fueled Propulsion Systems - An Overview," AGARD CP-450, pp. 1.1-1.73.

Erlebacher, G., Hussaini, M. Y., Speziale, C. G., and Zang, T. A. (197), "Toward the Large-Eddy Simulations of Compressible Turbulent Flows," ICASE Report No. 87-20.

Gutmark, E., Parr, T. P., Parr, D. M., and Schadow, K. C. (1990) "Active Control of a Premixed Flame," AIAA-90-2448.

Hedge, U. G., Reuter, D., Zinn, B. T., and Daniel B. R. (1987) "Fluid Mechanically Coupled Combustion Instabilities in Ramjet Combustors," AIAA-87-0216.

Jou, W.-H., and Menon, S. (1990) "Modes of Oscillations in a Nonreacting Ramjet Combustor," *J. Propulsion and Power*, Vol. 6, pp. 535-543. Vol. 6, pp. 535-543.

Kerstein, A. R., Ashurst, W. T., and Williams, F. A. (1988) "Field Equation for Interface Propagation in an Unsteady Homogeneous Flow Field," *Physical Rev. A.*, Vol. 37, No. 7, pp. 2728-2731.

Kerstein, A. R., and Ashurst, W. T. (1992) "Propagation Rate of Growing Interfaces in Stirred Fluids," to appear in *J. Fluid Mech.*

Langhorne, P. J., and Hooper, N. (1989) "Attenuation of Reheat Buzz by Active Control," AGARD-CP-450, pp. 10.1-10.16.

Leith, C. E. (1990) "Stochastic Backscatter in a Subgrid Model: 3D Compressible Flows," presented at the Intn. Workshop on Large Eddy Simulations, St. Peteresburg, Fl, December 19-21.

Menon, S., and Jou, W.-H. (1987) "Simulations of Ramjet Combustor Flow Fields, Part I: Numerical Model, Large-Scale and Mean Motion," AIAA-87-1421.

Menon, S., and Jou, W.-H. (1990) "Numerical Simulations of Oscillatory Cold Flows in an Axisymmetric Ramjet Combustor," *J. Propulsion and Power*, Vol. 6, No. 5, pp. 525-534.

Menon, S., and Jou, W.-H. (1991) "Large-Eddy Simulations of Combustion Instability in an Axisymmetric Ramjet Combustor," *Combustion Science and Technology*, Vol. 75, pp. 53-72.

Menon, S. (1990) "Numerical Simulation and Active Control of Combustion Instability in a Ramjet Combustor," AIAA Paper No. 90-3930.

Menon, S. (1992) "Active Combustion Control of Combustion Instability in a Ramjet Combustor using Large Eddy Simulations," *Combustion, Science and Technology*, Vol. 84, pp. 53-72.

Piomelli, U., Moin, P., and Ferziger, J. H. (1988) "Model Consistency in Large Eddy Simulation of Turbulent Channel Flows," *Phy. Fluids*, Vol. 31, pp. 1884-1891.

Piomelli, U., Cabot, W. H., Moin, P. and Lee, S. (1990) "Subgrid-Scale Backscatter in Transitional and Turbulent Flows," Proc. Summer Program, CTR, Stanford University, pp. 19-29.

Schadow, K. C., Gutmark, E., and Wilson, K. J. (1990) "Active Combustion Control in a Coaxial Dump Combustor," AIAA-90-2447.

Smith, D. A., and Zukoski, E. E. (1985) "Combustion Instability Sustained by Unsteady Vortex Combustion," AIAA-85-1248.

Squires, K., and Zeeman, O. (1990) "On the Subgrid-Scale Modeling of Compressible Turbulence," Proc. Summer Program, CTR, Stanford University, pp. 47-59.

Yakhot, V. (1989) "Propagation Velocity of Premixed Turbulent Flame," *Combustion Sci. and Tech.*, Vol. 60.

ACTIVE COMBUSTION CONTROL IN A RAMJET USING LARGE-EDDY SIMULATIONS

S. Menon

February 1991

QI²

ACTIVE COMBUSTION CONTROL
IN A RAMJET USING LARGE-EDDY SIMULATIONS

Suresh Menon

QUEST Integrated, Inc.

(formerly Flow Research, Inc.)

Kent, Washington

ABSTRACT

A large-eddy simulation model has been developed to study combustion instability in a ramjet combustor. A thin-flame model for premixed combustion is employed in the numerical scheme, which explicitly uses the local turbulent flame speed in the governing equation. Combustion instability in the ramjet has been numerically simulated. Two types of instability are observed: a small-amplitude, high-frequency instability and a large-amplitude, low-frequency instability. Both such instabilities have been experimentally observed, and various computed flow features are in good qualitative agreement with experimental observations. The information obtained from these simulations has been used to develop an active control strategy to suppress the instability. Control of both types of combustion instability was successfully achieved using the acoustic feedback technique, and the control could be used to turn the instability on and off. The control is effective over a range of time delays, and the pressure fluctuation levels in the combustor are significantly reduced when active control is used.

1. INTRODUCTION

Combustion instability in a ramjet engine is an extremely complex phenomenon involving nonlinear interactions among acoustic waves, vortex motion, and unsteady heat release. Typically, the instability manifests itself as a large-amplitude pressure oscillation in the low-frequency range (100-1000 Hz). This instability is related to longitudinal acoustic waves and is the most difficult to control. When the amplitude of the pressure oscillation reaches some critical limit, it can result in system failure, either by causing structural damage due to fatigue or by causing an engine "unstart," which occurs when the shock in the inlet duct can no longer be stabilized downstream of the choked inlet

throat and is expelled to form a bow shock ahead of the inlet. This phenomenon of engine unstart is a serious technical problem encountered in a ramjet engine. In recent years, both experimental (e.g., Schadow et al., 1987, 1990; Gutmark et al., 1989, 1990; Smith and Zukoski, 1985; Sterling and Zukoski, 1987; Hedge et al., 1987) and numerical (e.g., Menon and Jou, 1987, 1990, 1991; Jou and Menon, 1987, 1990; Kailasanath et al., 1989) investigations have been carried out to determine the mechanism of the combustion instability. Attempts to control combustion instability using both passive and active control techniques have also been carried out in the past (see Culick, 1989, for a review). Passive control methods that typically involve structural (i.e., geometrical) modifications have proven insufficient for controlling the low-frequency instability. Recent experimental studies (e.g., Poinsot et al., 1987; Langhorne et al., 1990; Schadow et al., 1990; Gutmark et al., 1990) suggest that the use of active control techniques may be a more effective approach for controlling the combustion instability in a ramjet. This paper discusses a study of active control techniques using large-eddy simulations (LES).

2. THE SIMULATION MODEL

The simulation model used in this study was developed through a series of numerical experiments starting with cold flow studies (Menon and Jou, 1987, 1990; Jou and Menon, 1987, 1990) and culminating in the simulation of combustion instability (Menon and Jou, 1991). The equations solved in this model are the full compressible Navier-Stokes equations formulated in an axisymmetric coordinate system. The numerical technique is an unsplit, second-order-accurate, finite-volume scheme based on MacCormack's method and is described elsewhere (Menon and Jou, 1987, 1990). The ramjet combustor modeled in these studies consists of an axisymmetric inlet duct connected to an axisymmetric dump combustor by a sudden expansion. A convergent-divergent nozzl 's attached downstream of the combustor. Figure 1a shows the typical ramjet configuration used in these studies.

2.1 The Numerical Model

The details of the numerical model and the validation studies have been described elsewhere (Menon and Jou, 1987, 1990; Jou and Menon, 1987, 1990) and will not be repeated here. However, some pertinent issues related to the implementation of the numerical boundary conditions are reviewed here.

For the spatially developing flow problem studied here, the inflow and outflow boundaries are computational boundaries. The implementation of proper inflow/outflow conditions is very important to ensure that no spurious (numerical) acoustic waves are generated. The ramjet is modeled here with a convergent-divergent nozzle attached downstream of the combustor, as in a real operating ramjet engine. The flow through this nozzle is choked, and the outflow at the downstream computational boundary is supersonic. Since at a supersonic outflow all characteristic waves (i.e., the acoustic waves, the entropy wave, and the vorticity wave) are outgoing, the imposed boundary conditions will not affect the interior flow field.

For the ramjet configuration shown in Figure 1a, subsonic inflow conditions are employed. These inflow conditions are similar to the conditions used in some of the experiments (e.g., Gutmark et al., 1989). Numerically, at the subsonic inflow three boundary conditions (the stagnation pressure, the stagnation temperature, and the local flow inclination) are specified corresponding to the three incoming characteristics (i.e., the vorticity wave, the entropy wave, and the right-running acoustic wave). The characteristic variable carried by the outgoing acoustic wave is determined by solving the pertinent decoupled interior characteristic equation. The application of these boundary conditions implies a certain "impedance" condition. Earlier, the characteristics of the current impedance condition were examined by a linearized analysis, and the condition was proven to be of the damping type. Thus, pressure disturbances reaching the inflow boundary will not be amplified.

In a realistic ramjet combustor, the upstream impedance condition is provided by the inlet shock, which under stable conditions resides downstream of the inlet throat. Thus, to simulate flow in a realistic ramjet combustor, the inlet nozzle must be included in the computational domain. Figure 1b shows a full ramjet configuration with a 320x64 grid distribution (only every other grid line is shown), which was used to discretize the computational domain. In such a ramjet geometry, the inflow is supersonic and all characteristics are incoming. Thus, all conditions can be specified. The supersonic inflow slows to a sonic condition (chokes) at the inlet throat and becomes supersonic again for a short distance downstream of the throat. Further downstream, the flow becomes subsonic due to the inlet shock. It has been noted earlier (e.g., Bogar and Sajben, 1979) that the flow oscillations downstream of the shock in the inlet diffuser may participate in the flow oscillations in the combustor. The shock also undergoes longitudinal oscillations that can, under some circumstances, become large-amplitude oscillations, resulting in the engine unstart phenomenon described earlier.

The full ramjet engine is currently being numerically modeled in a new study. Although a detailed analysis of this study will be presented in the future, some results are shown in Figure 2 to demonstrate the feasibility of modeling realistic flows in the full ramjet. Figure 2a shows a time sequence of vorticity contours during cold flow in a full ramjet engine. Figure 2b shows the typical Mach contours in the combustor. For this simulation, the shock undergoes only a small-amplitude oscillation about its stable location in the inlet diffuser. Analysis of the flow field indicates that the boundary layer on the inlet duct wall undergoes unsteady separation downstream of the inlet shock. This separated shear layer rolls up into coherent vortical structures, as seen in Figure 2a. The boundary layer sometimes reattaches on the inlet duct wall before finally separating at the dump plane. Downstream of the dump plane, this separated shear layer also undergoes vortex rollup, as seen in earlier cold flow studies (Menon and Jou, 1990). Complex vortex motions and merging processes are observed in the combustor as a consequence of the boundary layer separation in the inlet duct and the shear flow in the combustor. Many of the flow features observed during this simulation (and in other simulations not shown here) are in good qualitative agreement with the observations by Bogar and Sajben (1979). Currently, combustion is being initiated in the full ramjet, and the results will be reported in the future.

The results presented here are for the test configuration shown in Figure 1a, in which combustion instability has already been numerically simulated (Menon and Jou, 1991). The active control of the instability will be the focus of this paper.

2.2 The Combustion Model

To simulate combustion instability, an accurate evaluation of the chemical heat release is required. In particular, the amount of heat release and its time-dependent spatial distribution must be accurately computed. In a recent study (Menon and Jou, 1991), a thin-flame model (Williams, 1985; Kerstein et al., 1988) was incorporated. In this model, the local turbulent flame speed u_F appears explicitly and is determined as a function of the laminar flame speed u_l and the local subgrid turbulence intensity u' using the renormalization group (RNG) theory model of Yakhot (1989). The effects of detailed chemical kinetics are contained in the laminar flame speed, and a progress variable G is defined which is governed by the conservation equation

$$\frac{\partial \rho G}{\partial t} + \frac{\partial}{\partial x_i} \rho u_i G = - \rho u_F |\nabla G| \tag{1}$$

where u_i represents the fluid velocities, $G = 1$ for the fuel mixture, and $G = 0$ for the combustion product.

The turbulent flame speed u_F is given by the RNG model as

$$\frac{u_F}{u_l} = \exp\left[\frac{u'^2}{u_F^2}\right] \qquad (2)$$

The chemical heat release is a function of G and the specific chemical energy of the fuel mixture. The chemical energy of the mixture is included in the formulation by specifying the specific enthalpy h of the mixture in the energy equation as $h = C_p T + h_f G$. Here, h_f is the heat of formation of the premixed fuel, C_p is the specific heat of the mixture at constant pressure, and T is the temperature. The heat of formation of the fuel determines the amount of heat released during combustion and thus is a function of the equivalence ratio for a given fuel. The product temperature T_p can be estimated for a given heat of formation for the fuel by the relation $h_f = C_p(T_p - T_{fu})$, where T_{fu} is the fuel temperature at the inlet.

Due to the explicit appearance of the local flame speed in Equation (1), the amount of heat release does not depend on the computed internal structure of the flame. Even when numerical diffusion broadens the flame, the flame speed is not severely affected. The effect of numerical broadening was discussed earlier (Menon and Jou, 1991), and it was shown that numerical diffusion does not significantly affect the dynamics of the flame propagation. The model, as currently implemented, does not include flame broadening and flame extinction phenomena. These effects will have to be included eventually to generalize the combustion model.

2.3 The Subgrid Model

In a practical ramjet device, the Reynolds number of the flow is extremely high. Large-eddy simulations of such a flow would require a validated subgrid model; however, subgrid models for compressible flows have just begun to be investigated (e.g., Yoshizawa, 1986; Speziale et al., 1988). At present, it is not clear what would be an appropriate subgrid model for flows such as those in a ramjet combustor. It is, apparent, however that to close the combustion model described in Section 2.2, the subgrid turbulence intensity must be determined. Therefore, for the present application, a one-equation model for the subgrid turbulent kinetic energy is being investigated; this model is an extension of the Schumann's model (e.g., Schmidt and Schumann, 1989). With such a model, the subgrid

turbulence intensity in Equation (2) can be directly computed, and the subgrid stresses can be modeled.

At present, this model is still undergoing evaluation. Many issues still need to be resolved; these issues include, for example, the type of filtering to be used, the effect of variable grid distribution, the near-wall modifications to the eddy viscosity (e.g., Piomelli et al., 1989), and the proper closure for the Leonard and cross terms so that the filtered equations maintain Galilean invariance (e.g. Speziale, 1985; Germano, 1990).

Since a validated subgrid model is currently unavailable, all simulations carried out so far were for flows in a moderate Reynolds number range. This is considered a first step towards understanding the complex physical processes involved in the ramjet combustor. To model the dissipative effects of the subgrid turbulence, a constant eddy-viscosity model is employed. This eddy-viscosity is chosen to be the laminar dissipative coefficient at the reference temperature and can be viewed as a simple subgrid model, as noted by Ferziger and Leslie (1979). A uniform value of the subgrid turbulence intensity is also used; typically, this value is a small percentage of the reference velocity. Some important physical properties, such as the spatial nonuniformity of subgrid turbulence and its effect on the local flame speed and the amount of heat release, are not included at present. However, as shown earlier (Menon and Jou, 1991), the major qualitative interactions between the large-scale vortex structures and the combustion heat release have been captured by the present simulation model. The effect of nonuniform subgrid turbulence on the turbulent flame speed and on combustion instability will be included once the subgrid model has been fully implemented.

3. SIMULATION OF COMBUSTION INSTABILITY

The details of the simulation of combustion instability in a ramjet combustor are described elsewhere (Menon and Jou, 1991). The present focus is on active control of the numerically simulated combustion instability. Before describing the control studies, however, some important features of the computed instability are reviewed in this section.

In general, combustion instability in a combustor depends upon various parameters such as the system geometry, the flow parameters, the fuel type, and the equivalence ratio. In the earlier study (Menon and Jou, 1991), in addition to the flow parameters (e.g., the Mach number M and the Reynolds number Re) and the geometrical parameters (e.g., L_i, L, A_{inlet}/A^n ; see Figure 1a), two important thermochemical parameters were identified. One is $\theta = T_p/T_o$, which is the ratio of the product

temperature T_p to the stagnation temperature T_o.; the other is $\sigma = u_F/u_{ref}$, which is the ratio of the characteristic flame speed u_F to the characteristic reference velocity u_{ref}. For a fixed fuel mixture, θ can be related to the equivalence ratio ϕ, and σ can be related to the chemical kinetic rate and the level of subgrid turbulence. The effects of varying the geometrical parameters, the ratio between the inlet and throat areas (A_{inlet}/A^*), and the thermochemical parameters θ and σ have been studied (Menon and Jou, 1991). It was determined that increasing σ, with the other parameters held fixed, excites the large-amplitude, low-frequency pressure oscillations typical of combustion instability in a ramjet. This instability was also excited when the area ratio A_{inlet}/A^* was increased. The area ratio is increased by reducing the nozzle throat area A^*. This decreases the inlet mass flow rate and reduces the inlet mean flow velocity u_{in}. Thus, the effect of increasing the area ratio can be interpreted as an increase in the effective thermochemical parameter $\sigma^* = u_F/u_{in} = \sigma(u_{ref}/u_{in})$. This appears to indicate that σ^* may be a more general thermochemical parameter than σ.

Two simulations described in this section showed two different types of combustion instability: a small-amplitude, high-frequency combustion instability (Type I) and a large-amplitude, low-frequency combustion instability (Type II). Both types of instability have been observed in various experimental studies (e.g., Smith and Zukoski, 1985; Sterling and Zukoski, 1987; Schadow et al., 1987). Detailed analyses of these simulations have been described elsewhere (Menon and Jou, 1991). However, to put the results of the active control studies into perspective, a brief description of the pertinent features of the combustion instability is given in this section.

For all the simulations discussed in this paper, the reference Reynolds number and the reference Mach number were held fixed at Re = 10,000 and M = 0.32, respectively, based on the inlet duct diameter and the reference velocity of u_{ref} = 100 m/sec. A grid resolution of 256x64 was used for all the simulations, with the grid clustered in regions where high gradients are present, such as the boundary layer and the separated shear layer. For this grid resolution and the chosen Reynolds number, structures of the order of the boundary layer thickness could be resolved in the flow field (Menon and Jou, 1990). The thermochemical parameters θ and σ were also held fixed at θ = 5 and σ = 0.05. For θ = 5, the product temperature T_p was 1500 K. All system (geometrical) parameters, such as H, L_i, and L, were held fixed for both simulations except for the area-ratio parameter A_{inlet}/A^*, which was increased from 1.05 for the Type I instability simulation to 1.20 for the Type II simulation. This results in an increase in the thermochemical parameter σ^* from 0.042 to 0.048. In the following sections, some pertinent features of the Type I and Type II combustion instabilities are briefly described.

3.1 Small-Amplitude, High-Frequency Instability (Type I)

In a Type I combustion instability, the pressure oscillations initially show a large-amplitude, low-frequency oscillation that eventually decays so that a high-frequency oscillation at around 935 Hz dominates the pressure field. The peak-to-peak level of the high-frequency pressure fluctuation is around 15 percent of the mean pressure, as shown in Figure 3a. This level is around three times higher than that observed in earlier cold flow studies (Menon and Jou, 1990). Note that although the fluctuation level is small, it is by no means insignificant for a realistic ramjet combustor and may be sufficient to expel the inlet shock.

Flow visualization shows that the shear layer separating at the rearward-facing step rolls up into vortices; further downstream, these vortices undergo pairing, as observed in earlier cold flow studies. The flame front initially resides along the high shear region in the shear layer, and as the vortex rollup/pairing process occurs, the flame is entrained into the vortical structures. The typical flame structure and vorticity field distribution for this simulation is shown in Figures 3b and 3c. For comparison, an experimental visualization by Smith and Zukoski (1985) of premixed combustion in a two-dimensional combustor is shown in Figure 3d. Both the numerical and experimental visualization show qualitatively similar vortical structures in the shear layer.

Classical considerations using the Rayleigh criterion have been used in the past (e.g., Sterling and Zukoski, 1987; Hedge et al., 1987) to demonstrate that the unsteady fluctuations in heat release should be in-phase locally with the pressure fluctuations for the instability to occur. A local Rayleigh parameter $R(\vec{x}, t)$ is defined such that

$$R(\vec{x}) = \frac{1}{T}\int_T q'(\vec{x}, t)p'(\vec{x}, t)dt \qquad (3)$$

where T is the time period and $q'(\vec{x}, t)$ and $p'(\vec{x}, t)$ are the unsteady heat release term and the pressure fluctuation, respectively. When $R(\vec{x})$ is positive, local amplification of the instability occurs. When $R(\vec{x})$ is integrated radially, one obtains $R(x)$, which is the axial variation of the Rayleigh parameter. Alternatively, if $R(\vec{x}, t)$ is integrated in both the axial and radial directions, a volume-averaged parameter $\overline{R}(t)$ is obtained, which represents the time-dependent state of the combustion process in the combustor. If $\overline{R}(t)$ is further integrated in time, a global Rayleigh parameter R^* is obtained.

Both $R(x)$ and $\bar{R}(t)$ in the combustor were evaluated for this simulation. Figure 4a shows the time-dependent variation of the volume-averaged Rayleigh parameter $\bar{R}(t)$ normalized by R^* for two cycles of the high-frequency pressure fluctuation. Also shown is the normalized pressure fluctuation $(\Delta p/\bar{p})$ at the base of the step for this simulation period. This figure shows that during the high-frequency oscillations there are periods of time when the combustion process is damped. If we assume the pressure fluctuation shown in this figure is representative of the volume-averaged unsteady pressure field (an assumption that is strictly not valid since the amplitude and phase of the high-frequency oscillation are not constant in the combustor), then to obtain the observed variation in the Rayleigh parameter, the unsteady heat release term (Δq) should have a variation as sketched in Figure 4a. This indicates that the unsteady heat release fluctuations occur at a much higher frequency than the pressure fluctuation during the Type I instability. Figure 4b shows the axial variation of the Rayleigh parameter $R(x)/R^*$ for the time period shown in Figure 4a. Although the combustion instability is globally amplified, there are regions in the combustor where it is locally damped. The instability appears to be strongly amplified in the diffuser region where the vortices in the shear layer impinge on the wall. A similar amplification of the instability in the vortex impingement region was observed in experimental studies (Sterling and Zukoski, 1987).

3.2 Large-Amplitude, Low-Frequency Instability (Type II)

In a Type II combustion instability, the pressure fluctuations show a large-amplitude, low-frequency oscillation with peak-to-peak levels around 50 percent of the mean pressure, as shown in Figure 5a. The oscillation rapidly reaches a limiting cycle and shows a type of pressure signature that is typical of that observed during combustion instability. The flame propagation, however, is quite different from that observed during a Type I instability. A large hooked-flame structure propagates through the combustor at a low frequency, and associated with this flame is a large mushroom-shaped vortical structure. The combined vortex/flame structure propagates through the combustor at the same low frequency. Spectral analysis has shown that the dominant mode of oscillation is occurring at a frequency of around 166 Hz. The amplitude and phase of the pressure oscillation at various locations in the combustor were nearly the same, indicating that this pressure oscillation is similar to the bulk-mode oscillation observed in some experiments.

A typical flame structure and vorticity contour field are shown respectively, in Figures 5b and 5c. For comparison, the experimental visualization of Smith and Zukoski (1985) is shown in Figure 5d. Further analysis was carried out by Menon and Jou (1991), and it was shown that many

characteristics of Type II combustion instability, such as the pressure and velocity fluctuation levels, the phase relation between the pressure and velocity fluctuations, and various features of the vortex/flame structure propagation, qualitatively agreed with experimental observations.

The Rayleigh criterion for this instability was also computed. Figure 6a shows the variation of $\bar{R}(t)/R^*$ and the pressure fluctuation at the dump plane for one period of the low-frequency oscillation. During the Type II instability, the pressure amplitude and phase are nearly the same throughout the combustor, and thus the pressure fluctuation shown in Figure 6a can be considered to represent the volume-averaged pressure field in the combustor. Figure 6a shows that during the low-frequency oscillation there are two time periods during which the combustion process is locally damped. Again, this is due to a phase difference between the pressure fluctuations and the unsteady heat release term, as shown in Figure 6a. However, unlike the Type I instability case (Figure 4a), the fluctuation in the heat release term appears to be occurring at the same low frequency as the pressure fluctuation. The spatial variation of the Rayleigh parameter, $R(x)/R^*$, is shown in Figure 6b. As seen during the Type I instability (Figure 4b), the combustion process strongly drives the instability near the vortex impingement region in the diffuser. Figure 6b also shows that there is a region near the dump plane where the combustion process is locally damped. In contrast, during Type I instability (Figure 4b) multiple regions in the combustor show local damping of the instability.

4. ACTIVE CONTROL OF COMBUSTION INSTABILITY

Using the stored data for these two simulations, a new study was initiated to investigate techniques for controlling both types of instabilities. Experimentally, various approaches are being considered. In general, active control strategies fall in three categories: control using acoustic feedback (e.g., Lang et al., 1987; Poinsot et al., 1987; Gutmark et al., 1990; Schadow et al., 1990); control by unsteady modification of the inlet mass flow rate (e.g., Bloxsidge et al., 1988); and control by manipulation of the unsteady heat release in the combustor (e.g., Langhorne et al., 1990). Each of these methods has shown promise in laboratory tests. In this paper, the focus of the numerical experiments is the study of active control using acoustic feedback. Some results of active control using secondary fuel injection were recently presented (Menon, 1991).

4.1 Acoustic Feedback Control

Active control through acoustic forcing was demonstrated earlier by Lang et al. (1987) and Poinsot et al. (1987). The latter study showed that this technique provided the capability of turning the instability on or off at will, thereby providing a means to study the transient behavior. It was also shown that the power required for control was quite small and that control can be achieved over a wide range of phase differences. This indicates that the control technique is not an anti-sound approach, which would have required a specific phase relation. Recent studies (e.g., Schadow et al., 1990) have further demonstrated that acoustic feedback control of the combustion in a dump-combustor configuration is possible.

A typical acoustic feedback system used in the experiments involves a loudspeaker/microphone system in the active control loop. In this technique, the pressure signal is sensed at some chosen location using a microphone (or pressure transducer). The signal is analyzed, phase-shifted (or time-delayed), amplified, and then fed back at some other chosen location using a loudspeaker (see Figure 1a). Here, a similar technique has been studied numerically. To account for the effect of time delay in the control system, a control signal was chosen such that

$$p_{sp}'(t) = Ga \ p_{mic}'(t-\tau) \tag{4}$$

where the amplification parameter $Ga = A_g \dfrac{\bar{p}_{sp}}{\bar{p}_{mic}}$ with A_g a constant (typically, $A_g = 0.2$, unless otherwise specified). Here, $\bar{p}$ indicates the time mean value of the pressure, and the prime indicates unsteady fluctuation. Also, the subscripts sp and mic denote, respectively, the loudspeaker and the microphone. Once the acoustic pressure is determined by Equation (4), the axial acoustic velocity u_{sp}' generated by this pressure fluctuation at the loudspeaker surface is determined by using the acoustic relation $u_{sp}' = p_{sp}'/\rho c$. No transverse acoustic velocity fluctuations are assumed to occur (i.e., $v_{sp}' = 0$). Here, ρ and c are the unperturbed mean density and the speed of sound, respectively. Once p_{sp}' and u_{sp}' are determined, the pressure and velocity boundary conditions at the speaker surface become $p_{sp} = \bar{p}_{sp} + p_{sp}'$ and $u_{sp} = u_{sp}'$, $v_{sp} = 0$, respectively. The other boundary conditions at the loudspeaker surface are obtained by modeling the speaker surface as an adiabatic, noncatalytic surface (i.e., $\dfrac{dT}{dn} = 0$ and $\dfrac{dG}{dn} = 0$, where n is the normal direction). Typically, ten grid points along the base of the step were used to model the loudspeaker surface. The parameter τ is a specified time delay between the signal recorded by the microphone and the control signal used to drive the

loudspeaker. In the simulations, the time delay τ/T, where T is the time period of the oscillation ($T \approx 1.07$ msec for a Type I oscillation and $T \approx 6.02$ msec for a Type II oscillation), is specified prior to initiation of the active control. The time delay is chosen by analyzing the uncontrolled pressure signals in the simulations computed earlier; once chosen, the time delay is held constant for the entire duration of the control simulation. The effects of using different time delays have been investigated, and the results of these simulations are discussed below.

4.2 Active Control of Type I Instability

During a Type I instability, the pressure fluctuation at the base of the step shows a peak-to-peak level of around 15 percent of the mean pressure, as shown in Figure 3a. For reference, a short time interval of the pressure fluctuation is shown again in Figure 7a. A control system as shown in Figure 1a and the control law as given by Equation (4) were chosen for the study. Cross-correlation analysis of the uncontrolled pressure fluctuations at the microphone and speaker locations was carried out. The result is shown in Figure 7b. This figure shows that, for $\tau/T \approx 0$, the pressure fluctuations at the two locations are nearly perfectly *negatively* correlated. This indicates that a time delay close to zero should be effective. Figure 7c shows the pressure fluctuations at the base of the step with active control using $\tau/T = 0.03$. Clearly, the controller is quite effective; within two cycles of oscillation, it reduces the peak-to-peak pressure fluctuation level from 15 percent to less than 4 percent of the mean pressure. A 4 percent peak-to-peak fluctuation in this combustor is about the same level as seen during cold flow simulations (Menon and Jou, 1990).

Figure 7d shows the pressure signal at the dump plane with another time delay of $\tau/T = 0.15$ used for the control. The control is quite effective in this case as well, with the peak-to-peak pressure fluctuation level again decreasing to around 4 percent of the mean pressure. This figure also shows the effect of turning off the control at a later stage. The pressure fluctuation quickly recovers to the levels observed earlier with no control. Note that for $\tau/T = 0.15$, the correlation coefficient is still negative. This suggests that for a chosen time delay, if the correlation between the pressure signals from the microphone and loudspeaker locations is negative, then the control may be effective. This would imply that there may be a range of time delays for which control of the instability is possible. A similar observation was made in a recent experimental study (Schadow et al., 1990). In their test rig, the control was most effective within a specific phase range of 250 to 330 degrees.

That such an effectiveness range in terms of time delay exists can be ascertained from the simulations by comparing the simulation shown in Figure 7e with the earlier simulations (Figures 7c and 7d). Figure 7e shows the pressure signal using active control with $A_g = 1$ and a time delay of $\tau/T = 0.5$. For this chosen time delay, the correlation coefficient is strongly positive, as can be seen in Figure 7b. It appears that in this case the control signal has only a small effect on the high-frequency oscillation, and the peak-to-peak fluctuation level is not reduced.

The study described above showed that using a fixed time delay for the control signal was quite effective in reducing the pressure fluctuation level, provided the time delay was properly chosen. Cross correlations between the pressure fluctuations at the microphone and speaker locations during active control were also carried out for the simulations described above. Figures 8a and 8b show the cross correlation for the simulations shown in Figures 7c and 7d, respectively. For the chosen time delays, $\tau/T = 0.03$ (Figure 8a) and $\tau/T = 0.15$ (Figure 8b), the correlation coefficient remains negative during active control. For the case where control was ineffective with $\tau/T = 0.5$ (Figure 7e), the correlation coefficient remains positive during control (not shown).

Flow visualization of the flame propagation during active control showed that the flame structure does not change in any significant manner from the structure seen in the uncontrolled case (Figure 3b). Spectral analysis of the pressure fluctuation in the combustor showed that as the control becomes effective, the dominant frequency increases from 935 Hz to around 1.2 kHz. When the control is turned off, the frequency drops back to the original value.

In some experimental studies (e.g., Schadow et al., 1990; Wilson et al., 1991), the sensor (microphone) was located approximately one step height downstream of the dump plane, due to the restrictions imposed by the test rig configuration. To numerically determine the effect of sensor location on the control effectiveness, simulations were performed with the sensor located one step height downstream of the dump plane as in the experiments (location c, Figure 1a). Using cross-correlation data (not shown here), a time delay of $\tau/T = 0.3$ was chosen, for which the correlation was negative. Figure 9a shows the pressure signal for this case. Comparison with Figures 7c and 7d shows that, for this time delay, control of the pressure fluctuation is again achieved, with the peak-to-peak level dropping to less than 5 percent of the mean pressure. The importance of a proper choice of time delay is again demonstrated by carrying out another simulation with a time delay of $\tau/T = 0.15$, for which the correlation coefficient is slightly positive. Figure 9b shows the result of this simulation. Although the pressure fluctuation level drops from the 15 percent uncontrolled level to around 5 percent of the mean

pressure, comparison with Figure 9a shows that for this time delay the control was less effective.

4.3 Active Control of Type II Instability

The active control strategy employed for the control of a Type I instability was then applied to a Type II instability. A typical time trace of the uncontrolled pressure fluctuation at the base of the step during this instability is shown in Figure 10a. Cross correlation between the pressure signals from the dump plane and the diffuser location b showed that a peak negative correlation occurs around $\tau/T = 0.5$. This is shown in Figure 10b. Thus, it was expected that the control signal using a time delay of $\tau/T = 0.5$ would be effective. Figure 10c shows the pressure signal with the active control system turned on with $\tau/T = 0.5$ for the same time period as in Figure 10a. It is clear that the control strategy was quite effective in reducing the pressure fluctuation levels. In fact, the peak-to-peak level of oscillation, which was around 50 percent of the mean pressure for the uncontrolled case (Figure 10a), is now reduced to almost 4 percent (Figure 10c); this level is about the same as that achieved for the Type I instability. As seen in the figure, the control does take a certain amount of time (roughly equivalent to two periods of the low-frequency oscillation) to become effective. In another simulation (not shown), the control was turned on earlier, at around $t = 0.13$ msec (see Figure 5a), to determine if the controller is more effective if the low-frequency oscillations have not been established. It was determined (Menon, 1990) that in this case, the peak pressure level reached in the combustor is reduced, thereby increasing the effectiveness of the control system. Increasing the gain parameter A_g also reduces the overall time to achieve control, as described in Menon (1990). The effect of turning off the control is illustrated in Figure 10d, which shows the pressure signal after the control signal was turned off at the end of the simulation shown in Figure 10c. Although it takes a finite amount of time, the Type II instability does return.

Another simulation was carried out with a time delay of $\tau/T = 0.03$ between the sensor and control signal. In this case, cross correlation of the original signals (Figure 10b) indicates a strong positive correlation. Figure 10e shows the pressure signal for this control case; clearly indicating that the control is quite poor; however, it is interesting to note that the pressure fluctuation level does decrease slowly. Also shown in this figure is the computed Rayleigh parameter, $\bar{R}(t)/R^*$, and the projected variation of the unsteady heat release term. The Rayleigh parameter also decreases slowly, indicating that although the control is poor, it has a damping effect on the pressure oscillation.

The Rayleigh parameter for the case when control is effective (with $\tau/T = 0.5$) shows quite different behavior. The time variation of the Rayleigh parameter and the pressure fluctuation at the dump plane for such a case is shown in Figure 10f. The Rayleigh parameter indicates that the oscillation is still being driven during the early period of the control; as the control becomes effective, however, the Rayleigh parameter becomes very small, indicating that the instability is being damped.

The propagation of the vortex/flame structure seen in the uncontrolled case (Figure 5b) is also changed drastically, with the flame structure now taking a shape similar to that observed during the Type I instability simulation (Figure 3b). A typical flame structure in the combustor during control of the Type II instability is shown in Figure 11a, corresponding to the time shown in Figure 10c. When the control is turned off, the large-amplitude, low-frequency oscillation reappears (Figure 10d) and the flame structure begins to return to the large hooked shape seen in Figure 5b. This is shown in Figure 11b (corresponding to the time shown in Figure 10d). When control is turned on, the vortex structure in the shear layer changes from the large structure seen during instability (Figure 4c) to the relatively smaller vortices in the shear layer similar to those shown in Figure 3b. The vortex motion in the shear layer with active control is shown in Figure 11c. Subsequently, when the control is turned off, the amalgamation of the vortices in the shear layer into the large vortex reoccurs as the instability begins to reestablish in the combustor.

Spectral analysis of the pressure fluctuation in the combustor both with and without active control (Figures 10c and 10d, respectively) was carried out. When the control is first turned on, the dominant 166 Hz oscillation frequency increases to 175 Hz, but as the control becomes effective and the pressure fluctuation level drops, only a high-frequency fluctuation at around 1.2 kHz remains. This increase in fluctuation frequency during active control is similar to that observed during control of the Type I simulation described in Section 4.2. When the control is turned off, the dominant frequency begins to decrease and the amplitude increases until finally only the low-frequency, large-amplitude oscillation remains.

The Rayleigh criteria in the combustor during control sheds some light on the effect of active control. Figures 12a and 12b show, respectively, the variation of $R(t)/R^*$ and $R(x)/R^*$ in the combustor during active control. Figure 12a, which corresponds to a portion of the simulation shown in Figure 10f, shows that with active control there are multiple time periods during the oscillation when the instability is being damped. Figure 12b shows that during active control there are multiple regions in the combustor where the instability is being locally damped. This behavior is similar to that seen during

the Type I instability (Figures 4a and 4b) and quite different from that seen during the Type II instability (Figures 6a and 6b).

Although only a limited number of simulations with and without active control have been performed so far, some comments concerning the effect of active control on the pressure oscillation can be made from the analysis of the simulation data. The data show that with active control the large-amplitude, low-frequency oscillation seen during Type II instability is completely suppressed, and only a high-frequency oscillation around 1.2 kHz remains. The Type I oscillation also shows the same frequency with control. The analysis of pressure and vorticity spectra without control (see Menon and Jou, 1991) for both Type I and Type II instability show that a distinct peak at a frequency around 1.2 kHz is seen in the vorticity spectra. This suggests that this frequency is related to the vortex motion in the shear layer. Examination of the vorticity field in the shear layer during control (see for example Figure 11c) shows that the large vortex structure seen during Type II instability is now replaced with smaller vortices characteristic of vortex shedding in the shear layer. The large vortex formed during the Type II instability was shown (Menon and Jou, 1991) to be related to the large negative axial velocity fluctuations (associated with the large positive pressure fluctuations) occuring at the step location. Due to the negative velocity fluctuations, the vortex shedding mechanism was inhibited till the pressure fluctuation becomes negative and the velocity fluctuation becomes positive. Then, the entire seperated shear layer was forced into a large vortex. With active control, both the pressure and the velocity fluctuation levels are reduced significantly. The shear layer dynamics is no longer inhibited and thus, the characteristic vortex shedding mechanism dominates.

Finally, it is instructive to look at the acoustic power used to drive the loudspeaker during active control of the Type II instability. Figures 13a and 13b show the acoustic power as a function of time for the control simulations shown in Figures 10c and 10e, respectively. Here, the acoustic power (in watts) is defined as

$$P = 2\pi \int_{r_1}^{r_2} p_{sp}' u_{sp}' \, r \, dr \tag{5}$$

where r_1 and r_2 are the radial dimensions of the loudspeaker. Note that for the axisymmetric geometry, the modeled loudspeaker is actually a circular strip of thickness ($r_2 - r_1$). Figure 13a shows that, initially, the loudspeaker is driven at a high power level, but as the control becomes effective, the power level also drops off. Figure 13b shows that, for the case where the control is less effective, the power level is quite high for a longer period of time. However, it is interesting to note that as the

control slowly becomes effective (see Figure 10e) the power level also begins to drop off. These data indicate that for effective control of the Type II instability, a large power level is required only for a short time initially, and as the control becomes effective, the overall power required becomes quite low. The acoustic power required to drive the loudspeaker during control of the Type I instability (not shown here) is much lower (by an order of magnitude) when compared to the power requirements for the Type II control. Thus, the power requirement for controlling the Type I instability remains quite low at all times. This computed low-power requirement for achieving control is in qualitative agreement with the experimental results of Poinsot et al. (1987).

5. CONCLUSIONS

A large-eddy simulation model has been developed that contains the essential physics of combustion instability such as the acoustic wave motion, the interactions between the large eddies, and combustion and unsteady heat release during premixed fuel combustion in a ramjet. The combustion model used for the simulations explicitly incorporates the local turbulent flame speed and avoids the erroneous numerical heat release that would occur in a finite-rate chemistry model, while attempting to resolve the internal structure of the flame. Two types of combustion instability have been identified from the simulation results: a small-amplitude, high-frequency instability and a large-amplitude, low-frequency instability. Both types of instability have been experimentally observed, and many of the qualitative features of the numerically computed instabilities are in good agreement with the experimental observations.

The data stored during the simulations were then utilized to study closed-loop techniques to control the unstable pressure oscillations. The first phase of this study involved the application of acoustic feedback control techniques. It has been demonstrated here that active control of both types of instability can be accomplished by such a technique. Furthermore, it was shown that the instabilities could be turned on and off. This capability can be used to study and understand the transient process prior to the growth of the instability. Both the control and recovery of the Type II instability take a relatively longer time period than the Type I instability.

The effect of varying the time delay between the sensor and control signals was also studied, and it was shown that control is possible for different choices of the time delay. This clearly demonstrates that active control is not an anti-sound approach, which would have required a specific phase relation. This finding is in qualitative agreement with experimental observations. The results obtained so far

also suggests that cross-correlation analysis of the signals from the sensor and the driver (loudspeaker) locations could be utilized to devise an effective control signal. Note, however, that in the present study a constant time delay was used for the control signal. This approach was found to be effective, since for the Reynolds number simulated here, the original uncontrolled flow field had a single dominant frequency during both Type I and Type II instability. In a realistic combustor, the flow field will be highly turbulent and the pressure spectra could contain multiple distinct frequencies. In such a case, a constant time delay controller may not be effective, and a more complex control signal will be required. For example, the controller may require a dynamically changing time delay to respond to the changes in the flow field during active control. High Reynolds number flows will be simulated in the near future once the subgrid model has been fully implemented. More complex controllers can then be investigated.

It was also shown in this study that the acoustic power required to drive the loudspeaker is high for only a short initial period; as the control becomes effective, the power requirement becomes quite low. Again, this finding agrees with earlier experimental observations (e.g., Poinsot et al., 1987). Although these results appear to suggest the potential of using acoustic feedback control in a practical combustor, such a system still needs to be demonstrated, especially experimentally. Realistic combustors, which typically operate in the megawatt range, are extremely hot and noisy environments. Acoustic drivers that can survive such a hostile environment and deliver high power output may not exist. Therefore, to develop controllers for practical combustors, another approach to control the combustion instability is currently being explored. This technique uses secondary fuel injection, both steady and unsteady (e.g., Langhorne et al., 1990); results obtained so far suggest this approach may be more practical for realistic combustors. Some results of numerical simulations using steady and pulsed secondary fuel injection were recently reported (Menon, 1991). Further investigation of this type of controller is currently being carried out and will be reported in the future.

ACKNOWLEDGEMENT

REFERENCES

Bloxsidge, G. J., Dowling, A. P., Hooper, N., and Langhorne, P. J. (1988) "Active Control of Reheat Buzz," *AIAA J.*, Vol. 26, pp. 783-790.

Bogar, T. J., and Sajben, M. (1979) "The Role of Convective Perturbations in Supercritical Inlet Oscillations," CPIA Publication No. 412.

Culick, F. E. C. (1989) "Combustion Instabilities in Liquid-Fueled Propulsion Systems - An Overview," AGARD CP-450, pp. 1.1-1.73.

Ferziger, J., and Leslie, D. C. (1979) "Large-Eddy Simulations: A Predictive Approach to Turbulent Flow Computations," AIAA-79-1471.

Germano, M. (1990) "Averaging Invariance of the Turbulent Equations and Similar Subgrid Modeling," CTR-116, Center for Turbulence Research, Stanford University.

Gutmark, E., Parr, T. P., Hanson-Parr, D. M., and Schadow, K. C. (1989) "On the Role of Large and Small-Scale Structures in Combustion Control," *Combustion Sci. and Tech.*, Vol. 66, pp. 107-126.

Gutmark, E., Parr, T. P., Parr, D. M., and Schadow, K. C. (1990) "Active Control of a Premixed Flame," AIAA-90-2448.

Hedge, U. G., Reuter, D., Zinn, B. T., and Daniel, B. R. (1987) "Fluid Mechanically Coupled Combustion Instabilities in Ramjet Combustors," AIAA-87-0216.

Jou, W.-H., and Menon, S. (1987) "Simulations of Ramjet Combustor Flow Fields, Part II. Origin of Pressure Fluctuations," AIAA-87-1422.

Jou, W.-H., and Menon, S. (1990) "Modes of Oscillations in a Nonreacting Ramjet Combustor Flow," *J. Propulsion and Power*, Vol. 6, No. 5, pp. 535-543.

Kailasanath, K., Gardner, J. H., Oran, E. S., and Boris, J. P. (1989) "Effects of Energy Release on High Speed Flows in an Axisymmetric Combustor," AIAA-89-0385.

Kerstein, A. R., Ashurst, W. T., and Williams, F. A. (1988) "Field Equation for Interface Propagation in an Unsteady Homogeneous Flow Field," *Physical Rev. A.*, Vol. 37, No. 7, pp. 2728-2731.

Lang, W., Poinsot, T., and Candel, S. (1987) "Active Control of Combustion Instability," *Comb. and Flame*, Vol. 70, pp. 281-289.

Langhorne, P. J., Dowling, A. P., and Hooper, N. (1990) "Practical Active Control System for Combustion Oscillations," *J. Propulsion and Power*, Vol. 6, No. 3, pp. 324-333.

Menon, S. (1990) "Numerical Simulation and Active Control of Combustion Instability in a Ramjet," AIAA-90-3930.

Menon, S. (1991) "Active Control of Combustion Instability in a Ramjet Using Large-Eddy

Simulations," AIAA-91-0411,

Menon, S., and Jou, W.-H. (1987) "Simulations of Ramjet Combustor Flow Fields, Part I: Numerical Model, Large-Scale and Mean Motions," AIAA-87-1421.

Menon, S., and Jou, W.-H. (1990) "Numerical Simulations of Oscillatory Cold Flows in an Axisymmetric Ramjet Combustor," *J. Propulsion and Power*, Vol. 6, No. 5, pp. 525-534.

Menon, S., and Jou, W.-H. (1991) "Large-Eddy Simulations of Combustion Instability in an Axisymmetric Ramjet Combustor," *Combustion Sci. and Tech.*, Vol. 75, pp. 53-72.

Piomelli, U., Ferziger, J., and Moin, P. (1989) "New Approximate Boundary Conditions for Large-Eddy Simulations of Wall-Bounded Flows," *Physics of Fluids*, Vol. 1, pp. 1061-1068.

Poinsot, T. J., Bourienne, F., Esposito, E., Candel, S., and Lang, W. (1987) "Suppression of Combustion Instability by Active Control," AIAA-87-1876.

Schadow, K. C., Gutmark, E., Parr, T. P., Parr, D. M., Wilson, K. J., and Crump, J. H. (1987) "Large-Scale Coherent Structures as Drivers of Combustion Instability," AIAA-87-1326.

Schadow, K. C., Gutmark, E., and Wilson, K. J. (1990) "Active Combustion Control in a Coaxial Dump Combustor," AIAA-90-2447.

Schmidt, H., and Schumann, U. (1989) "Coherent Structure of the Convective Boundary Layer Derived from Large-Eddy Simulations," *J. of Fluid Mechanics*, Vol. 200, pp. 511-562.

Smith, D. A., and Zukoski, E. E. (1985) "Combustion Instability Sustained by Unsteady Vortex Combustion," AIAA-85-1248.

Speziale, C. (1985) "Galilean Invariance of Subgrid-scale Stress Models," *J. of Fluid Mechanics*, Vol. 156, pp. 55-62.

Speziale, C., Erlebacher, G., Zang, T. A., and Hussaini, M. Y. (1988) "The Subgrid-Scale Modeling of Compressible Turbulence," *Phys. Fluids*, Vol. 31, pp. 940-942.

Sterling, J. D., and Zukoski, E. E. (1987) "Longitudinal Mode Combustion Instabilities in a Dump Combustor," AIAA-87-0220.

Williams, F. A. (1985) *Combustion Theory*, Second Edition, Benjamin/Cummings Publishing Co.

Wilson, K. J., Gutmark, E., Schadow, K. C., and Smith, R. A. (1991) "Active Control of a Dump Combustor with Fuel Modulation," AIAA-91-0368.

Yakhot, V. (1989) "Propagation Velocity of Premixed Turbulent Flame," *Combustion Sci. and Tech.*, Vol. 60, pp. 191-214.

Yoshizawa, A. (1986) "Statistical Theory for Compressible Turbulent Shear Flows with the Application to Subgrid Modeling," *Physics of Fluids*, Vol. 29, pp. 2152-2164.

FIGURE CAPTIONS

FIGURE 1 The axisymmetric ramjet configuration; (a) the ramjet geometry without the inlet nozzle and the active control system, (b) the full ramjet geometry with a 320 x 64 grid distribution.
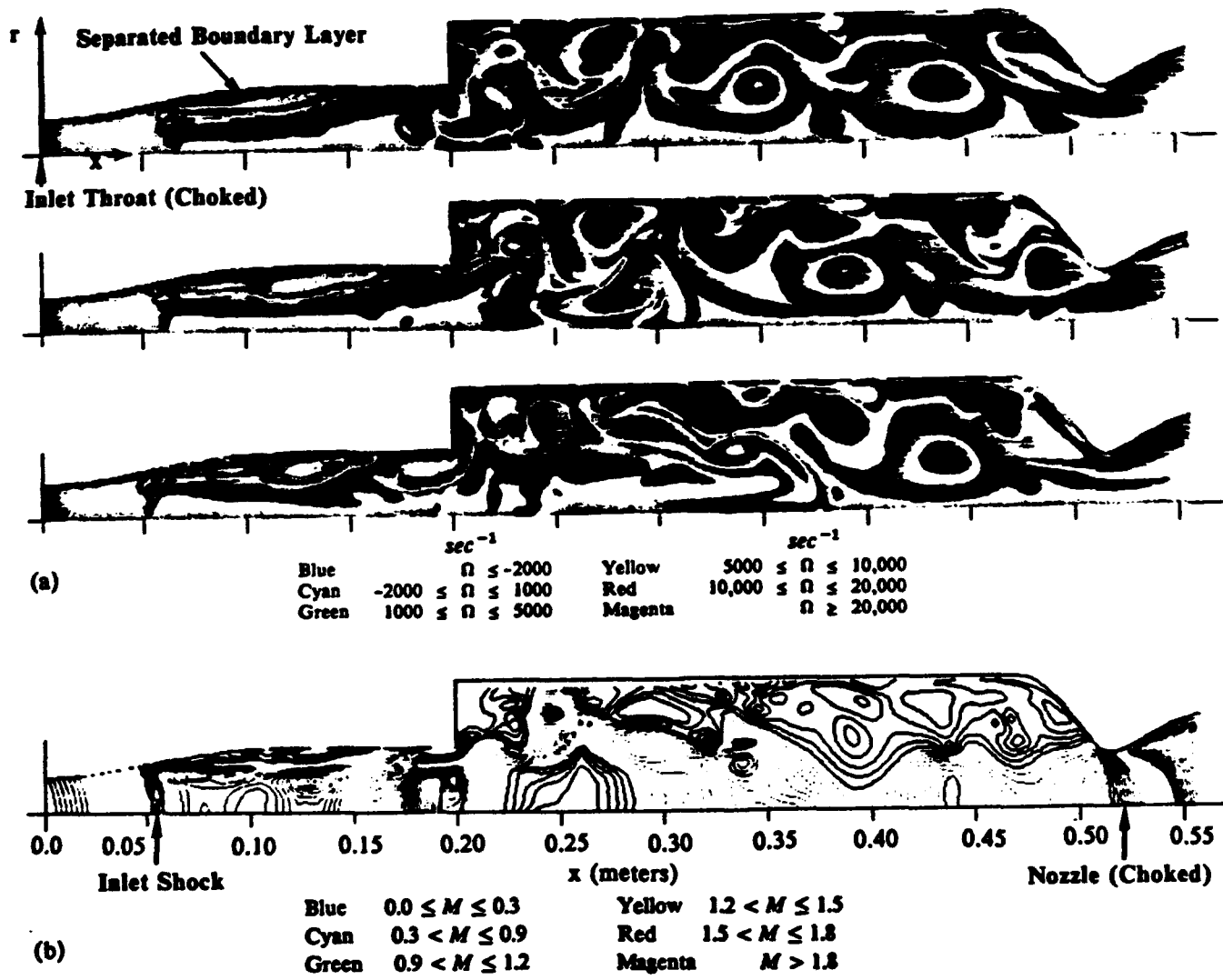
FIGURE 2 Typical cold flow field in a full ramjet engine; (a) time sequence of vorticity contours, (b) mach contours.
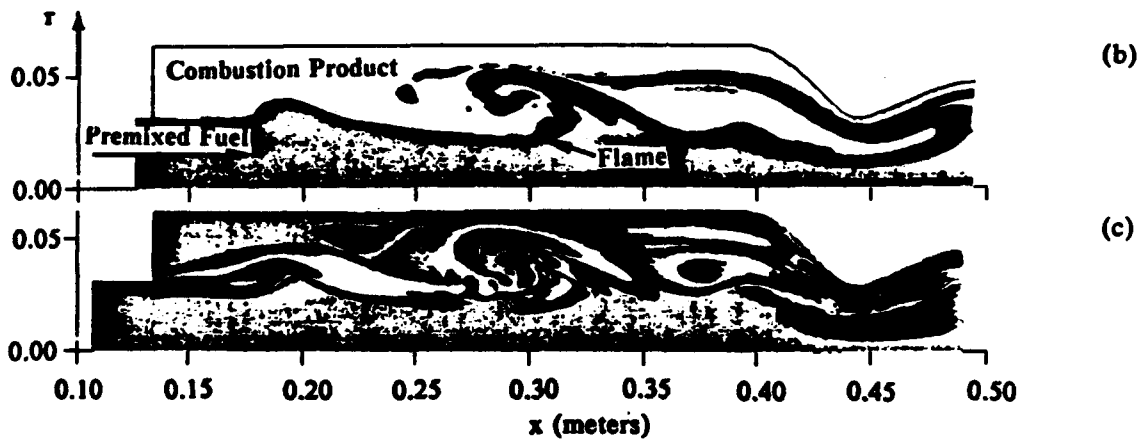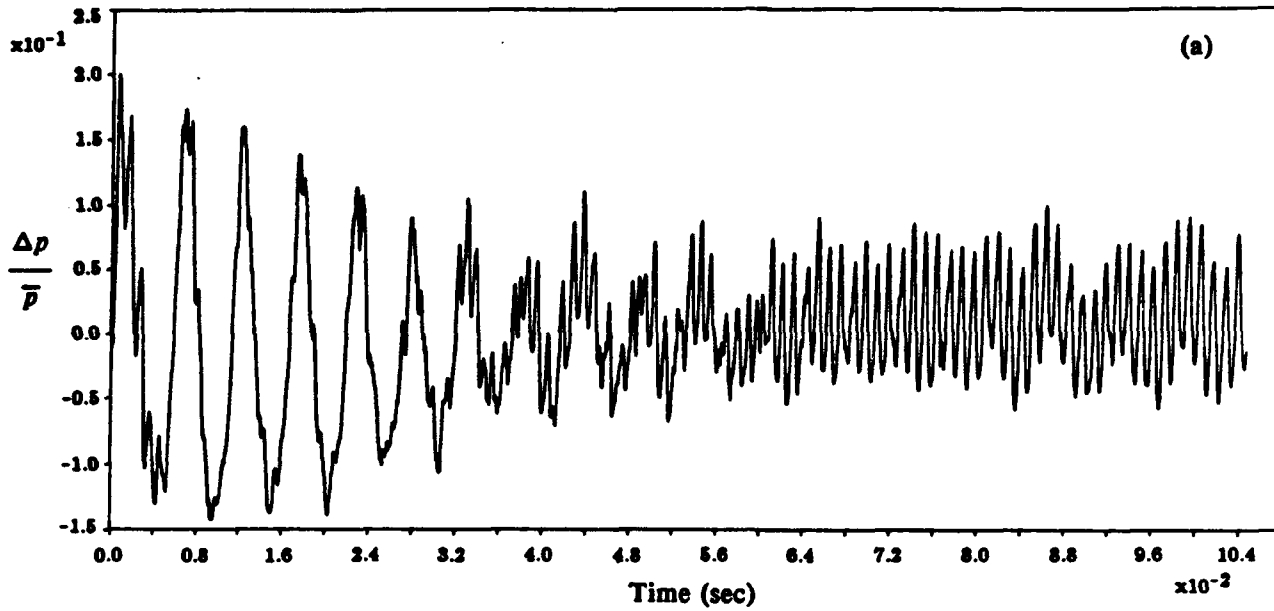
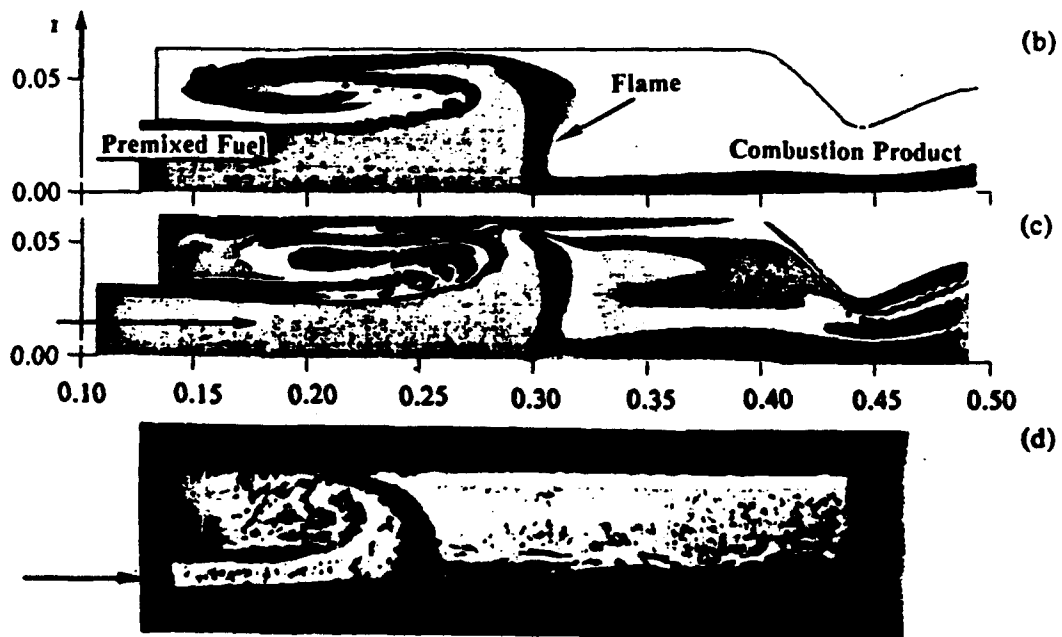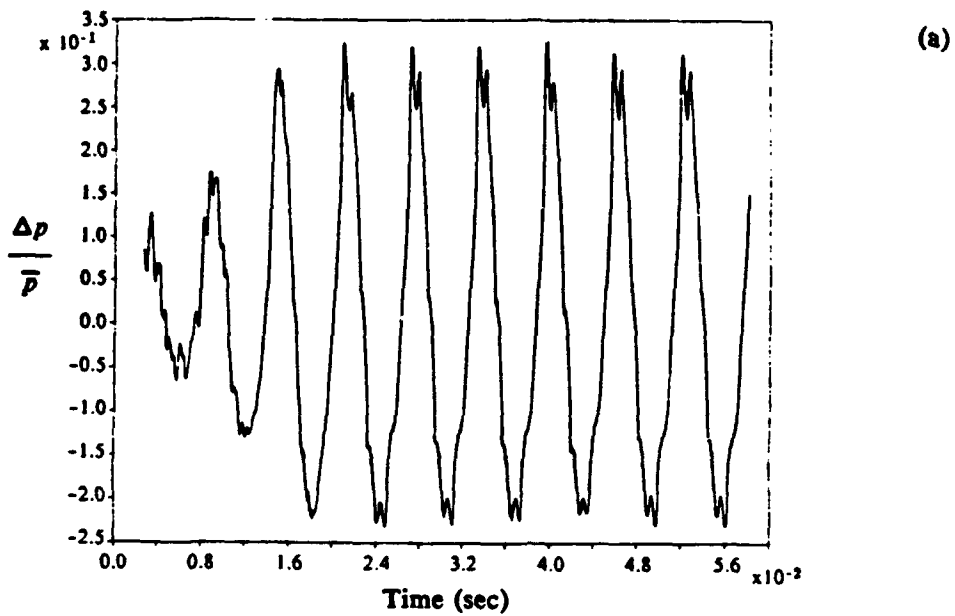FIGURE 3 Typical flow features observed during Type I instability; (a) pressure fluctuation at the base of the step, (b) flame structure, (c) vorticity field, (d) experimental. (Smith and Zukoski, 1985)

FIGURE 4 Rayleigh criteria in the combustor for a Type I instability; (a) temporal variation of $R(t)$, (b) spatial variation of $R(x)$.

FIGURE 5 Typical flow features observed during Type I instability; (a) pressure fluctuation at the base of the step, (b) flame structure, (c) vorticity field, (d) experimental. (Smith and Zukoski, 1985)

FIGURE 6 Rayleigh criteria in the combustor for Type II instability; (a) temporal variation of $R(t)$, (b) spatial variation of $R(x)$.
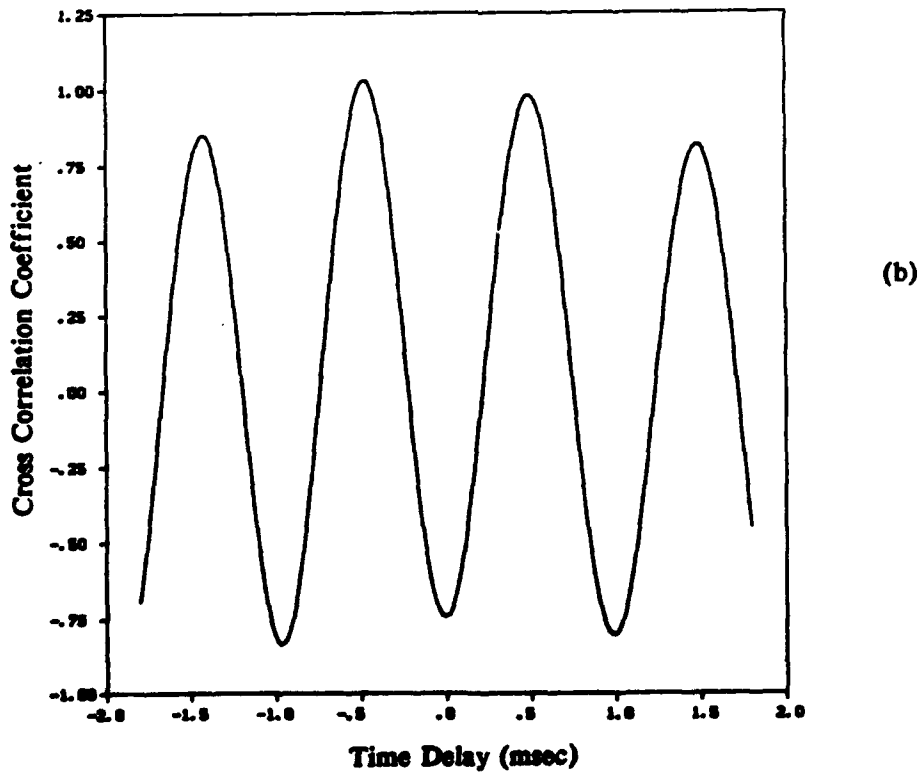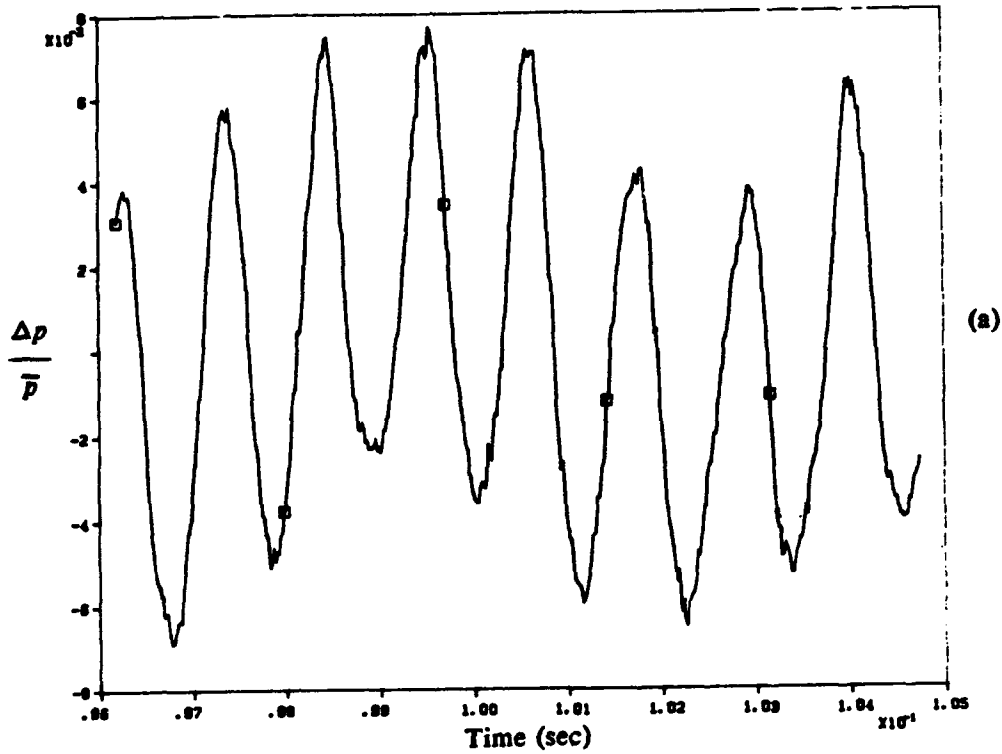
FIGURE 7 The effect of active control on the Type I instability, sensor at location b; (a) control OFF; reference signal, (b) correlation between the pressure signals at the speaker and microphone locations (control OFF), (c) control ON with $\tau/T = 0.03$, (d) control ON/OFF with $\tau/T = 0.15$, (e) control ON with $\tau/T = 0.5$.
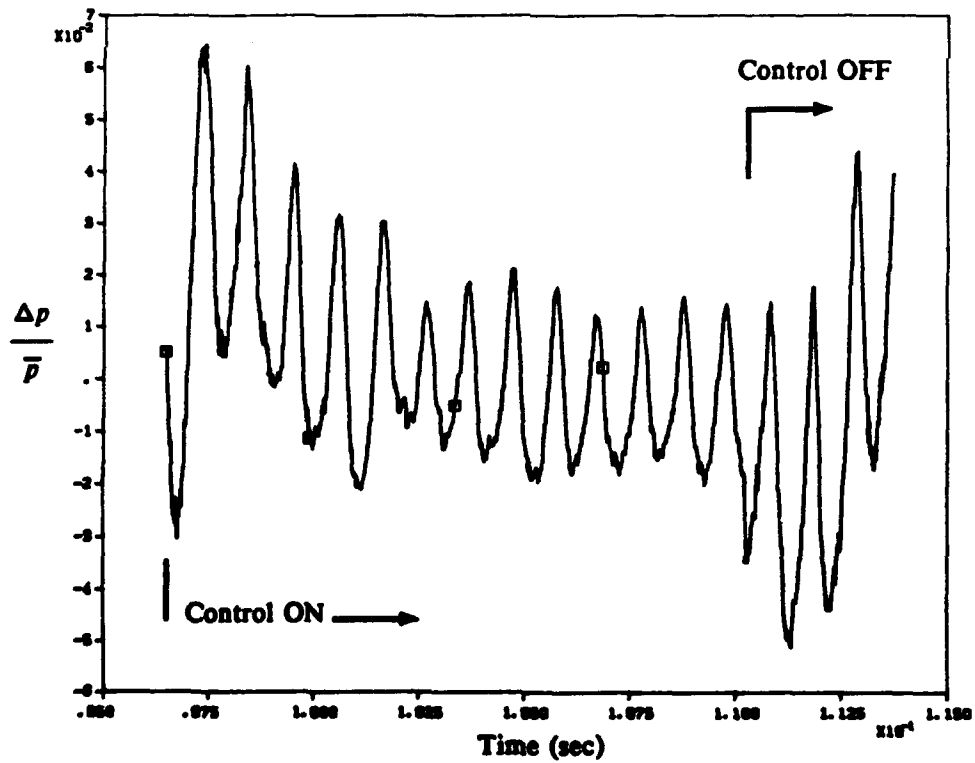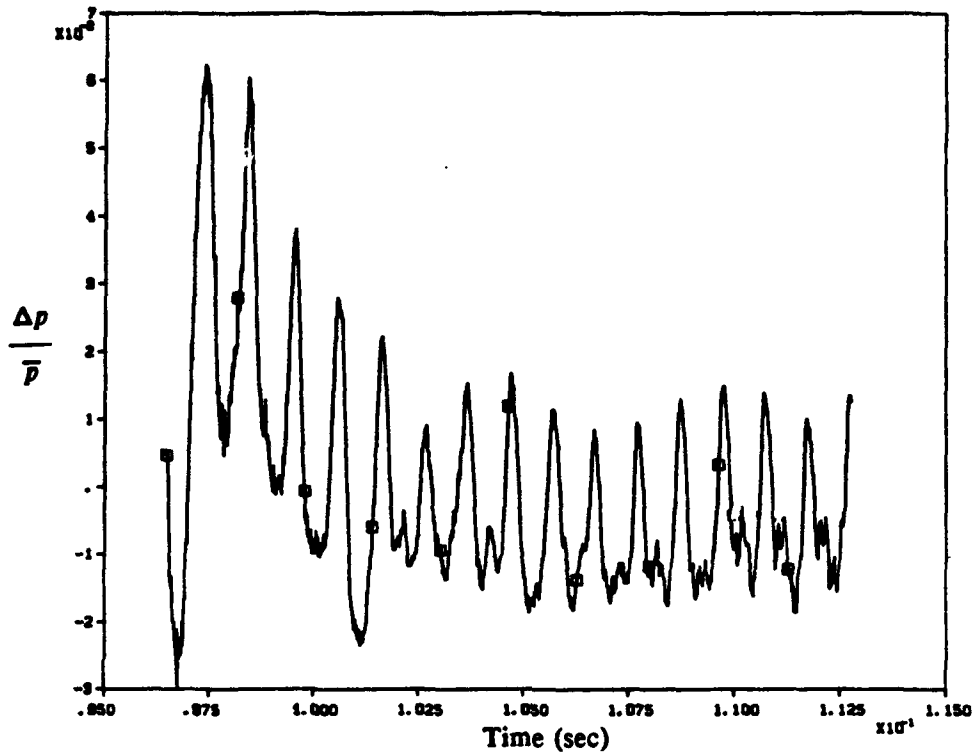
FIGURE 8 Correlation between the pressure signals at the speaker and microphone locations during active control; (a) $\tau/T = 0.03$, (b) $\tau/T = 0.15$.

FIGURE 9 The effect of active control on the Type I instability, sensor at location c; (a) control ON with $r/T = 0.30$, (b) control ON with $r/T = 0.15$.
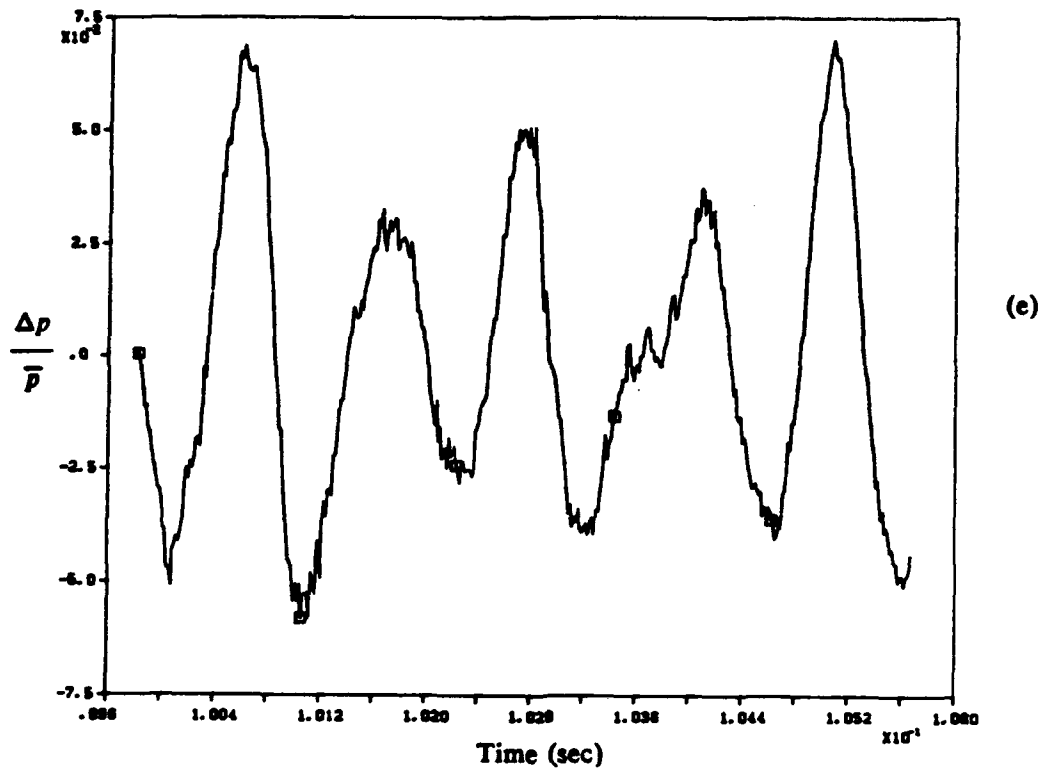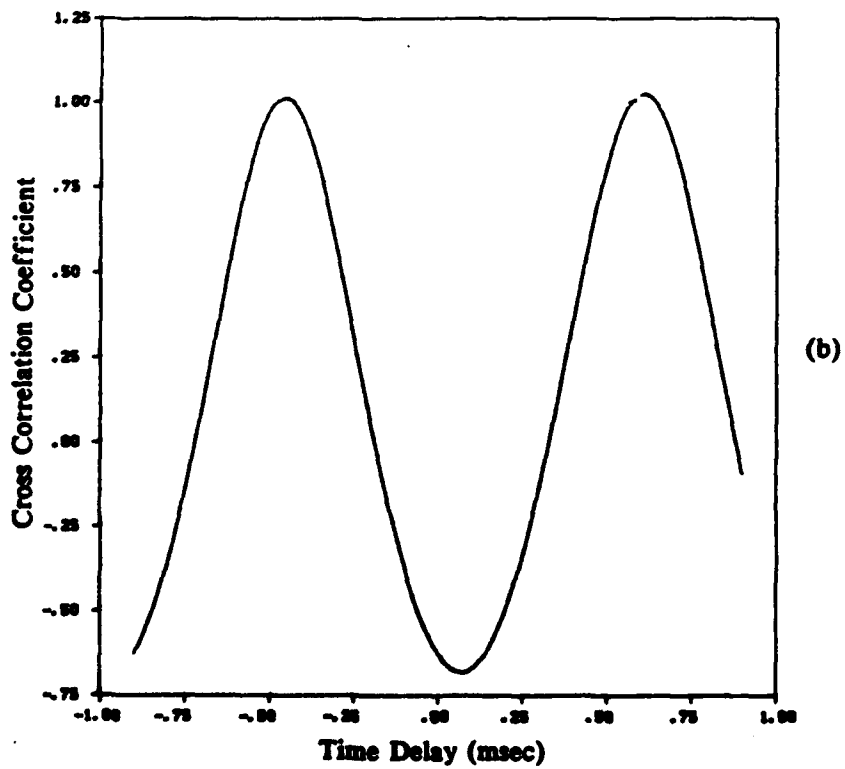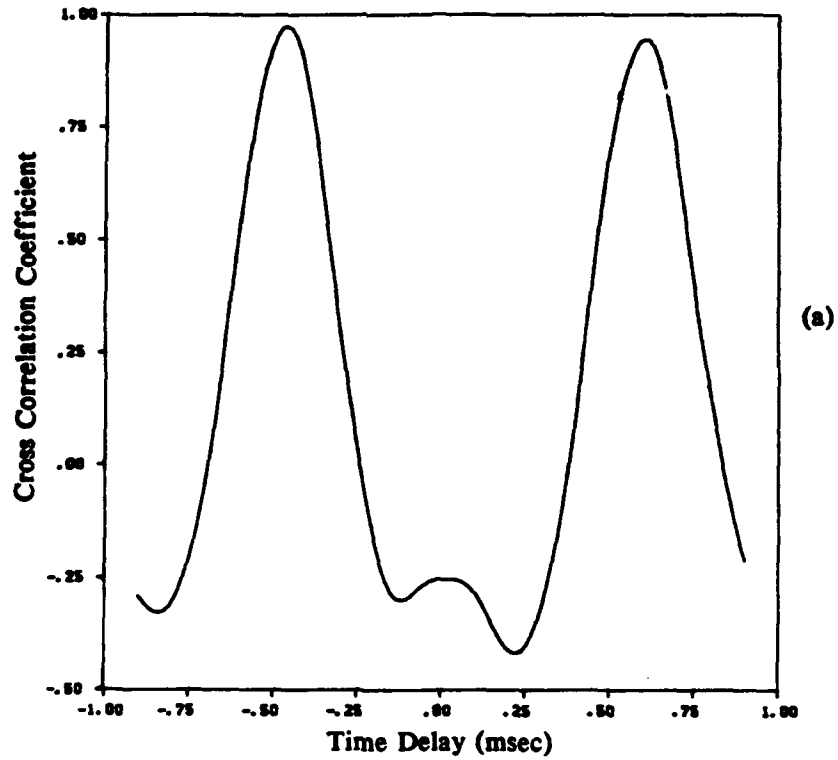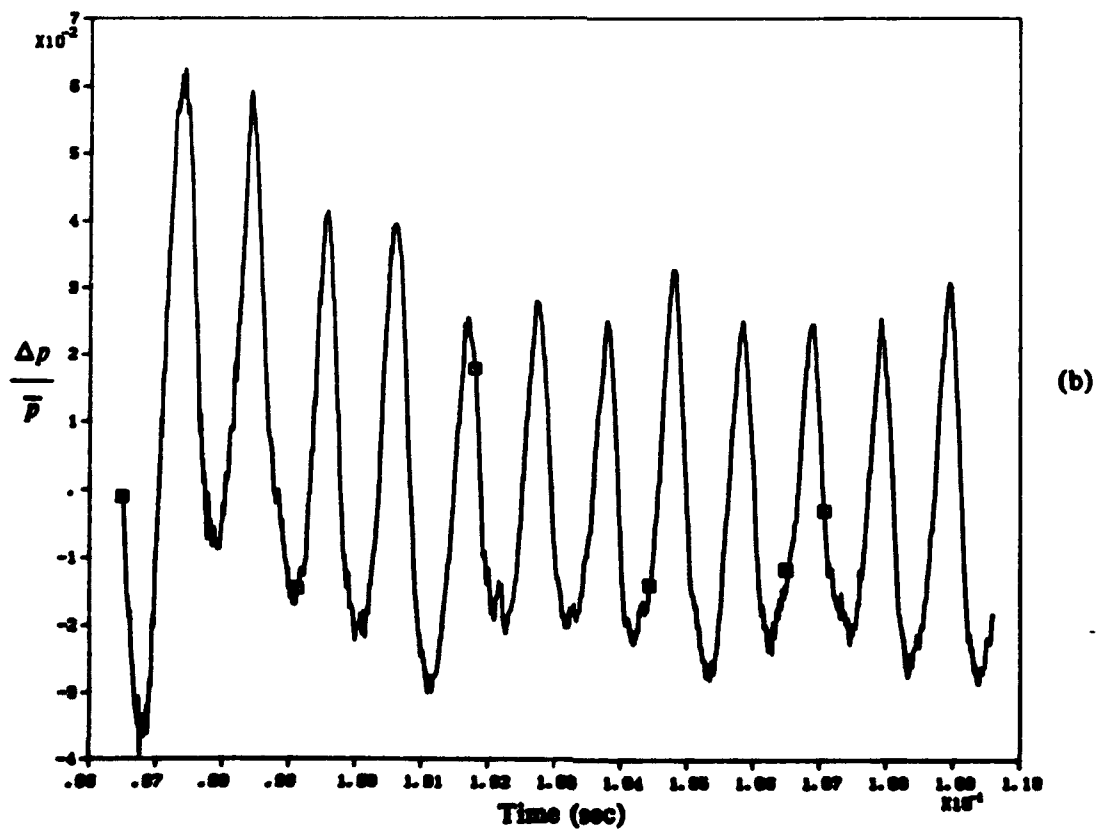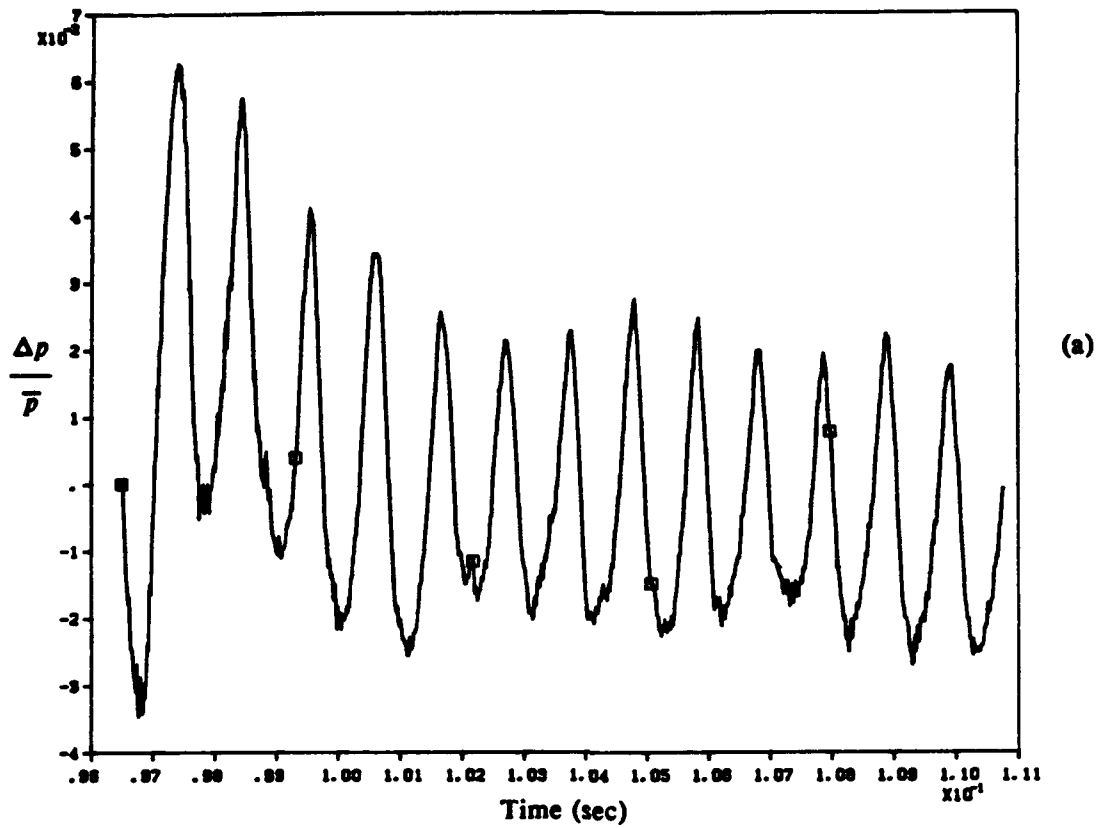
FIGURE 10 The effect of active control on the Type II instability; (a) control OFF, reference signal, (b) correlation between pressure signals at the speaker and microphone locations (control OFF), (c) control ON with $r/T = 0.5$, (d) control OFF, after control ON in Figure 10c, (e) control ON with $r/T = 0.03$, (f) control ON with $r/T = 0.5$.

FIGURE 11 Typical flame and vortex structure during active control of Type II instability; (a) flame, control ON with $r/T = 0.5$, (b) flame, control OFF, (c) vorticity, control ON.

FIGURE 12 Rayleigh criteria in the combustor during control of a Type II instability; (a) temporal variation of $R(t)$, (b) spatial variation of $R(x)$.

FIGURE 13 Acoustic power of the loudspeaker during active control of Type II instability; (a) control ON with $r/T = 0.5$, (b) control ON with $r/T = 0.03$.

Gain — Time Delay — Microphone

Loudspeaker

s_2 s_1 | a
$H = 0.03175\ m$
c
b

Inlet

$\dfrac{d}{2} = 0.03175\ m$

Combustor

Choked Nozzle

r

x

$L_i = 0.1344\ m$

$L = 0.36\ m$

(a)

Inlet Nozzle

(b)

FIGURE 1 The axisymmetric ramjet configuration; (a) the ramjet geometry without the inlet nozzle and the active control system, (b) the full ramjet geometry with a 320 x 64 grid distribution.

r ↑ Separated Boundary Layer

Inlet Throat (Choked)

	sec^{-1}			sec^{-1}	
Blue	$\Omega \leq -2000$		Yellow	$5000 \leq \Omega \leq 10,000$	
Cyan	$-2000 \leq \Omega \leq 1000$		Red	$10,000 \leq \Omega \leq 20,000$	
Green	$1000 \leq \Omega \leq 5000$		Magenta	$\Omega \geq 20,000$	

(a)

0.0   0.05   0.10   0.15   0.20   0.25   0.30   0.35   0.40   0.45   0.50   0.55

Inlet Shock   x (meters)   Nozzle (Choked)

Blue	$0.0 \leq M \leq 0.3$		Yellow	$1.2 < M \leq 1.5$
Cyan	$0.3 < M \leq 0.9$		Red	$1.5 < M \leq 1.8$
Green	$0.9 < M \leq 1.2$		Magenta	$M > 1.8$

(b)

FIGURE 2   Typical cold flow field in a full ramjet engine; (a) time sequence of vorticity contours, (b) mach contours.

FIGURE 3 Typical flow features observed during Type I instability; (a) pressure fluctuation at the base of the step, (b) flame structure, (c) vorticity field, (d) experimental. (Smith and Zukoski, 1985)

FIGURE 4 Rayleigh criteria in the combustor for a Type I instability; (a) temporal variation of R(t), (b) spatial variation of R(x).

FIGURE 5 Typical flow features observed during Type I instability; (a) pressure fluctuation at the base of the step, (b) flame structure, (c) vorticity field, (d) experimental. (Smith and Zukoski, 1985)
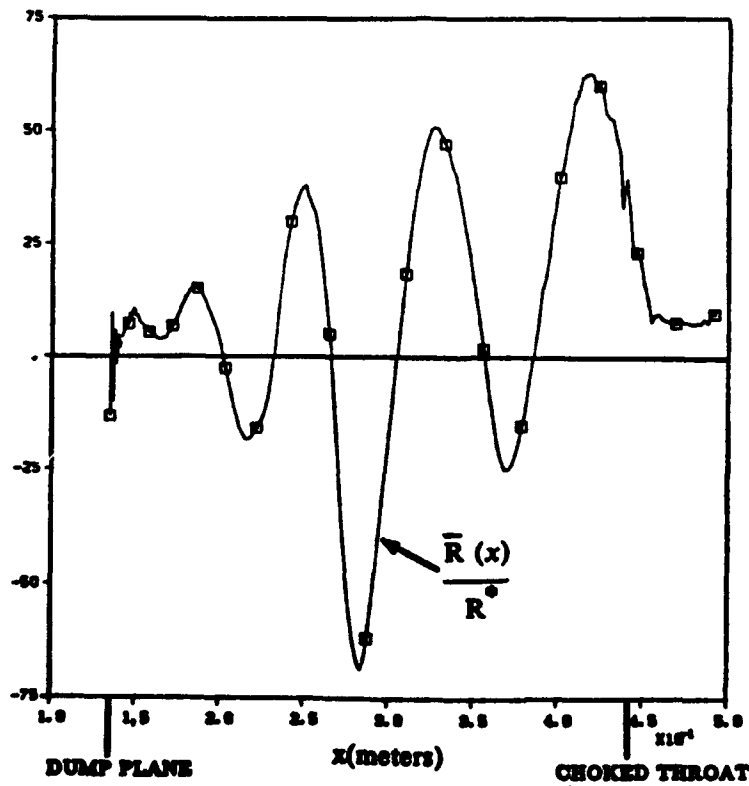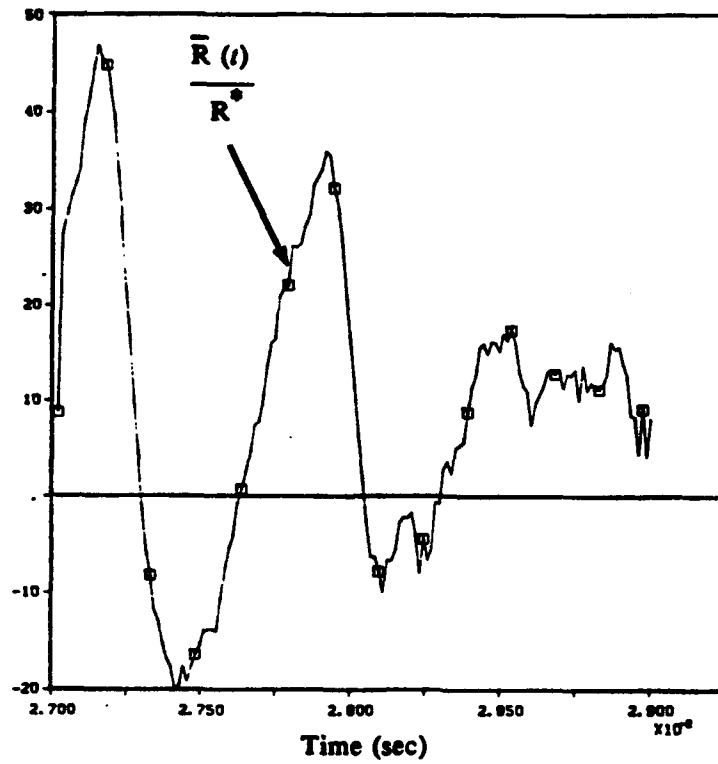
FIGURE 6 Rayleigh criteria in the combustor for Type II instability; (a) temporal variation of R(t), (b) spatial variation of R(x).

FIGURE 7 The effect of active control on the Type I instability, sensor at location b; (a) control OFF; reference signal, (b) correlation between the pressure signals at the speaker and microphone locations (control OFF), (c) control ON with $\tau/T = 0.03$, (d) control ON/OFF with $\tau/T = 0.15$, (e) control ON with $\tau/T = 0.5$.

FIGURE 7 The effect of active control on the Type I instability, sensor at location b (Cont.); (c) control ON with r/T = 0.03, (d) control ON/OFF with r/T = 0.15.

FIGURE 7 The effect of active control on the Type I instability, sensor at location b (Cont.); (e) control ON with $r/T = 0.5$.

FIGURE 8 Correlation between the pressure signals at the speaker and microphone locations during active control; (a) $\tau/T = 0.03$, (b) $\tau/T = 0.15$.

FIGURE 9 The effect of active control on the Type 1 instability, sensor at location c; (a) control ON with $r/T = 0.30$, (b) control ON with $r/T = 0.15$.

(a)

$\dfrac{\Delta p}{\bar{p}}$

Time (sec)

(b)

$\dfrac{\Delta p}{\bar{p}}$

Time Delay (msec)
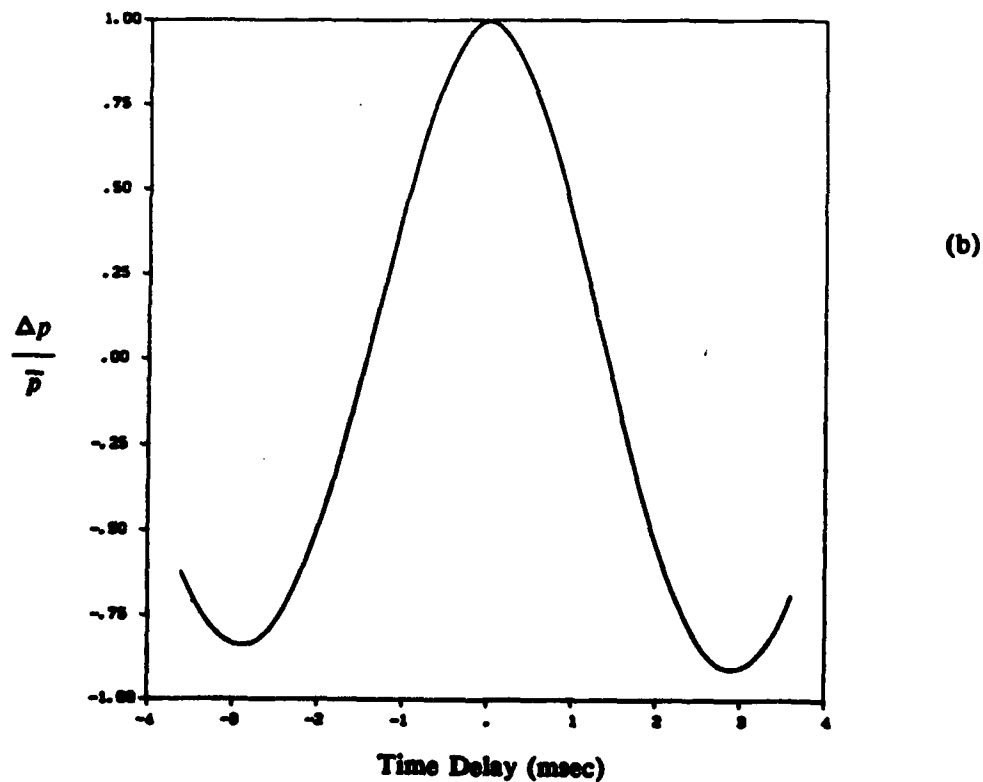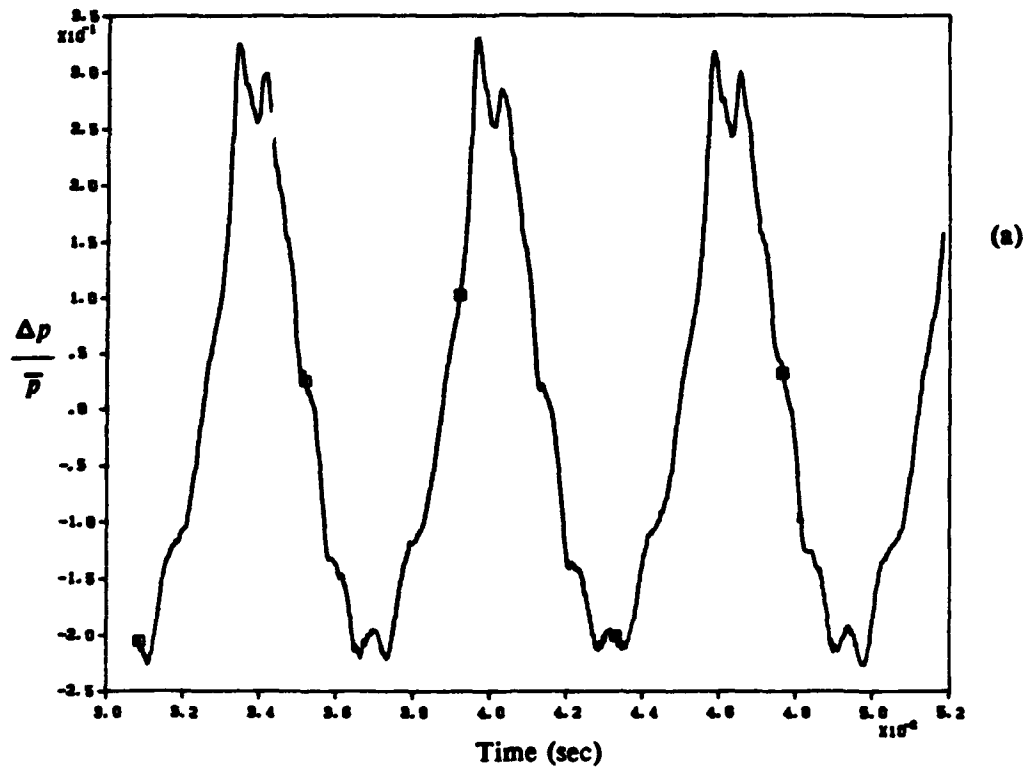
FIGURE 10 The effect of active control on the Type II instability; (a) control OFF, reference signal, (b) correlation between pressure signals at the speaker and microphone locations (control OFF), (c) control ON with $\tau/T = 0.5$, (d) control OFF, after control ON in Figure 10c, (e) control ON with $\tau/T = 0.03$, (f) control ON with $\tau/T = 0.5$.

FIGURE 10 The effect of active control on the Type II instability (Cont.); (c) control ON with $\tau/T = 0.5$, (d) control OFF, after control ON in Figure 10c.
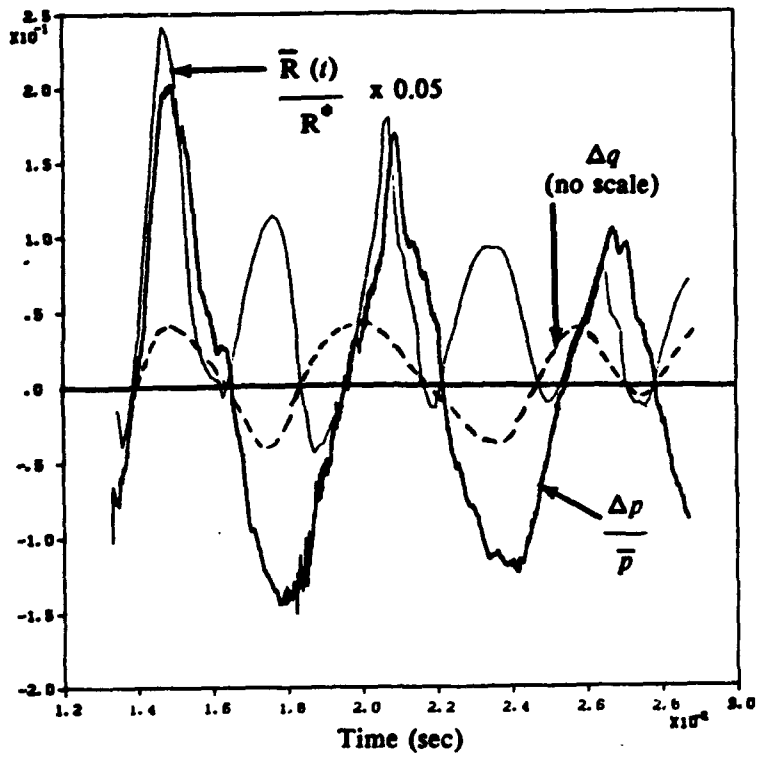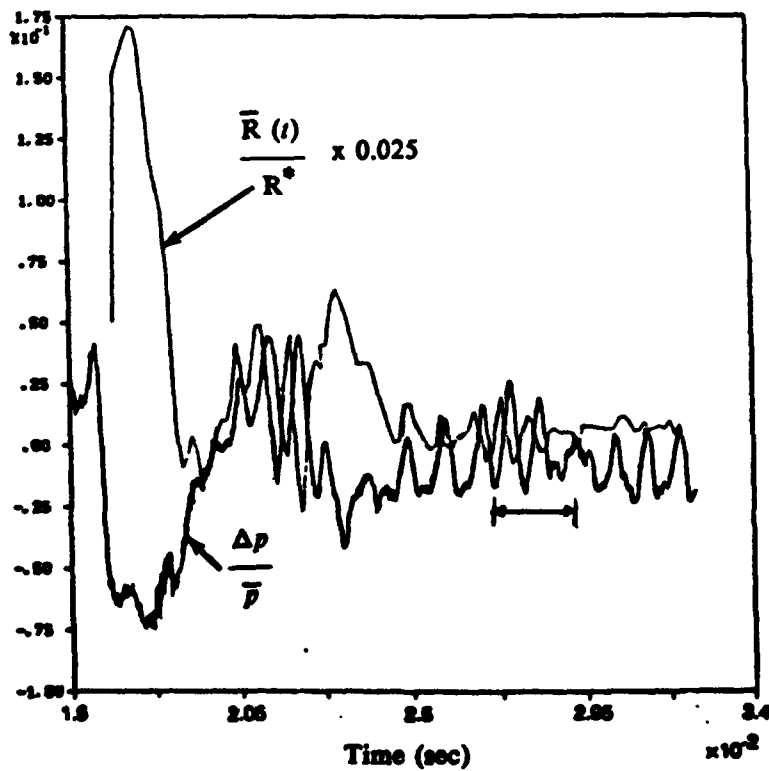
FIGURE 10 The effect of active control on the Type II instability (Cont.); (e) control ON with r/T = 0.03, (f) control ON with r/T = 0.5.
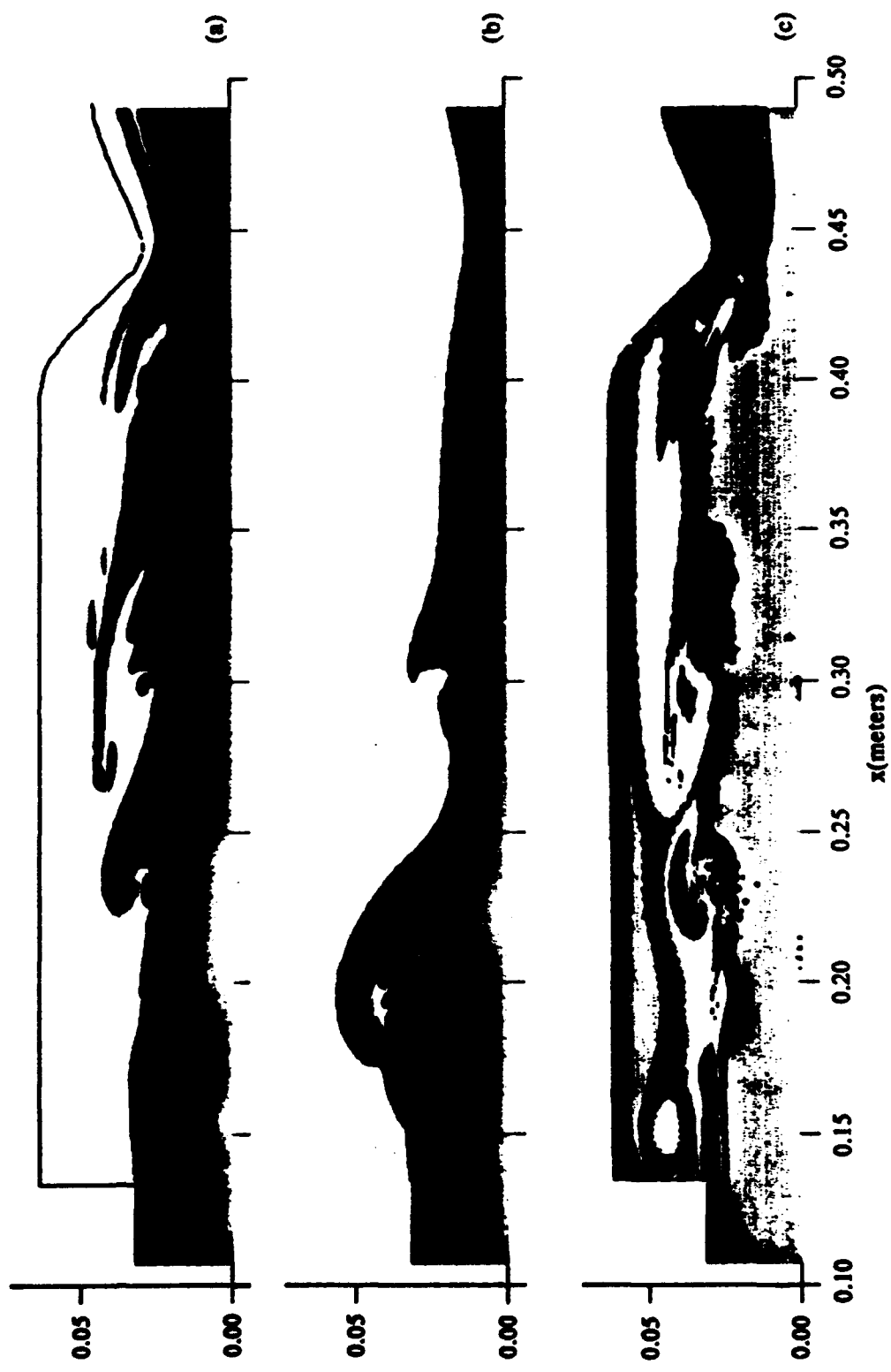
FIGURE 11 Typical flame and vortex structure during active control of Type II instability:
(a) flame, control ON with $r/T = 0.5$, (b) flame, control OFF, (c) vorticity, control ON.

FIGURE 12 Rayleigh criteria in the combustor during control of a Type II instability; (a) temporal variation of R(t), (b) spatial variation of R(x).
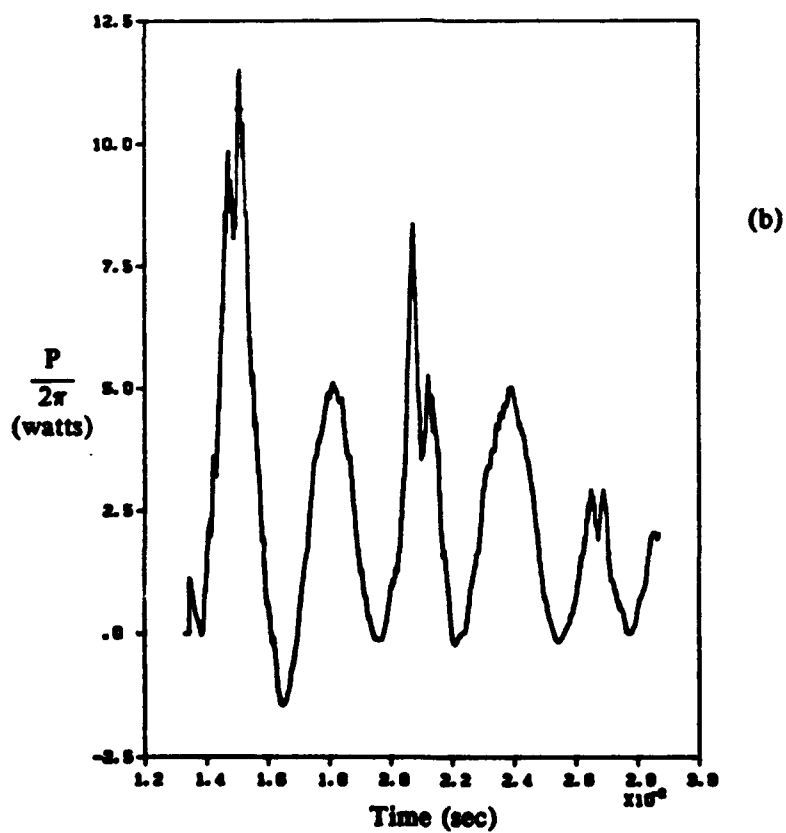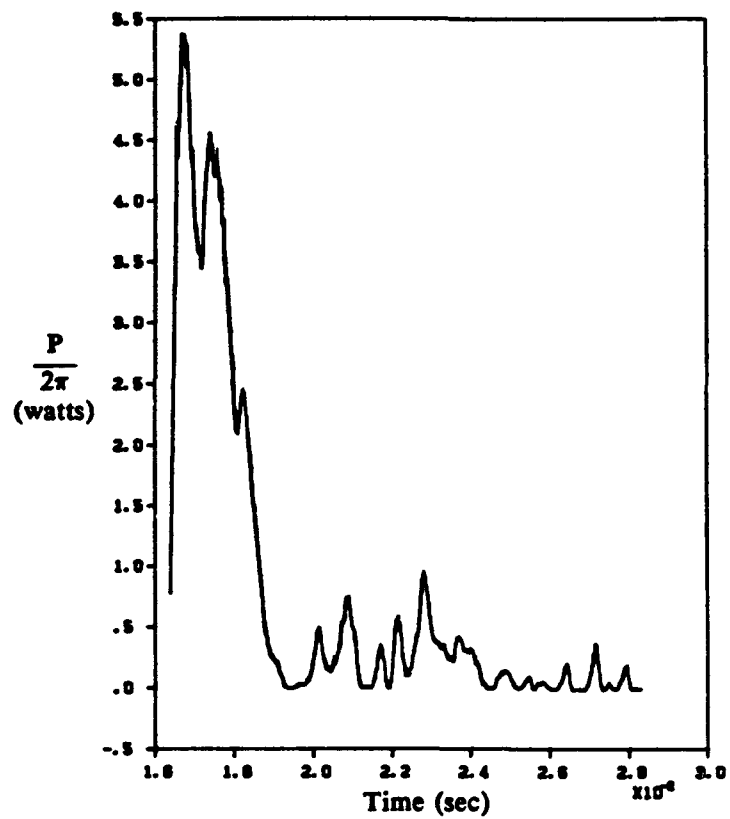
FIGURE 13 Acoustic power of the loudspeaker during active control of Type II instability; (a) control ON with $r/T = 0.5$, (b) control ON with $r/T = 0.03$.

AIAA 92-0777
A Numerical Study of Secondary Fuel Injection Techniques for Active Control of Combustion Instability in a Ramjet

S. Menon
QUEST Integrated, Inc.
Kent, WA

30th Aerospace Sciences Meeting & Exhibit
January 6-9, 1992 / Reno, NV

A NUMERICAL STUDY OF SECONDARY FUEL INJECTION TECHNIQUES FOR ACTIVE CONTROL OF COMBUSTION INSTABILITY IN A RAMJET

Suresh Menon[*]
Quest Integrated, Inc.
(formerly Flow Research, Inc.)
Kent, Washington

ABSTRACT

Combustion instability in a ramjet combustor has been numerically simulated using a large-eddy simulation (LES) technique. Premixed combustion in the combustor is simulated using a thin-flame model that explicitly determines the turbulent flame speed as a function of the laminar flame speed and subgrid turbulent kinetic energy. Two different inlet duct length, a short inlet and a long inlet configurations were modeled. Low frequency, large amplitude pressure oscillations characteristic of combustion instability is simulated in both the configurations. Active control using secondary fuel injection upstream of the flame holder employing different types of control algorithms have been investigated. Results show that control of the instability can be successfully achieved in some cases, while in other cases, the control algorithm is only partially effective.

1. INTRODUCTION

Combustion instability in a ramjet engine is an extremely complex phenomenon involving nonlinear interactions among acoustic waves, vortex motion and unsteady heat release. Typically, the instability manifests itself as a large-amplitude pressure oscillation in the low-frequency range (100-800 Hz) and is very difficult to control. When the amplitude of the pressure oscillation reaches some critical limit, it can cause structural damage due to fatigue or can cause an engine "unstart," which occurs when the shock in the inlet duct is expelled to form a bow shock ahead of the inlet. This phenomenon of engine unstart is one of the most serious technical problems encountered in developing an operational ramjet engine.

In recent years, both experimental (e.g., Schadow et al., 1989; Smith and Zukoski, 1985; Hedge et al., 1987) and numerical (e.g., Menon and Jou, 1990, 1991; Jou and Menon, 1990) investigations have been conducted to determine the mechanism of the combustion instability. Attempts to control combustion instability using both passive and active control techniques have also been carried out in the past (Culick, 1989). Passive control methods that typically involve structural (i.e., geometrical) modifications have proven insufficient for controlling the low-frequency instability. Recent experimental studies (e.g., Langhorne and Hooper, 1989; Schadow et al., 1990; Gutmark et al., 1990) suggest that active control techniques may be more effective in controlling the combustion instability in a ramjet. In parallel to the experimental studies, a numerical study of active control methods is also being carried out. Earlier, the result of numerical studies of active control using acoustic feedback techniques was reported (Menon, 1990, 1991) and it was shown that

combustion instability can be successfully controlled using such techniques provided certain feedback criteria are satisfied. Although, the results are in good agreement with experimental observations, it is well known that in realistic ramjet combustors, acoustic feedback control using loudspeakers as the controller may not be practical due to the prevailant hostile (hot) environment in the combustor. This paper describes a numerical study of another type of active control technique which uses secondary injection of the premixed fuel as the controller. Such a technique has been shown experimentally to be a more practical and effective control system (e.g., Langhorne and Hooper, 1989)

2. THE SIMULATION MODEL

The simulation model used in this study was developed through a series of numerical experiments starting with cold flow studies (Menon and Jou, 1987, 1990; Jou and Menon, 1987, 1990) and culminating in the simulation of combustion instability (Menon and Jou, 1991). The equations are the full compressible Navier-Stokes equations formulated in the axisymmetric coordinate system. The original numerical technique is an unsplit second-order-accurate, finite-volume scheme based on MacCormack's method; it has been described elsewhere (Menon and Jou, 1987, 1990). In the present study, a fourth-order-accurate spatial differencing scheme (Baylis et al., 1985) has been used for most of the simulations. The modeled ramjet combustor consists of an axisymmetric inlet duct connected to an axisymmetric dump combustor by a sudden expansion. A convergent-divergent nozzle is attached downstream of the combustor. Figure 1 shows the typical ramjet configuration used in these studies. Two different inlet duct lengths were used in the present study: a short inlet with $L_i/H = 6.3$ and a long inlet with $L_i/H = 22.4$, where H is the step height. The long inlet duct configuration is similar to an experimental test rig currently being used for active control studies at the Naval Weapons Center, China Lake (e.g., Schadow, et al, 1990). Experiments have suggested that with a long inlet duct, the inlet duct acoustics plays a major role in the determining the dominant frequency of the combustion instability. As shown below, such an observation can also be made from the results of the long inlet simulations.

For the spatially developing flow problem studied here, the implementation of proper inflow/outflow conditions is very important to ensure that no spurious (numerical) acoustic waves are generated. In the current model, a convergent-divergent nozzle is attached downstream of the combustor. This is similar to a real operating ramjet configuration. The flow through this nozzle is choked, and the outflow at the downstream computational boundary is supersonic. Since at

a supersonic outflow all characteristic waves (i.e., the acoustic waves, the entropy wave and the vorticity wave) are outgoing, the imposed boundary conditions will not affect the interior flow field.

In the present study, the inlet nozzle typical of a ramjet engine is not included as a part of the computational domain. Thus, a subsonic inflow conditions similar to those in some experiments (Schadow et al., 1990) are used at the inlet. Three boundary conditions: the stagnation pressure, the stagnation temperature and the flow inclination are specified corresponding to the three incoming characteristics (i.e., the vorticity wave, the entropy wave and the right-running acoustic wave). The characteristic variable carried by the left-running acoustic wave is determined by solving the pertinent characteristic equation. The application of these boundary conditions implies a certain "impedance" condition. Earlier, the behavior of this impedance condition was examined by using a linearized analysis, and the condition was proven to be of the damping type. Thus, pressure disturbances reaching the inflow boundary will not get amplified.

The upstream boundary conditions for the flow in the combustor can be specified correctly if the inlet nozzle is included in the computational domain. In such a case, the inflow is also supersonic and the flow chokes at the inlet throat and then subsequently becomes subsonic due to the inlet shock that resides under stable conditions in the divergent part of the inlet nozzle. The upstream condition for the flow in the combustor is then specified by the condition just downstream of the inlet shock. Simulations including the inlet nozzle in the computational domain was carried out earlier (Menon, 1991a) and it was shown that the shock undergoes longitudinal oscillations in response to the upstream propagating acoustic waves from the combustor and results in the unsteady separation of the inlet duct wall boundary layer. This separated shear layer rolls up into coherent vortices within the inlet duct itself and this vortex train interacts with the vorticies being shed at the dump plane. Many of the observed features of the flow field were in good qualitative agreement with the experimental observations (e.g., Bogar and Sajben, 1979).

Although, combustion instability has been simulated in the full ramjet engine, active control studies have not yet been carried out in such configurations, since, it is first neccessary to ensure that the simulated control techniques work in configurations that are being studied experimentally. Therefore, all active control studies discussed in this paper are being carried out using the configuration shown in Figure 1.

2.1 The Combustion Model

In premixed combustion, the amount of heat release per unit area of flame is determined by the local flame speed and by the specific chemical energy available in the fuel. If a finite-rate chemical mechanism for premixed combustion is employed in an LES, the numerical simulation must implicitly compute the local flame speed. Unfortunately, this is difficult to achieve in practice. The flame speed depends upon the dissipation mechanism and therefore, the internal structure of the flame sheet. Because the number of grid points are limited in LES, the flame sheet cannot be resolved adequately. Also, all numerical schemes involve some form of artificial dissipation, either explicitly added to stabilize the computations or implicitly present due to the differencing algorithm. As a result, the computed flame structure will be numerically diffused and the temporal-spatial distribution of the heat release could be overwhelmed by numerical diffusion.

The problems associated with employing a classical finite-rate model can be circumvented by using a thin flame

model. In this approach, the flame thickness is considered small compared to the smallest turbulent length scale (i.e., the Kolmogorov scale), and if the changes in the reaction-diffusion structure due to turbulent straining are also small, then the reaction zone can be considered to be asymptotically thin. Within the thin flame approximation, a model equation for premixed combustion is considered in which the local flame speed explicitly appears. If the local flame speed u_F is known, a progress variable G can be defined that is governed by the equation (Kerstein et al., 1988; Menon and Jou, 1991):

$$\frac{\partial \rho G}{\partial t} + \frac{\partial}{\partial s_i} \rho u_i G = - \rho u_F |\nabla G| \qquad (1)$$

where ρ is the density and u_i is the fluid velocity. Equation (1) describes the convection of the flame by the local fluid velocity and the flame propagation into the unburnt mixture through a Huygens type mechanism, $u_F |\nabla G|$. Here, by definition, $G = 1$ corresponds to the premixed fuel state, $G = 0$ corresponds to the fully burnt state and the flame is located at a prescribed $G = G_o$ level surface, where, $0 < G_o < 1$. For laminar premixed combustion, the local flame speed u_F is the laminar flame speed S_L which contains the information on the chemical kinetics and the molecular dissipation. When Equation (1) is applied to turbulent flows, the local flame speed u_F is taken to be the local turbulent flame speed u_T, where u_T is a prescribed function of local turbulence intensity u' and the laminar flame speed S_L (here treated as a constant chemical property, though in reality it is sensitive to the strain field affecting the flame). The implementation of the thin flame model as a part of the LES transport equations therefore explicitly requires the specification of the subgrid turbulent kinetic energy to determine the turbulent flame speed. This is accomplished in the present study by explicitly computing the subgrid turbulent kinetic energy as described in Section 2.2.

The next issue that must be addressed is the determination of the functional relation: $u_T = u_T(S_L, u')$. It appears that a general functional relationship between the turbulent flame speed, the laminar flame speed and the turbulence intensity which is valid for all types of fuel and flow conditions is difficult to develop (Kerstein and Ashurst, 1992). Yakhot (1988) used renormalization theory to develop a relation of the form $u_T/S_L = \exp(u'^2/u_T^2)$ which was shown to reduce to the linear scaling, $u_T/S_L \approx (1 + u'/S_L)$ in the high u'/S_L limit, and to the Clavin-Williams relation $u_T/S_L \approx (1 + (u'/S_L)^p)$, where $p = 2$ in the low u'/S_L limit. He also showed that, at least for high u'/S_L cases, this expression shows good agreement with experimental data. However, recently, Kerstein and Ashurst (1992) showed that for low u'/S_L, the Clavin-Williams expression maybe incorrect and proposed a scaling with $p = 4/3$. In the present study, both Yakhot's expression and the more simplified approximations (linear scaling, i.e., $p = 1$ for $u'/S_L > 1$ and the modified Clavin-Williams relation, i.e., $p = 4/3$ for $u'/S_L < 1$) were investigated. Yakhot's relation is a nonlinear equation that requires iteration at every grid point and at every time step to determine the turbulent flame speed. This is computationally very expensive and therefore, to reduce computational effort, an approach is being implemented in which a look-up table of $u_T = u_T(S_L, u')$ is first generated and then the turbulent flame speed is determined by using interpolation routines. However, since this approach is still under development, in this study, the more simpler relations described above have been used to determine the turbulent flame speed.

In addition to the specification of the turbulent flame speed, the effect of heat release must be included to couple the effect of combustion with the large-scale transport. The

chemical energy of the mixture is included in the formulation by specifying the specific enthalpy h of the mixture in the energy equation as $h = C_p T + h_f H(G - G_o)$. Here, h_f is the heat of formation of the premixed fuel, C_p is the specific heat of the mixture at constant pressure, and T is the temperature. Also, $H(s)$ is an Heavyside function that is used to determine the location of the flame. Here, the Heavyside function is defined such that $H(s) = 1$ when $s = 0$ and zero elsewhere. The heat of formation of the fuel determines the amount of heat released during combustion and thus is a function of the equivalence ratio for a given fuel. The product temperature T_p can be estimated for a given heat of formation by the relation $h_f = C_p(T_p - T_{fu})$, where T_{fu} is the fuel temperature at the inlet. In the simulations, the combustion product temperature is initially specified, and the heat of formation is determined from the above noted expression for h_f.

If the Heavyside function, $H(G - G_o)$ is used in the static enthalpy expression to identify a level surface $G = G_o$ as the flame location, it results in an infinitely thin flame wherever the $G = G_o$ level surface exists, with the fuel temperature T_{fu} on the $G > G_o$ side and the product temperature T_p on the $G < G_o$ side. This sharp discontinuity in temperature is impossible to resolve numerically when the G-equation is solved as a part of the LES transport equations. Consequently, numerical instability can (and does) occur. To avoid this unavoidable complication, the current approach resolves the flame as a numerically diffused flame in the $0 < G < 1$ region. However, due to the explicit appearance of the local flame speed in Equation (1), the amount of heat release does not depend on the computed internal structure of the flame. Even when numerical diffusion broadens the flame, the flame speed is not severely affected. The effect of numerical broadening was discussed earlier (Menon and Jou, 1991) and it was shown that numerical diffusion does not significantly affect the dynamics of the flame propagation.

The proper implementation of the thin flame by identifying a specified level surface as the flame surface can be accomplished by a new approach that has been recently developed in which the G-equation is solved within the subgrid domain rather than in the resolved scale domain. In this approach, the subgrid domain is further discretized into small cells to resolve the micro-scales that effect the flame propagation and the turbulent mixing processes. This approach has an added advantage, in addition to the correct implementation of the thin flame model, since, within the small scale (i.e., subgrid), the flame propagates at its laminar speed (which is well defined for a given fuel) rather than at the modeled turbulent flame speed. Any arbitrariness in choosing a turbulent flame speed model can be avoided, and in fact, the subgrid processes provides a mechanism to determine the turbulent speed based on the flame propagation and turbulent mixing processes occurring at the small (subgrid) scales. Preliminary evaluation of this approach (Menon, 1991b, Menon et al., 1992) has clearly shown the potential of this new "subgrid" flame model. At present, this approach is being implemented to study combustion instability in ramjets and the results will be described in the future.

2.3 The Subgrid Model

In a practical ramjet device, the Reynolds number of the flow is extremely high. A LES of such a flow requires a validated subgrid model. Subgrid models for compressible flows have just begun to be investigated (e.g., Speziale et al., 1987, Zeeman and Squires 1990). At present, it is not clear what is an appropriate subgrid model for flows such as those in a ramjet combustor. The earlier simulations (Menon and Jou, 1991) with the short inlet duct length were carried out using a constant eddy viscosity model and a constant turbulent

flame speed for flows in a moderate Reynolds number range. Some important physical properties, such as the spatial nonuniformity of subgrid turbulence and its effect on the local flame speed and the amount of heat release, were not included in this approach. However, as shown earlier (Menon and Jou, 1991), the major qualitative interactions between the large-scale vortex structures and the combustion heat release could be captured by the constant flame speed model. In the present study, the effect of nonuniform subgrid turbulence on the turbulent flame speed and on combustion instability has been included by using a subgrid model for turbulent kinetic energy and then determining the turbulent flame speed based on the scaling relationships described in Section 2.1. The subgrid model used for this study is described in this section.

Recently, Zeeman (1990) has proposed a model for the subgrid eddy viscosity which requires the determination of the subgrid turbulent kinetic energy. He employed concepts from the traditional Reynolds-averaged second-order closure approach to derive this model and showed that this eddy viscosity model reduces to the Smagorinsky's model in the incompressible limit. Although this model has been tested only for simple problems, such as decaying, compressible homogeneous turbulence (Zeeman and Squires, 1990), the relevant feature of this model is that the subgrid kinetic energy is computed in terms of the resolved fields to determine the subgrid eddy viscosity. Since, the subgrid kinetic energy distribution is essential for the specification of the turbulent flame speed, this model has been implemented to determine its applicability for LES of reacting flow fields.

The formulation begins by considering a one-equation model for the subgrid turbulent kinetic energy, and then neglecting the convective term Dk/Dt by using inertial range scaling to show that the convective term is much smaller than the source terms of this k-transport equation. (This approximation is probably inappropriate for the current problem and will be relaxed in the future. This would result in a one-equation subgrid model for the subgrid kinetic energy.) Without going into the details of this formulation (see Zeeman, 1990; Zeeman and Squires, 1990) a final expression for the subgrid kinetic energy is obtained as:

$$k = 2C\Delta^2 |\bar{s}_{ij}|^2 + C\Delta^2 \frac{\nabla \bar{p} \cdot \nabla \widetilde{T}}{\bar{\rho} \widetilde{T} Pr_t} - \frac{\sqrt{2C}}{3} \Delta^2 |\bar{s}_{ij}| \frac{\delta \widetilde{u}_i}{\delta x_i} \quad (2)$$

Here, Δ is the characteristic filter size, $\widetilde{u}_i$, $\bar{\rho}$, $\bar{p}$ and $\widetilde{T}$ are, respectively, the Favre-filtered (Erlebacher et al., 1988) large-scale (resolved) velocity, density, pressure and temperature, and $k = \frac{1}{2}(\widetilde{u_i^2})$ is the subgrid turbulent kinetic energy. Also, $\bar{s}_{ij} = \frac{1}{2}(\frac{\delta \widetilde{u}_i}{\delta x_j} + \frac{\delta \widetilde{u}_j}{\delta x_i})$ is the strain tensor in terms of the resolved velocity field. The constants C and Pr_t are chosen for the present study to be 0.06 and 0.8, respectively.

The subgrid eddy viscosity ν_t is related to the subgrid kinetic energy by the expression:

$$\nu_t = C k^{\frac{1}{2}} \Delta \quad (3)$$

Once k is known, the subgrid turbulence intensity u' ($u' = \sqrt{2k}$) and the turbulent flame speed u_T can be determined. This model is also used to determine the turbulent subgrid fluxes appearing in the momentum equations. Thus, the subgrid stresses in the momentum transport, $\tau_{ij}' = \bar{\rho}(\widetilde{u_i u_j} - \widetilde{u}_i \widetilde{u}_j) \approx \bar{\rho} \widetilde{u_i' u_j'}$ is given as

$$\tau_{ij}' - \frac{1}{3} \tau_{kk}' \delta_{ij} = -2\nu_t \bar{s}_{ij} \quad (4)$$

Closure of the subgrid terms appearing in the energy transport is also accomplished using the eddy viscosity model.

The typical term that needs to be modeled is: $q_i' = \bar{\rho}c_v(\widetilde{Tu_i} - \widetilde{T}\widetilde{u_i}) \approx \bar{\rho}c_v\widetilde{T'u_i'}$. This term is modeled as

$$\bar{\rho}c_v\widetilde{T'u_i'} = -\sigma_{ij}\frac{\partial\widetilde{T}}{\partial x_i} \qquad (5)$$

where, σ_{ij} is determined from the relation:

$$\sigma_{ij} = \frac{\nu_t}{Pr_t}\delta_{ij} - \frac{\nu_t}{3}\frac{\Delta}{\sqrt{k}}\bar{S}_{ij} \qquad (6)$$

Some modifications are required to implement this model in axisymmetric flows and in flows with complex geometries. The primary issue is to include the effect of walls. It is well known that walls can inhibit the growth of turbulent structures and also reduce the length scale. Although a stretched grid is used near the wall (which will reduce the length scale) an additional correction has been used to ensure that the subgrid stress variation is modeled correctly near the wall. Here, the wall damping model of Piomelli et al. (1988) is used to redefine the filter width as $\Delta = \Delta_g[1 - \exp(-y^{+3}/A^{+3})]$ where Δ_g is the characteristic grid size, $y^+ = yu_\tau/\nu$ is the distance from the wall in wall units and $A^+ = 25$. With this definition, the subgrid stress τ_{yy}' varies as y^{+3} near the wall. Care also needs to be taken when evaluating Equation (6) near the wall, since, as $y \to y_{wall}$, $\Delta \to 0$ and so does the subgrid kinetic energy $k \to 0$.

A major issue for LES of complex flows is whether the primary assumption that the subgrid scales are primarily dissipative (and contain negligible kinetic energy) is valid. Past direct numerical simulations of relatively simpler flows (e.g., Piomelli et al., 1990) have demonstrated that the unresolved scales can contain significant kinetic energy and thus the phenomena of backscatter (transfer of energy from the small scales to the large scales) will have to be taken into account. Thus, in general, equation (4) will not correctly reflect the process of energy transfer at the filter cutoff. To determine a more general subgrid model for the eddy viscosity that takes into account the energy transfer to and from the subgrid scales, we are currently studying a modified subgrid model that has an additional term for the backscatter component. A stochastic backscatter model was recently developed by Chasnov (1991) for application as a subgrid model. However, this model was developed in the spectral space and, as such, is not practical for application to complex flows and to complex geometries. Here, we consider an approach in the physical space that contains the elements of the model developed by Chasnov in the spectral space. A backscatter model was also recently shown by Leith (1990). By carrying out a simple phenomenological analysis, a similar model has been developed that uses the results of the study by Chasnov. The basic properties that are used to derive the backscatter model are: (1) forward scatter and backscatter are modeled by two distinctly different mechanisms, (2) forward scatter is modeled by an eddy damping term as in the spectral formulation (results in an expression similar to equation 4), (3) backscatter is modeled by a random force (as in the spectral formulation) which satisfies certain constraints (it is uncorrelated in time with a zero mean, and, to ensure that it adds a finite amount of energy to the turbulence, the force is proportional to $\Delta t^{-1/2}$). These properties are discussed in more detail by Chasnov (1991).

Thus, the total subgrid eddy viscosity is a sum of two terms: an eddy damping term ν_e and a random "diffusion" term such that:

$$\nu_T(\vec{x}, t) = \nu_e(\vec{x}, t) - F_r(\vec{x}, t) \qquad (7)$$

where ν_T is the total subgrid eddy viscosity and $F_r(\vec{x}, t)$ is the random diffusion term. The model of the anisotropic part of the subgrid Reynolds-stress term is then written as

$$\tau_{ij}' - \frac{1}{3}\tau_{kk}'\delta_{ij} = -2\nu_T\bar{S}_{ij} = -2\nu_e\bar{S}_{ij} + F_r\bar{S}_{ij} \qquad (8)$$

The eddy damping term ν_e is chosen to be the same as the original forward scatter eddy viscosity, ν_1, given by equation (3). We define the backscatter contribution to the subgrid stress equation (8) using the points noted above and by using simple dimensional analysis. Without going into details (Menon, 1991b) the random diffusion term is given as:

$$F_r\bar{S}_{ij} = C_{BS}\,\text{rand}\,\frac{\Delta^2}{\sqrt{\Delta t}}|\bar{s}|\,\bar{S}_{ij}^{1/2} \qquad (9)$$

where $|\bar{s}| = |\bar{S}_{ij}\bar{S}_{ij}|^{1/2}$, rand is a random number with zero mean and unit variance and C_{BS} is a constant of $O(1)$ taken here to be 0.1. On using equations (3) and (9) in equation (8), the final expression for the two-term subgrid model is

$$\tau_{ij}' - \frac{1}{3}\tau_{kk}'\delta_{ij} = -2\nu_t\bar{S}_{ij} + C_{BS}\,\text{rand}\,\frac{\Delta^2}{\sqrt{\Delta t}}|\bar{s}|\,\bar{S}_{ij}^{1/2} \quad (10)$$

This model is now being evaluated for application to the combustion instability. Some preliminary validation studies that have been carried out to determine the behavior of this subgrid model is discussed in the next section.

3. SIMULATION OF COMBUSTION INSTABILITY

Before describing the active control results, the features of the simulated combustion instability in the ramjet is described. As noted before, combustion instability has been simulated to two different types of configurations: a short inlet combustor and a long inlet combustor. The details of the simulation of combustion instability in the short inlet combustor are discussed elsewhere (Menon and Jou, 1991) and therefore, will only be briefly described here. Most of the simulations discussed in this section deals with the long inlet combustor.

In general, combustion instability in a combustor depends upon various parameters such as the system geometry, the flow parameters, the fuel type, and the equivalence ratio. In the earlier study (Menon and Jou, 1991), in addition to the flow parameters (e.g., the Mach number M and the Reynolds number Re) and the geometrical parameters (e.g., L_i, L, A_{inlet}/A^*; see Figure 1), two important thermochemical parameters were identified. One is $\theta = T_p/T_o$, which is the ratio of the product temperature to the stagnation temperature T_o; the other is $\sigma = u_p/u_{in}$, which is the ratio of the characteristic flame speed to the characteristic inlet velocity u_{in}. For a fixed fuel mixture, θ can be related to the equivalence ratio ϕ, and σ can be related to the chemical kinetic rate and the level of subgrid turbulence. The effects of varying the geometrical parameters, the ratio between the inlet and throat areas A_{inlet}/A^*, and the thermochemical parameters θ and σ have been studied (Menon and Jou, 1991). It was determined, that increasing σ with the other parameters held fixed excites the large-amplitude, low-frequency pressure oscillations typical of combustion instability in a ramjet.

The simulation of combustion instability in the short inlet configuration employed a constant eddy viscosity subgrid model and also assumed that the turbulent flame speed is a constant, around 5 percent of the mean inlet velocity. For this simulation, the reference Mach number was $M = 0.32$ and the reference Reynolds number was 10000, based on the inlet duct diameter and a reference velocity of $u_{in} = 100$ m/sec. For the long inlet combustor, the subgrid model described in Section 2.2 was used to determine the subgrid stresses and the turbulent flame speed in the combustor. Two simulations with Mach number 0.32 and 0.17 were carried out using the long inlet duct configuration for the same reference Reynolds number of 20000. The thermochemical

parameters θ and σ were held fixed at $\theta = 5$ and $\sigma = 0.05$ for the short inlet studies while for the long inlet cases, only $\theta = 5$ was held fixed (since now, u_f is no longer a constant). For $\theta = 5$, the product temperature T_p was 1500 K. All system (geometrical) parameters such as H and L, were held fixed for both simulations except for the inlet duct length which was increased from $L_i/H = 6.3$ for the short inlet case to $L_i/H = 22.4$ for the long inlet cases.

3.1 Combustion Instability in the Short Inlet Combustor

Combustion instability in the short inlet case was simulated earlier (Menon and Jou, 1991) and was shown to be characterized by a large-amplitude, low-frequency pressure oscillation with peak-to-peak levels around 50 percent of the mean pressure, as shown in Figure 2a. The oscillation rapidly reaches a limiting cycle and shows a type of pressure signature that is typical of what is observed during combustion instability. A large hooked-flame structure propagates through the combustor at a low frequency, and associated with this flame is a large mushroom-shaped vortical structure. The combined vortex/flame structure propagates through the combustor at the same low frequency. Spectral analysis showed that the dominant mode of oscillation is occurring at a frequency of around 166 Hz. The amplitude and phase of the pressure oscillation at various locations in the combustor was nearly the same, indicating that this pressure oscillation is similar to the bulk-mode oscillation observed in some experiments.

The typical flame structure and the vorticity field are shown in Figures 2b and 2c. For comparison, the experimental visualization of Smith and Zukoski (1985) is shown in Figure 2d. Further analysis was carried out by Menon and Jou (1991), and it was shown there that many characteristics of this type of combustion instability, such as the pressure and velocity fluctuation levels, the phase relation between the pressure and velocity fluctuations, and various features of the vortex/flame structure propagation, qualitatively agreed with the experimental observations.

3.2 Combustion Instability in the Long Inlet Combustor

For the long inlet combustor, the first issue addressed was the evaluation of the new subgrid model for application to complex reacting flows. Typically, validation studies of new subgrid models are carried out by comparing the results of LES (using the subgrid model) to the results obtained by direct numerical simulations. However, such an approach is impractical not only at present, but also in the foreseeable future, due to the intense computational effort (both time and memory) that will be required to carry out direct simulations of reacting flows in complex geometries. Even LES of combustion instability is very expensive. Therefore, in the approach chosen here, two identical simulations with the same subgrid model was carried out, but with two different grid resolutions. Changing the grid resolution results in a change in the filter width Δ. This should impact the dissipative process modeled by the subgrid model since the grid scale cutoff moves to lower wavenumbers with decrease in grid resolution. The contribution of the backscatter term to the subgrid model can also be evaluated by carrying out such simulations since a cutoff at the lower wavenumber will cause more energy-containing eddies to be filtered out. However, for the preliminary evaluations discussed here, the backscatter contribution has been neglected; the behavior of the backscatter component will be described in the future.

Two approaches to analyze the computed results can then be used. The first approach is to look at the characteristic spectra (e.g., frequency, etc.) of the relevant flow properties such as the pressure, vorticity and the velocity to determine if changing the filter width effects the frequency and phase

of the dominant oscillations. Note that, for the present combustion instability studies, the frequency content of the dominant oscillations is important for developing control strategies. Such an analysis of the computed simulations have been carried out and some of the pertinent results are discussed in this section.

The second approach is much more complicated. This method uses a masking technique (Domaradzki et al., 1990) which essentially involves filtering the high resolution simulation results with a mask that mimics the effect of the filter used for the coarse grid. Then the energy transfer near the cutoff computed using the masking technique can be compared to the actual energy transfer predicted by using the subgrid model in the coarse grid simulation. Such a technique has been successfully used by Domaradzki et al. (1990) and Chasnov (1991); however, all their studies were carried out in spectral space and for simple flows (low Reynolds number homogeneous turbulence without boundary effects) for which direct simulation and Fourier transform analysis was possible. The applicability of this approach to study LES data in physical space is not yet clear, but is under study.

To evaluate the subgrid model, two large-eddy simulations were carried out with grid resolution of 320 x 64 and 256 x 32, respectively, using identical geometrical configurations, flow parameters and the same subgrid model. For the first series of simulations, the subgrid model was implemented for the momentum and energy transport closure, but the coupling between the subgrid kinetic energy and the turbulent flame speed was not carried out. A constant turbulent flame speed model was used for these tests. Subsequently, the flame speed was coupled to the subgrid model.

Figures 3a and 3b show respectively, the pressure spectra at the base of the rearward facing step obtained using the fine mesh and the coarse mesh with a constant turbulent flame speed of 5 m/s. The spectral analysis was carried out by using both the maximum entropy method (Menon and Jou, 1987, 1990) and the standard FFT method with and without a prewhitening filter. Similar frequencies were observed in all these spectral analysis. In the spectral data shown here, only the frequency information is considered accurate; therefore, no amplitude information is shown. It can be seen that the fine and coarse mesh simulations show a dominant frequency of around 234 Hz and 244 Hz, respectively. The difference between the value of the frequency is less than 5 percent and thus, it appears that for the test conditions chosen here, the coarse grid is capable of reproducing the same dominant mode of oscillation seen in the fine mesh simulation. The amplitude of the pressure oscillation at this frequency was also measured and compared. Very similar levels were present in both these simulations. The axial variation of the pressure amplitude in the inlet (shown below) suggests that this frequency is the standing half-wave acoustic mode; a simple determination of the acoustic frequency by using the relation $f = a/2L_i$ with $L_i = 0.711$ m and using the speed of sound based on the temperature at the inlet gives the same frequency. Thus, it appears that the inlet duct acts as a long-wavelength acoustic resonator.

Figures 4a and 4b show respectively, the vorticity spectra in the separated shear layer just downstream of the step for these two simulations. The low frequency seen in the pressure spectra also dominates the vorticity spectra. Flow visualization of the flow field showed that a large vortex is shed at this frequency. The higher frequencies present in the vorticity spectra is related to the initial vortex shedding at the step which occurs when the pressure in the combustor is low and inlet flow velocity is accelerating. However, as the flow continues to accelerate, the vortices rollup into a large coherent vortex which then propagates downstream at the

5

low frequency. The details of the vortex formation and the phase relation between the pressure and the axial velocity fluctuations during this process has been discussed in more details in Menon and Jou (1991) for the short inlet case. The present results are in agreement with these earlier observations and also with experimental data (e.g., Smith and Zukoski, 1985; Yu et al., 1991); therefore, this discussion is not repeated here.

The above two simulations were carried out with a constant turbulent flame speed. To determine if inclusion of the variable turbulent flame speed model effects the dominant mode, another simulation was carried out with the turbulent flame speed computed as a function of the laminar flame speed S_L and the turbulence intensity u'. For this simulation, the coarse grid resolution was employed and a laminar flame speed of $S_L = 0.5$ m/s was used. This value of S_L was chosen rather arbitrarily; however, experimental data (Gulder, 1990) shows that this value of S_L is in within the range determined for many types of hydrocarbon fuels (e.g., methane-air).

Figure 5a shows the computed pressure spectra for this simulation. The dominant frequency is nearly the same as seen in the earlier simulations (Figure 3). This indicates that the pressure oscillation is being controlled by the inlet duct acoustics. Since this simulation data was then used to study active control techniques, further analysis of the data was carried out. Some of the pertinent results are discussed here. Figure 5b shows the pressure trace at the base of the step for this simulation. The low frequency oscillation with a peak-to-peak level of around 30 percent of the mean pressure is seen. This is somewhat lower than the level seen in the earlier short inlet case but is consistent with the levels observed in a similar experimental test configuration. Also interesting to note is that the pressure oscillation no longer maintains a constant amplitude in time when compared to the earlier short inlet case (Figure 2a).

The amplitude of the 244 Hz pressure oscillation in the inlet and in the combustor was computed and the axial variation of the amplitude normalized by the pressure amplitude at the base of the step is shown in Figure 6a. Note that the s-axis is shown relative to the location of the step. Although the amplitude values as computed by the FFT analysis is not considered very accurate (due to the finite amount of temporal data available), the axial variation suggests the presence of standing half-wave acoustic mode in the combustor. The amplitude is a maximum in the combustor and the level in nearly unchanged in the entire combustor. Figure 6b shows the spectra of the axial velocity at the centerline just upstream of the dump plane. The same low frequency seen in the pressure and vorticity spectra is present in the velocity fluctuations.

Some experiments have suggested that the instability mechanism may not be purely acoustic in nature and there may be a convective component to the instability which is related to vortex motion in the combustor (e.g., Yu et al., 1991). Numerical studies of cold flows (Menon and Jou, 1990; Jou and Menon, 1990) in ramjet combustors have also shown that a coupled acoustic-vortex mode can exist in ramjet combustors. The frequency determined based on this coupled mode oscillation is different from that of a pure acoustic resonant mode. To determine if a similar mechanism may be present in reacting flows, another simulation was carried out, similar to that shown in Figure 5, but with a reference inlet Mach number of 0.17. Figure 7a shows the pressure spectra at the base of the step for this simulation and Figure 7b shows the pressure trace at the same location. It can be seen that with the decrease in the Mach number (obtained by decreasing the inlet flow velocity), the dominant frequency

shifts down to around 87 Hz. A higher harmonic of this oscillation at 178 Hz is also seen in the pressure spectra. The peak-to-peak pressure fluctuation level remains relatively unchanged from that seen in the earlier simulation (Figure 5). Decrease in the instability frequency with the decrease in the inlet velocity has also been observed in experimental configurations (Dowling, 1990; Yu et al., 1991). This result suggests that the instability mode of oscillation may have a convective component. The acoustic oscillation at the 244 Hz seen in the earlier simulation is no longer dominant in the combustor; however, the pressure and the axial velocity spectra in the inlet do show the presence of this frequency. This can be seen in Figures 7c and 7d which show respectively, the pressure spectra in the middle of the inlet duct and the axial velocity spectra just upstream of the dump plane.

The phase relation between the pressure and velocity fluctuations can be determined from Figures 8a and 8b which show respectively, the Mach 0.32 and Mach 0.17 cases. For the higher Mach number case, the pressure at the base of the step and the centerline axial velocity at the dump plane are clearly out-of-phase. The velocity fluctuation peak-to-peak level is around 70 percent of the mean velocity and the oscillation frequency is the same as the frequency seen in the pressure field. However, for the lower Mach number case, the velocity fluctuation shows both the low frequency of 87 Hz and also the high frequency of 244 Hz. The peak-to-peak level of the low frequency is again around 70-80 percent of the mean velocity but the higher frequency shows a much lower fluctuation level. The pressure fluctuation on the other hand, shows only the low frequency mode.

Flow visualization of the flame and vortex structures are shown in Figures 9a through 9d. Two time snapshots are shown: Figures 9a and 9b shows respectively, the flame structure and vorticity field at an instant when there is a large vortex/flame structure present in the middle of the combustor. Figures 9c and 9d shows respectively, another instant when there is no large structure present and a vortex has just been shed from the step corner. Analysis of the subgrid kinetic energy field (not shown) indicates that significant amount of subgrid kinetic energy is associated with the large vortex. Since an increase in subgrid kinetic energy implies an increase in the turbulent flame speed (which is a measure of the turbulent reaction rate), this suggests that significant reaction processes occur around large vortices

The simulated data on the combustion instability in both the short and the long inlet duct configurations were then used to study active control techniques. This study is still underway; however, some interesting results have been obtained and are discussed in the next section.

4. ACTIVE CONTROL OF COMBUSTION INSTABILITY

Various active control techniques have been studied in the past. The acoustic feedback technique has been successfully used to control combustion instability, both experimentally and numerically. In the present effort, the focus is on a technique that involves manipulating the unsteady heat release in the combustor to control the low-frequency oscillations. An approach successfully demonstrated by Langhorne and Hooper (1989) employed secondary (premixed) fuel injection just upstream of the flame holder. In this technique, the control system uses additional heat release to modify the acoustic energy balance in the combustor. Langhorne and Hooper (1989) showed that both steady and pulsed secondary fuel injection can result in effective control of the instability. They also showed that an increase in the maximum available thrust is possible since the controller allows stable combustion at a higher fuel-air ratio than possible without active control.

6

In the following, we describe some results obtained using secondary fuel injection as a control system. Both steady and unsteady secondary fuel injection are being studied. The secondary premixed fuel is introduced typically one step height upstream of the step. Normal injection (in the negative r direction) is modeled in all the present simulations. Note that, when secondary fuel is introduced in the inlet, the primary and the secondary fuel streams are both (cold) premixed fuel and the net effect of secondary injection is a modification (increase) of the total mass flow into the combustor.

Although, the choice of location (i.e., upstream of the flameholder) is similar to the experimental approach, there are, however, some major differences. For example, in the experiments, to achieve control multiple secondary fuel injectors were employed around the circumference of the inlet duct. With such a configuration the interaction of the secondary stream with the primary stream is probably highly three-dimensional. With the current axisymmetric simulation model, the effect of three dimensionality cannot be addressed. After further evaluation of the subgrid model, full three-dimensional simulations are planned in the near future on the iPSC/i860 massively parallel processor. (The current axisymmetric code is already running on this machine and the 3D code is currently being ported over). With full three-dimensional simulations, more realistic control studies will become feasible.

Another difference between the experimental study of Langhorne and Hooper (1989) and the present effort is that, in the experiments, the primary stream was always steady (because a choked inlet was employed) and the only unsteadiness introduced was from the secondary fuel injection. In the present study, the inflow, as noted above, is subsonic and unsteady. This implies that the secondary fuel stream has to be injected with proper phase to the primary unsteady stream, and, this makes the control approach more complicated.

To develop a control strategy, we followed a technique similar to that used earlier for acoustic feedback control and also somewhat similar to the experimental approach. First, a cross-correlation analysis between the (earlier recorded) pressure fluctuation at the base of the step and the pressure signal at a chosen sensor location (at present, the sensor signal is the wall pressure near the downstream diffuser) is carried out to determine the time delay for peak negative correlation. For example, this time delay is around 2 msec for the 244 Hz pressure oscillation. Earlier acoustic feedback control studies (Menon, 1991a) have suggested that as long as the correlation coefficient is negative, the control strategy will be successful. This implied that a wide range of time delays can be used for active control and this result was in good agreement with experimental observations. In the present study, we are attempting to determine if a similar general criteria can be established for the secondary fuel control method.

A general controller is first defined such that:

$$\dot{m}_{sec} = G_0\, p_s'(t - \tau) \tag{11}$$

where, τ is a prescribed time-delay, $\dot{m}_{sec}$ is the secondary mass flow rate and p_s' is the unsteady pressure at the sensor location. G_0 is a transfer function that may or may not be a constant. Some preliminary estimate for G_0 can be obtained from linearized analysis that was recently carried out by Pung et al. (1991). They showed that G_0 can be related to the heat content of the fuel (h_f) and the mean inlet speed of sound.

Equation (11) cannot be used directly, since it would result in a negative secondary fuel rate whenever the pressure

fluctuation becomes negative. For the present controller this has no meaning and therefore, must be avoided. Various modified versions of this controller are being evaluated. The type of controller used will be defined when describing the results.

In addition to prescribing the secondary fuel flow rate, additional conditions are necessary for implementing the injection boundary conditions. The shape (width) of the injector is defined by the number of grid points used to model the injection zone. In all the simulations discussed here, five grid points with nearly uniform spacing were used to model the injector. The secondary fuel temperature was always taken to be same as the temperature (T_{fs}) of the primary stream at the inlet and the flow inclination was always specified for normal injection (i.e., $s = 0$). The injection pressure was chosen depending upon the type of injection control system used. For steady injection, the injection pressure was the same as the primary inflow reference pressure. For pulsed or unsteady injection, the injection pressure can be a function of time if such a control algorithm is used. Finally, the injection velocity is determined by using $\dot{m}_{sec}$ and other flow parameters.

In the following, we describe some results of the active control studies that showed some interesting features. As noted before, additional study of active control techniques are being carried out and further results will be reported in the future. Control studies of combustion instability in both the short and the long inlet were carried out and are described separately.

4.1 Secondary Fuel Injection Control in the Short Inlet Combustor

The control of the low-frequency instability simulated in the short inlet configuration (Menon and Jou, 1991) using secondary fuel injection was studied using both steady and pulsed injection. For these studies, the secondary fuel flow rate was determined by defining a parameter, $\dot{M} = \dot{m}_{sec}/\dot{m}_{ref}$ where, $\dot{m}_{ref}$ was the mass flow rate based on the reference conditions at the inlet. A value of $\dot{M} = 0.3$ was chosen for these simulations.

Figure 10a shows the result of a control simulation with a steady secondary fuel injection in the inlet duct. Both the pressure at the base of the step and the centerline axial velocity are shown in this figure. Although, the control is not very effective, the peak-to-peak pressure fluctuation level does decrease from the original 50 percent level to around 30 percent of the mean pressure. The velocity fluctuation remains out-of-phase with the pressure oscillation and the peak-to-peak level of velocity fluctuation decreases from the 100 percent of the mean velocity seen in the uncontrolled instability (Menon and Jou, 1991) to around 50 percent level with control. Also, note that, although the amplitude decreases, the dominant frequency is unchanged.

Figure 10b shows the pressure fluctuation occurring when a control strategy of pulsed injection was employed. In this approach, the secondary fuel was injected similar to the steady injection approach but only when the sensor pressure was low, i.e., when $p_s' < 0$. No time delay was used for this simulation. This control system appears to be quite effective in controlling the low-frequency instability, with the pressure fluctuation level decreasing to around 5 percent of the mean pressure. However, the control does take around three cycles of oscillation before becoming effective. The typical flame structure before the control begins is shown in Figure 10c. The characteristic hooked vortex/flame structure seen during the low frequency instability is seen at this time. Figure 10d shows an instant later in time when the control is becoming effective and shows that the hooked structure is no longer

present in the combustor. The low-frequency oscillation seen during combustion instability is no longer present and the spectra shows only a high frequency oscillation which appears to be related to the primary vortex shedding process.

4.2 Secondary Fuel Injection Control in the Long Inlet Combustor

Active control using secondary fuel injection was also applied to the simulated instability in the long inlet combustor. First, the steady and pulsed injection approach used for the short inlet simulations were implemented and their effectiveness evaluated. The results (not shown here) were not very encouraging. The instability was not controlled and in fact, for the steady injection case the instability amplitude actually starts grow. It became evident that for the long inlet case, much more sophisticated approach was required if the control strategy is to succeed.

Figure 11a shows a pressure signal at the base of the step for an active control study of the Mach 0.32 simulated instability. For this simulation, the controller, equation (11) was used but with a modification. A time delay of 2 msec was used and the secondary fuel injection was only carried out whenever $p_s'(t - \tau) > 0$. When the sensor signal showed a negative value, the injection was turned off. This approach is similar to the approach used by Langhorne and Hooper (1989). The injection pressure was chosen to be the reference inlet pressure and the gain parameter G_s was chosen to be 2.5×10^{-6}. The control simulation was begun from a previous time of the earlier uncontrolled simulation (Figure 5b). The results show that the pressure oscillation is not very effectively controlled; however, with time the peak-to-peak pressure fluctuation level drops from the original 30 percent value to around 15 percent. The reduction in the pressure level appears to be a function of time and may be due to the unsteady control injection coupling with the unsteady mass flow of the primary stream. For the values used here, the secondary mass flow rate was approximately 10 percent of the reference mass flow rate at the inlet. But, since the actual inflow at the inlet is unsteady, the instantaneous ratio of $\dot{m}_{sec}/\dot{m}_{in}$ fluctuates. Further analysis of the effect of the behaviour of this type of controller is underway. The spectral analysis of the pressure fluctuation at the base of the step is shown in Figure 11b. The dominant oscillation frequency seen in the uncontrolled simulation is still present in this spectra. This suggests that the inlet duct acoustics is still controlling the combustion instability. A low frequency of around 75 Hz is also seen in the spectra. It is unclear at present as to the source of this mode of oscillation and in any case, this frequency value is probably not reliable due to insufficient data for analysis.

The control strategy used for the Mach 0.32 case described above was then used to control the Mach 0.17 simulated instability (described earlier in Figure 6). The only difference was that, for this case, a time delay of 6 msec was used (which was chosen based on cross-correlation analysis of the 87 Hz oscillation). Figure 12a shows the pressure time trace at the base of the step for this control simulation. Some interesting observations can be made by comparing Figure 12a with Figure 6b. First, the peak-to-peak fluctuation level is not decreased significantly; however, the amplitude level is no longer a constant and ranges from 15 percent to 30 percent of the mean pressure. Second, the original pressure spectra (Figure 6a) had shown a dominant frequency around 87 Hz in the combustor. Now, the pressure signal no longer shows that frequency and the time trace actually shows that the fluctuation frequency is switching from one type of oscillation to another type. The appearance of two modes during control was also reported by Langhorne and Hooper (1989) although the physical mechanism behind their two-mode

oscillation and the present data may be different due to the significant differences between their setup and the current simulation. Spectral analysis of the pressure signal was then carried out. Figure 12b shows the pressure spectra for this case. The two dominant frequencies are at 122 Hz and 253 Hz. The latter value is close to the 244 Hz mode seen earlier and appears to suggest that the inlet acoustics is again starting to dominant the pressure oscillation. The lower frequency may be an upward shift of the original 87 Hz frequency caused by an increase in the effective Mach number at the dump plane (since the total flow rate has gone up with secondary injection). However, it must be pointed out that the pressure signal that was analysed did not have sufficient amount of temporal data to ensure the accuracy of the computed frequencies. The fact that the original frequency changes when control is applied indicates that a fixed time-delay controller cannot be used when attempting to inhibit this type of instability. Therefore, a time-dependant time-delay controller is being investigated.

5. CONCLUSIONS

A large-eddy simulation model has been developed that contains the essential physics of combustion instability such as the acoustic wave motion, interactions between large eddies, and combustion and unsteady heat release during premixed fuel combustion in a ramjet. The combustion model used for the simulations explicitly incorporates the local turbulent flame speed and avoids the erroneous numerical heat release that would occur in a finite-rate chemistry model while attempting to resolve the internal structure of the flame. A subgrid model that models the forward scatter and the backscatter as two distinctly different mechanism is proposed for large-eddy simulations of combustion instability. The forward scatter subgrid model determines the subgrid turbulent kinetic energy which is used to evaluate both the subgrid Reynolds stresses and the turbulent flame speed. Preliminary evaluation of the capability and behavior of the subgrid model has provided some confidence in the current model.

Combustion instability has been numerically simulated in two different ramjet configurations: a short inlet combustor and a long inlet combustor. Many features of the computed instability are in good agreement with experimental observations. Two different Mach number simulations were carried out for the long inlet combustor. Analysis of the data in the higher Mach number case suggests that the inlet acoustic mode determines the oscillation frequency in the combustor. However, when the Mach number was reduced, a lower dominant oscillation frequency was excited which suggests that a coupled acoustic-vortex mode may also occur in reacting flows. Further simulations with parametric variation of the inlet duct length and the flow Mach number are planned to evaluate the importance of the inlet duct acoustic resonant mode and the coupled acoustic-vortex mode in establishing combustion instability.

The data stored during the simulations were then utilised to study active techniques to control the unstable pressure oscillations. Secondary fuel injection control systems have been studied using various types of control algorithms. Both steady and pulsed secondary fuel injection upstream of the flameholder was studied in the short inlet duct combustor. When the control is effective there is an order of magnitude drop in the pressure fluctuation level, and, the large-amplitude, low-frequency oscillation is replaced by a small-amplitude, high-frequency oscillation. However, when the control is only partially effective, although the amplitude is reduced, the dominant frequency remains unchanged.

The control strategy used in the short inlet studies was then implemented in the long inlet combustor. However, control was completely ineffective indicating that a more sophisticated controller is required. A new controller was then evaluated that used a time delayed pressure signal from a sensor to specify the secondary fuel flow rate. This controller was partially effective with only a factor of 2 decrease in the fluctuation level but left the frequency unchanged. In another simulation, the secondary fuel injection at the instability frequency resulted in the excitation of two different frequencies. Such a behavior has been observed in some experiments.

Results obtained so far using secondary fuel injection controllers indicate that a more careful study is warranted to determine how the secondary fuel flow in the inlet interacts with the unsteady primary fuel stream and how it affects the instability mechanism.

ACKNOWLEDGEMENT

REFERENCES

Baylis, A., Parikh, P., Maestrello, L., and Turkel, E. (1985) "A Fourth-Order Scheme for the Unsteady Compressible Navier-Stokes Equations," ICASE Report No. 85-44.

Bogar, T. J., and Sajben, M. (1979) "The Role of Convective Perturbations in Supercritical Inlet Oscillations," CPIA Publications No. 412.

Chasnov, J. R. (1991) "Simulation of the Kolmogorov Inertial Subrange using an Improved Subgrid Model," Phys. Fluids A., Vol. 3, pp. 188-200.

Culick, F. E. C. (1989) "Combustion Instabilities in Liquid-Fueled Propulsion Systems - An Overview," AGARD CP-450, pp. 1.1-1.73.

Domaradski, J. A., Rogallo, R. S., and Wray, A. A. (1990) "Interscale Energy Transfer in Numerically, Simulated Homogeneous Turbulence," Proc. Summer Program, CTR, Stanford University, pp. 1-11.

Dowling, A. P. (1989) "Reheat Buzz - An Acoustically Coupled Combustion Instability," AGARD CP-450.

Erlebacher, G., Hussaini, M. Y., Speziale, C. G., and Zang, T. A. (197), "Toward the Large-Eddy Simulations of Compressible Turbulent Flows," ICASE Report No. 87-20.

Fung, Y. T., Yang, V., and Sinha, A. (1991) "Active Control of Combustion Instabilities with Distributed Actuators," to appear in Combustion, Science and Technology.

Gutmark, E., Parr, T. P., Parr, D. M., and Schadow, K. C. (1990) "Active Control of a Premixed Flame," AIAA-90-2448.

Gulder, O. L. (1990) "Turbulent Premixed Flame Propagation Models for Different Combustion Regimes," 23rd Symposium (Intn.)on Combustion, The Combustion Institute, pp. 743-750.

Hedge, U. G., Reuter, D., Zinn, B. T., and Daniel B. R. (1987) "Fluid Mechanically Coupled Combustion Instabilities in Ramjet Combustors," AIAA-87-0216.

Jou, W.-H., and Menon, S. (1989) "Modes of Oscillations in a Nonreacting Ramjet Combustor Flow," J. Propulsion and Power, Vol. 6, pp. 535-543.

Kerstein, A. R., Ashurst, W. T., and Williams, F. A. (1988) "Field Equation for Interface Propagation in an Unsteady Homogeneous Flow Field," Physical Rev. A., Vol. 37, No. 7, pp. 2728-2731.

Kerstein, A. R., and Ashurst, W.T. (1992) "Propagation Rate

of Growing Interfaces in Stirred Fluids," to appear in J. Fluid Mech.

Langhorne, P. J., and Hooper, N. (1989) "Attenuation of Reheat Buzz by Active Control," AGARD-CP-450, pp. 10.1-10.16.

Leith, C. E. (1990) "Stochastic Backscatter in a Subgrid Model: 2D Compressible Flows," presented at the Intn. Workshop on Large Eddy Simulations, St. Petersburg, Fl, December 19-21.

Menon, S., and Jou, W.-H. (1987) "Simulations of Ramjet Combustor Flow Fields, Part I: Numerical Model, Large-Scale and Mean Motion," AIAA-87-1421.

Menon, S., and Jou, W.-H. (1990) "Numerical Simulations of Oscillatory Cold Flows in an Axisymmetric Ramjet Combustor," J. Propulsion and Power, Vol. 6, No. 5, pp. 525-534.

Menon, S., and Jou, W.-H. (1991) "Large-Eddy Simulations of Combustion Instability in an Axisymmetric Ramjet Combustor," Combustion Science and Technology, Vol. 75, pp. 53-72.

Menon, S. (1990) "Numerical Simulation and Active Control of Combustion Instability in a Ramjet Combustor," AIAA Paper No. 90-3930.

Menon, S. (1991a) "Active Combustion Control of Combustion Instability in a Ramjet Combustor using Large Eddy Simulations," to appear in Combustion, Science and Technology.

Menon, S. (1991b) "A New Subgrid Model for Large-Eddy Simulations of Turbulent Reacting Flows," Final Report to NASA Ames Research Center, Quest TR-535, October.

Menon, S., McMurtry, P. A., and Kerstein, A. R. (1991) "A Linear Eddy Mixing Model for LES of Turbulent Reacting Flows," to appear in Large-Eddy Simulations of Complex Engineering and Geophysical Flows, Ed. B. Galperin, Cambridge University Press.

Piomelli, U., Moin, P., and Ferziger, J. H. (1988) "Model Consistency in Large Eddy Simulation of Turbulent Channel Flows," Phys. Fluids, Vol. 31, pp. 1884-1891.

Piomelli, U., Cabot, W. H., Moin, P. and Lee, S. (1990) "Subgrid-Scale Backscatter in Transitional and Turbulent Flows," Proc. Summer Program, CTR, Stanford University, pp. 19-29.

Schadow, K. C., Gutmark, E., Parr, T. P., Parr, D. M., Wilson, K. J., and Crump, J. H. (1987) "Large-Scale Coherent Structures as Drivers of Combustion Instability," AIAA-87-1326.

Schadow, K. C., Gutmark, E., and Wilson, K. J. (1990) "Active Combustion Control in a Coaxial Dump Combustor," AIAA-90-2447.

Smith, D. A., and Zukoski, E. E. (1985) "Combustion Instability Sustained by Unsteady Vortex Combustion," AIAA-85-1248.

Yakhot, V. (1988) "Propagation Velocity of Premixed Turbulent Flames," Combustion Sci. and Tech., Vol. 60.

Yu, K. H., Trouve, A., and Daily, J. W. (1991) "Low-Frequency Pressure Oscillations in a Model Ramjet Combustor," J. Fluid Mech., Vol. 232, pp. 47-72.

Zeman, O. (1990) "Dilatation Dissipation: the Concept and Application in Modeling Compressible Mixing Layers," Phys. Fluids, Vol. 2, pp. 178-188.

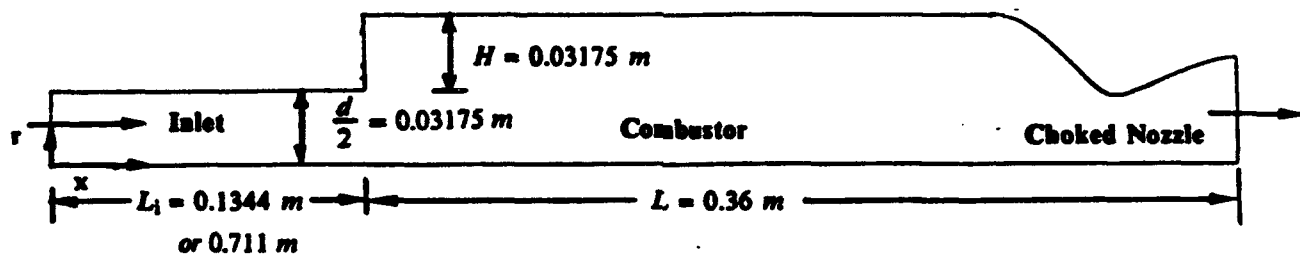Zeman, O., and Squires, K. (1990) "On the Subgrid-Scale Modeling of Compressible Turbulence," Proc. Summer Program, CTR, Stanford University, pp. 47-59.
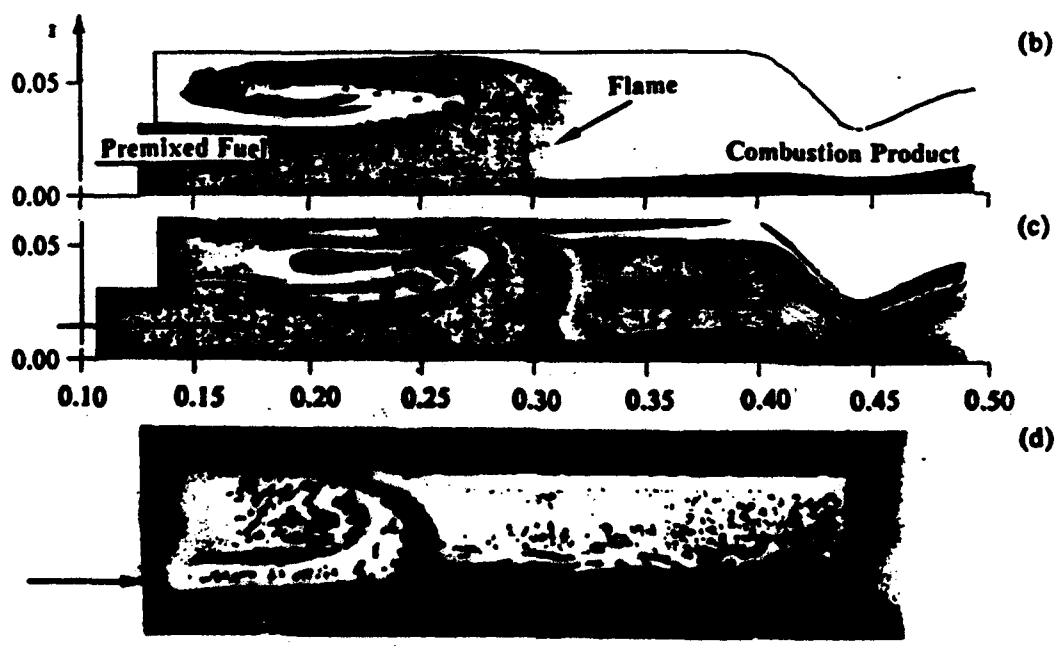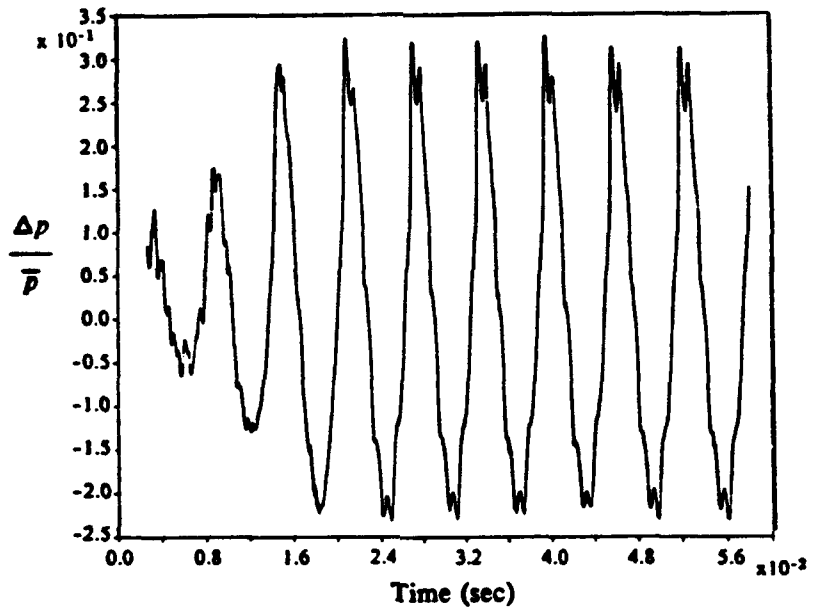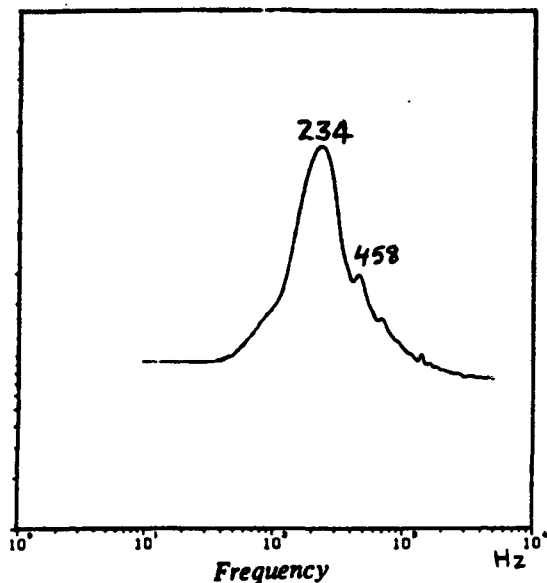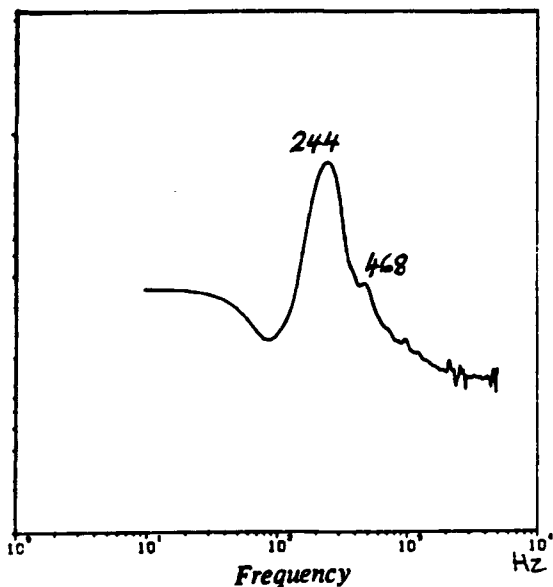
Figure 1. The Ramjet Combustor

Figure 2. Typical flow features observed during combustion instability in the ramjet combustor with a short inlet. (a) Pressure oscillation at the base of the step, (b) flame structure, (c) Vortex structure, and, (d) Experimental (Smith and Zukoski, 1985).
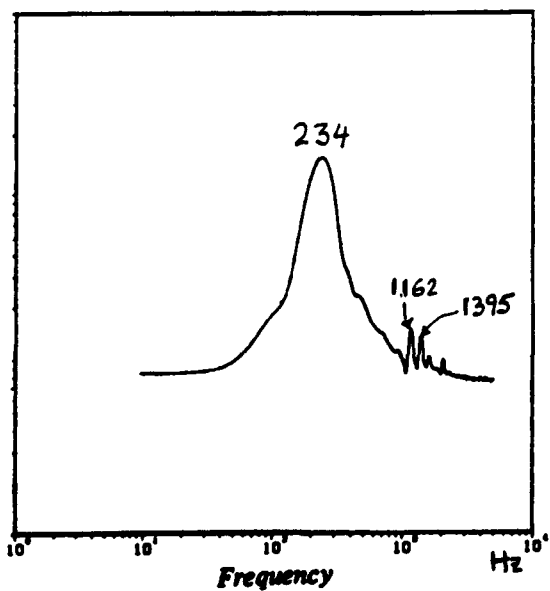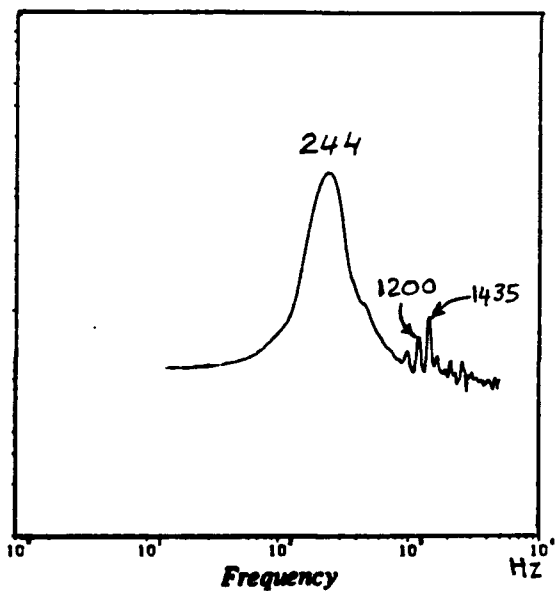
(a) 320 x 64 mesh

(b) 256 x 32 mesh

Figure 3. Pressure spectra in the long inlet combustor using the subgrid model for different grid resolutions. Constant turbulent flame speed case.

(a) 320 x 64 mesh

(b) 256 x 32 mesh

Figure 4. Vorticity spectra in the long inlet combustor using the subgrid model for different grid resolutions. Constant turbulent flame speed case.

234

Frequency Hz

(a) Pressure spectra

$\frac{\Delta p}{\bar{p}}$

TIME (sec)
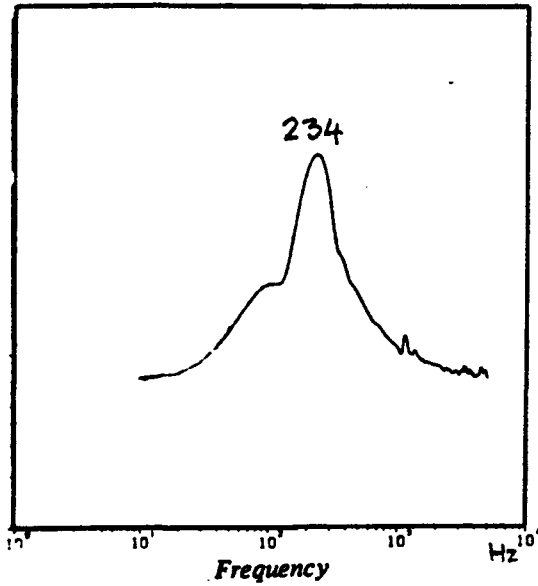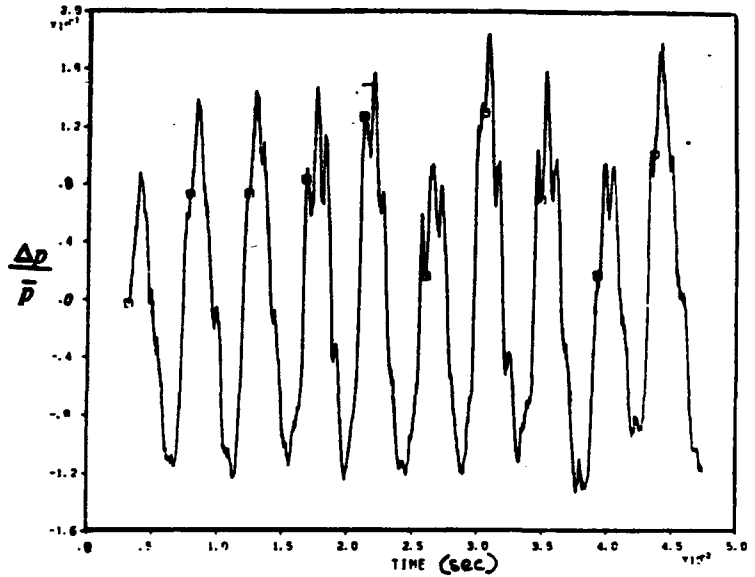
(b) Pressure time trace

Figure 5. Pressure spectra and time trace at the base of the step in the long inlet combustor. Variable turbulent flame speed case with reference Mach number of 0.32 and a grid resolution of 256 x 32.

$\frac{|p'|}{|p_{ref}'|}$

X_r/H STEP
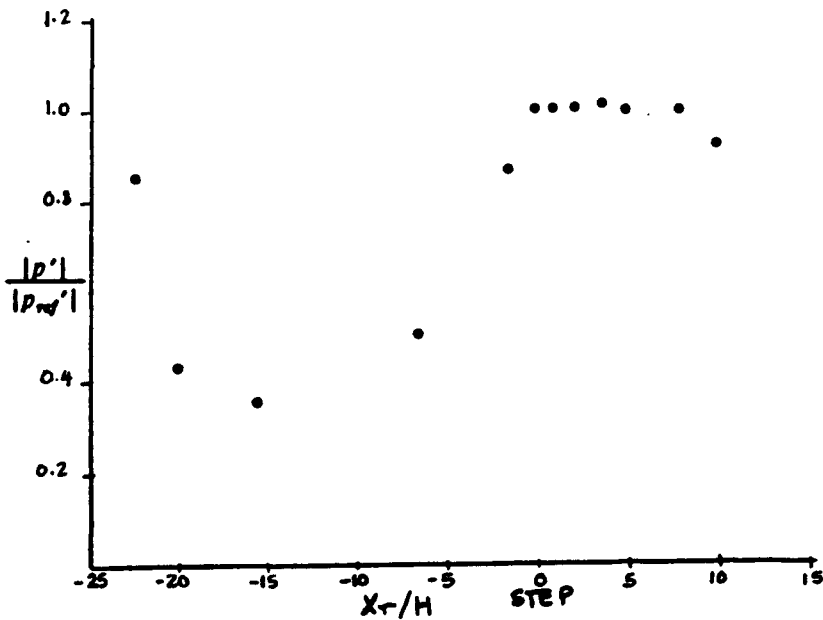
(a) Pressure amplitude variation for the 244 Hz oscillation

234

Frequency Hz
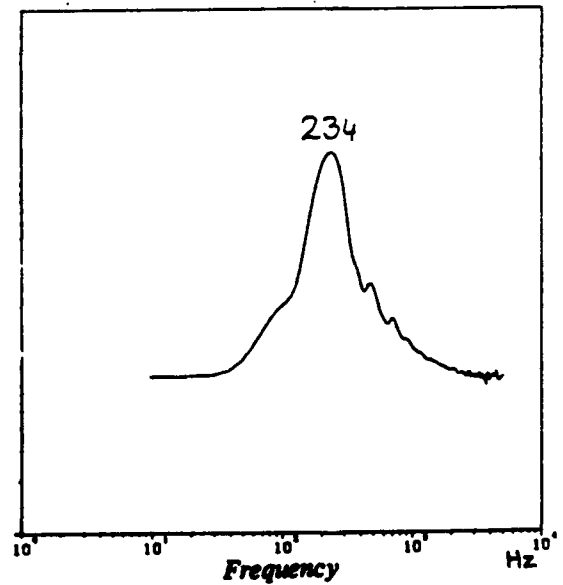
(b) Centerline axial velocity spectra

Figure 6. Centerline axial velocity spectra at the dump plane and the amplitude variation of the pressure fluctuation in the long inlet combustor. Variable turbulent flame speed case with the reference Mach number of 0.32 and a grid resolution of 256 x 32.
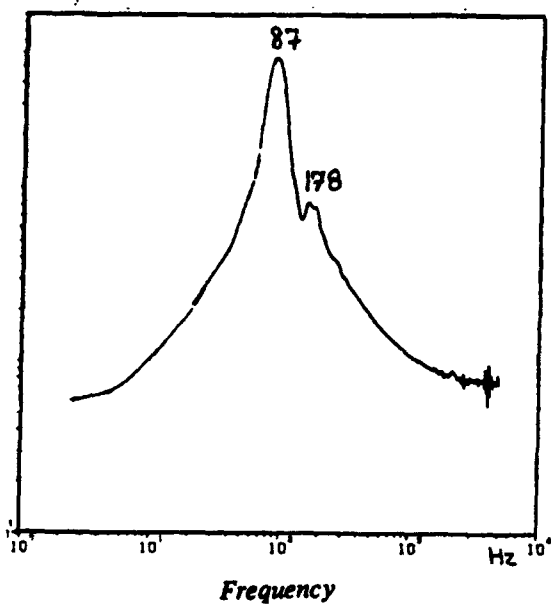
(a) Pressure spectra at the dump plane
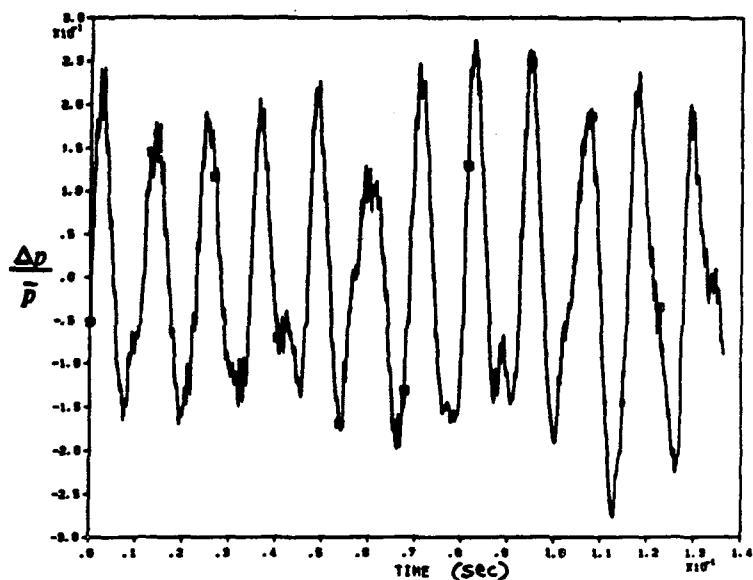
(b) Pressure time trace at the dump plane
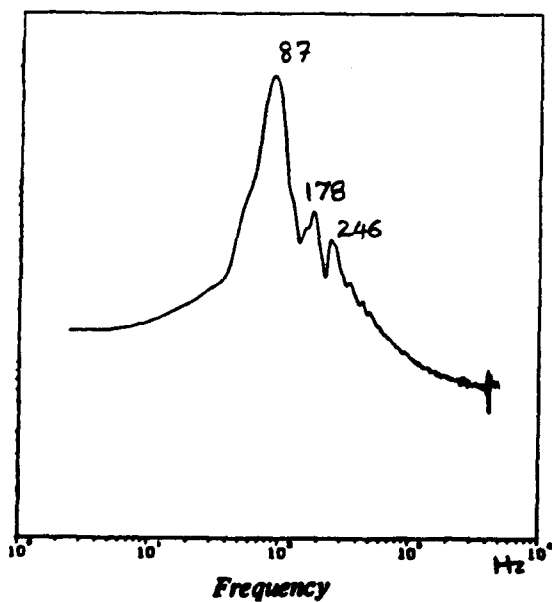
(c) Pressure spectra in the inlet
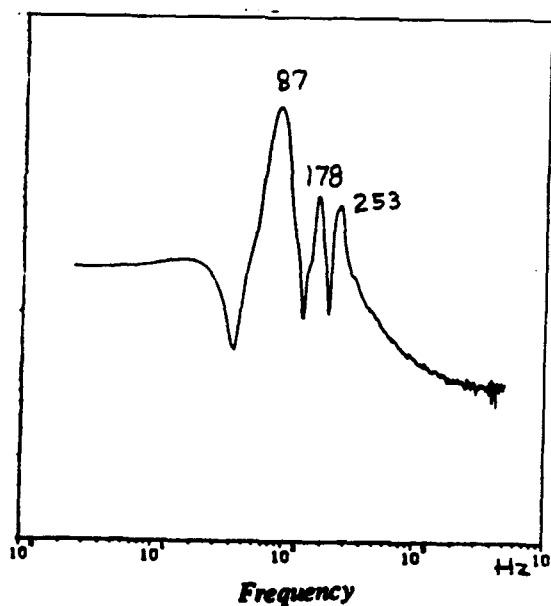
(d) Centerline axial velocity spectra

Figure 7. Pressure spectra and time trace in the long inlet combustor. Variable turbulent flame speed case with reference Mach number of 0.17 and a grid resolution of 256 x 32.

(a) Mach = 0.32   (b) Mach = 0.17
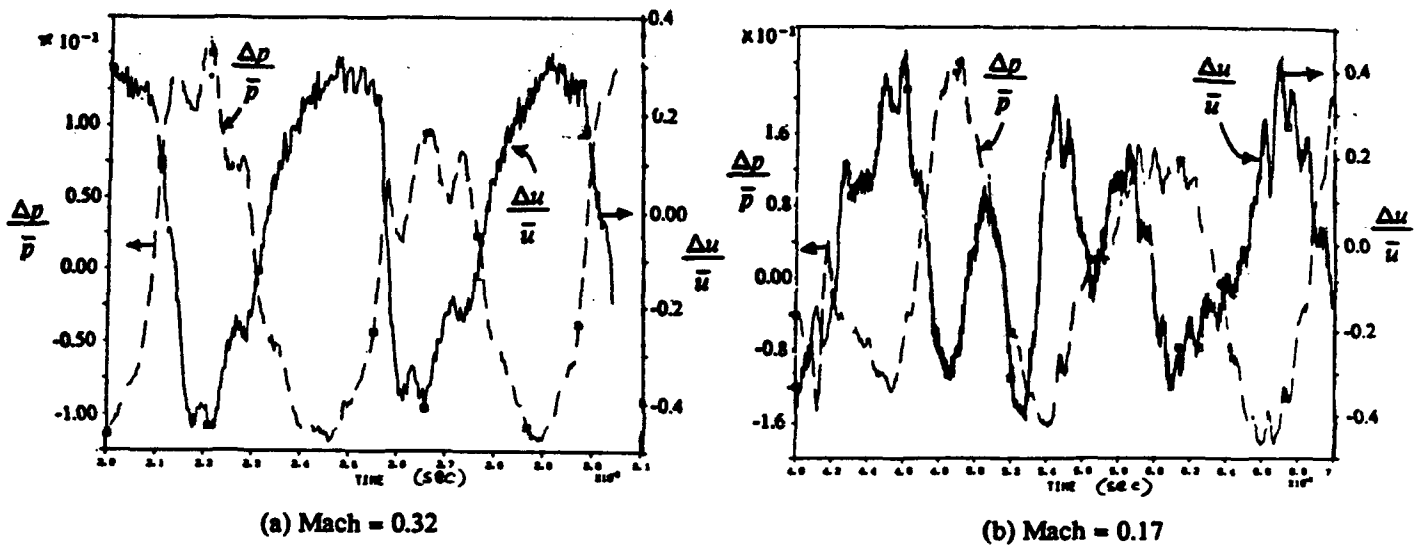
Figure 8. Pressure fluctuation at the step and centerline axial velocity fluctuation at the dump plane for two Mach number cases
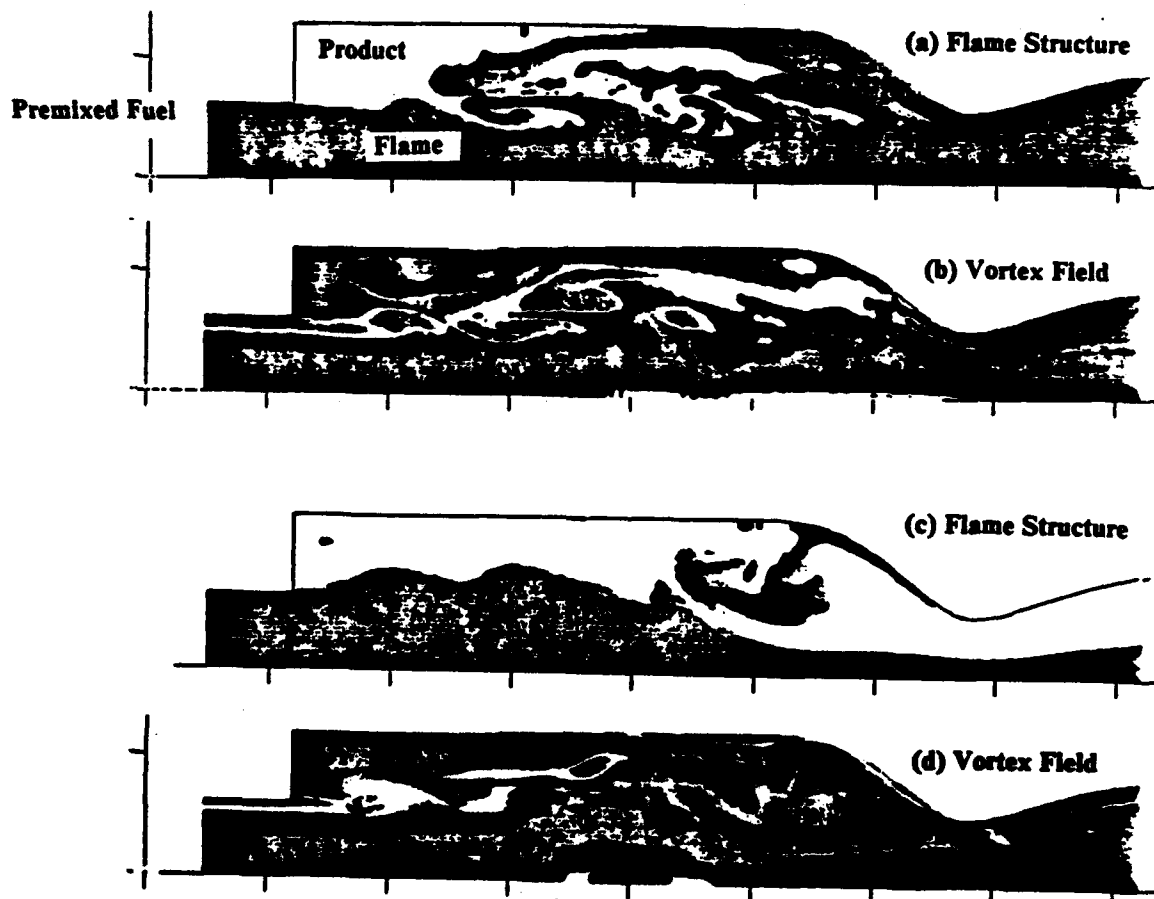
Figure 9. The flame and vortex structure in the combustor at two different times
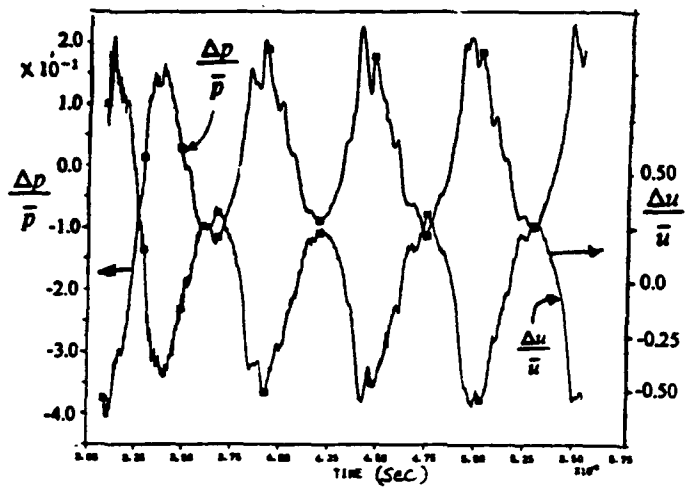
(a) Steady injection
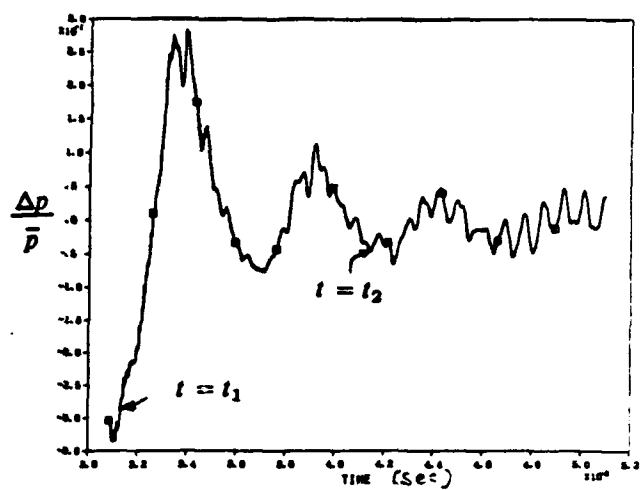
(b) Pulsed injection
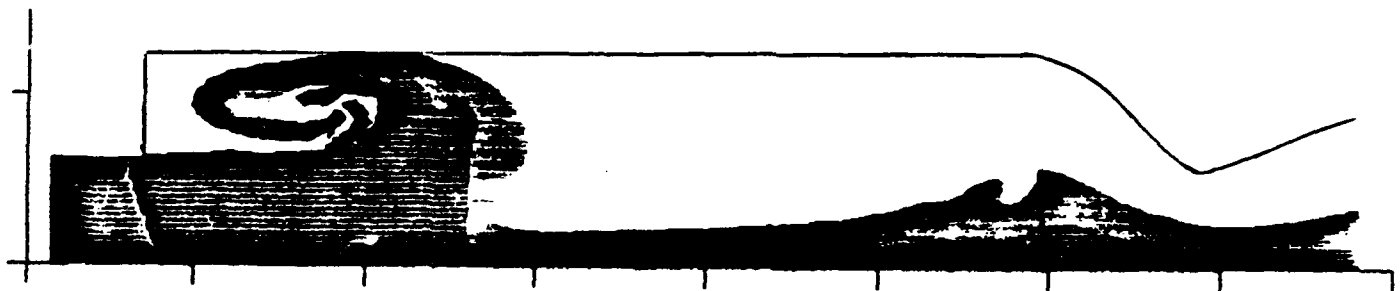
(c) Flame structure at $t = t_1$ for the pulsed injection case
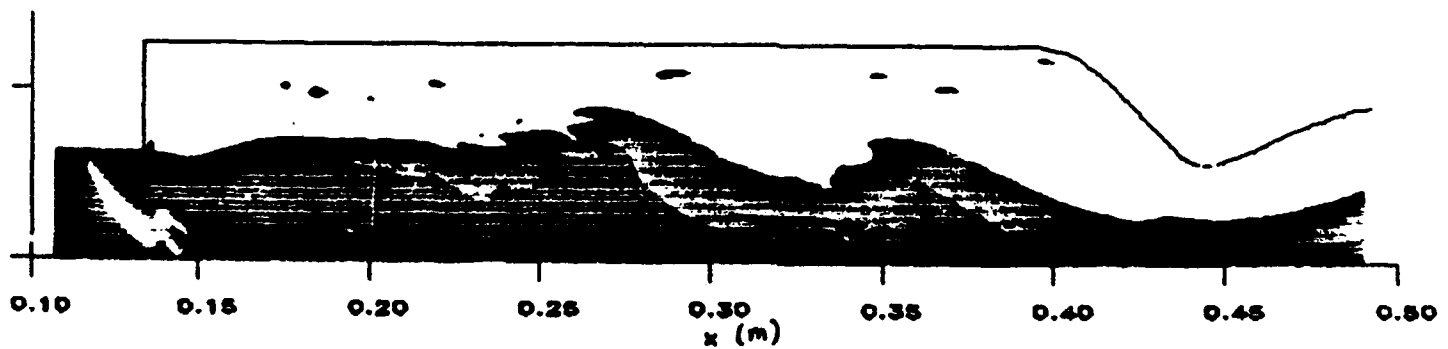
(d) Flame structure at $t = t_2$ for the pulsed injection case

Figure 10. Active control of combustion instability in the short inlet combustor
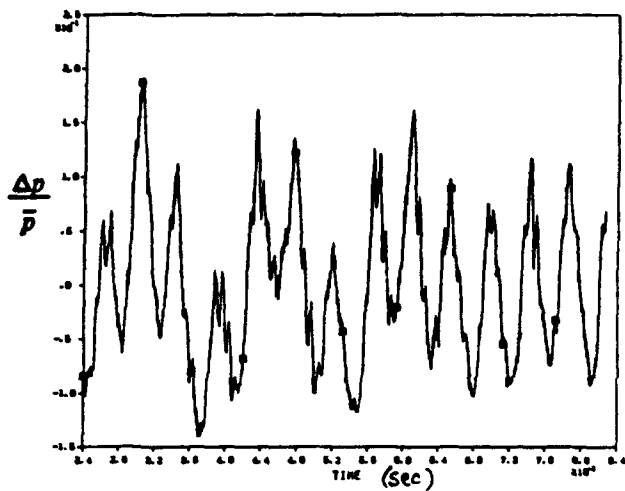
(a) The pressure fluctuation at the base of the step
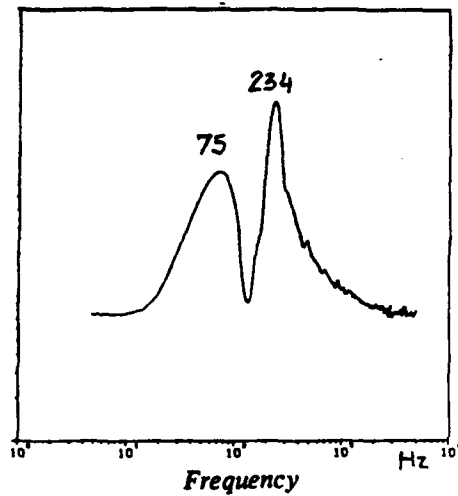
(b) The pressure spectra

Figure 11. Pressure fluctuation and spectra during active control of instability in the long inlet combustor using a time-delay feedback controller for the Mach = 0.32 case.
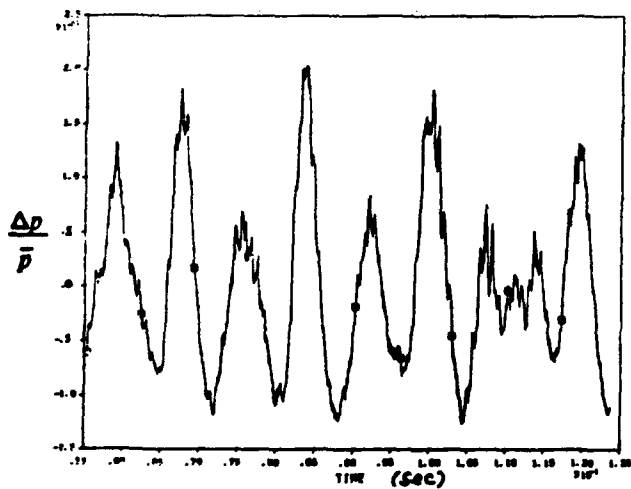
(a) The pressure fluctuation at the base of the step
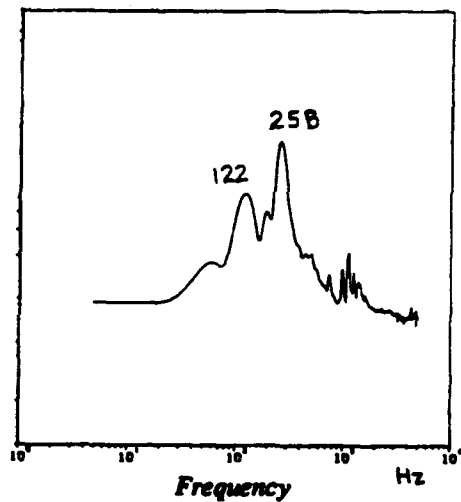
(b) The pressure spectra

Figure 12. Pressure fluctuation and spectra during active control of instability in the long inlet combustor using a time-delay feedback controller for the Mach = 0.17 case.

AIAA-91-0411

Active Control of Combustion Instability in a Ramjet Using Large-Eddy Simulations

S. Menon, QUEST Integrated, Inc.
(formerly Flow Research, Inc.)
Kent, WA

29th Aerospace Sciences Meeting
January 7-10, 1991/Reno, Nevada

ACTIVE CONTROL OF COMBUSTION INSTABILITY IN A RAMJET
USING LARGE-EDDY SIMULATIONS

Suresh Menon*
Quest Integrated, Inc.
(formerly Flow Research, Inc.)
Kent, Washington

ABSTRACT

Combustion instability in a ramjet combustor has been numerically simulated using a large-eddy simulation (LES) technique. Premixed combustion in the combustor is simulated using a thin-flame model that explicitly uses the local turbulent flame speed in the governing equation. Two types of instability are observed: a small-amplitude, high-frequency instability and a large-amplitude, low-frequency instability. Both such instabilities have been experimentally observed, and various computed flow features are in good qualitative agreement with experimental observations. The information obtained from these simulations has been used to develop active control strategies to suppress the instabilities. Two active control techniques have been investigated: an acoustic feedback technique and secondary (both steady and unsteady) fuel injection. Control of both types of combustion instability was successfully achieved using the acoustic feedback technique, and the control could be used to turn the instability on and off. Secondary fuel injection also shows promise as an active control technique to suppress combustion instability.

1. INTRODUCTION

Combustion instability in a ramjet engine is an extremely complex phenomenon involving nonlinear interactions among acoustic waves, vortex motion and unsteady heat release. Typically, the instability manifests itself as a large-amplitude pressure oscillation in the low-frequency range (100-800 Hz) and is very difficult to control. When the amplitude of the pressure oscillation reaches some critical limit, it can cause structural damage due to fatigue or can cause an engine "unstart," which occurs when the shock in the inlet duct is expelled to form a bow shock ahead of the inlet. This phenomenon of engine unstart is one of the most serious technical problems encountered in developing an operational ramjet engine. In recent years, a major research program was undertaken, both experimentally (e.g., Schadow et al., 1987; Gutmark et al., 1989; Smith and Zukoski, 1985; Sterling and Zukoski, 1987; Hedge et al., 1987) and numerically (e.g., Menon and Jou, 1990a, 1990b; Jou and Menon, 1990; Kailasanath et al., 1989), to determine the mechanism of the combustion instability. Attempts to control combustion instability using both passive and active control techniques have also been carried out in the past (see Culick, 1989, for a review). Passive control methods that typically involve structural (i.e., geometrical) modifications have proven insufficient for controlling the low-frequency instability. Recent experimental studies (e.g., Gulati and Mani, 1990; Langhorne and Hooper, 1989; Schadow et al., 1990; Gutmark et al., 1989, 1990) suggest that the use of active control techniques may

be a more effective approach for controlling the combustion instability in a ramjet. To complement the experimental studies at the Naval Weapons Center (NWC) (e.g., Schadow et al., 1990, Gutmark et al., 1990) a numerical approach to study active control methods is also being developed. Some results of active control using acoustic feedback techniques were reported earlier (Menon, 1990). This paper continues the acoustic feedback control study and also describes another active control technique using secondary fuel injection that has been shown experimentally to be an effective control system (e.g., Langhorne and Hooper, 1989; Gutmark et al., 1990).

2. THE SIMULATION MODEL

The simulation model used in this study was developed through a series of numerical experiments starting with cold flow studies (Menon and Jou, 1987, 1990a; Jou and Menon, 1987, 1990) and culminating in the simulation of combustion instability (Menon and Jou, 1990b). The equations solved in this model are the full compressible Navier-Stokes equations formulated in the axisymmetric coordinate system. The numerical technique is an unsplit second-order-accurate, finite-volume scheme based on MacCormack's method; it has been described elsewhere (Menon and Jou, 1987, 1990a). The ramjet combustor modeled in these studies consists of an axisymmetric inlet duct that is connected to an axisymmetric dump combustor by a sudden expansion. A convergent-divergent nozzle is attached downstream of the combustor. Figure 1a shows the typical ramjet configuration used in these studies.

2.1 The Numerical Model

The details of the numerical model and the validation studies have been described elsewhere (Menon and Jou, 1987, 1990a; Jou and Menon, 1987, 1990) and will not be repeated here. However, some pertinent issues related to the implementation of the numerical boundary conditions are reviewed here.

For the spatially developing flow problem studied here, the inflow and outflow boundaries are computational boundaries. The implementation of proper inflow/outflow conditions is very important to ensure that no spurious (numerical) acoustic waves are generated. In the ramjet model simulated here, a convergent-divergent nozzle is attached downstream of the combustor. This is similar to a real operating ramjet configuration. The flow through this nozzle is choked, and the outflow at the downstream computational boundary is supersonic. Since at a supersonic outflow all characteristic waves (i.e., the acoustic waves, the entropy wave and the vorticity wave) are outgoing, the imposed boundary conditions will not affect the interior flow field.

For the ramjet configuration shown in Figure 1a, subsonic inflow conditions are employed. These inflow conditions are similar to the conditions used in some of the experiments (e.g., Gutmark et al., 1989). Numerically, at the subsonic inflow three boundary conditions (the stagnation pressure, the stagnation temperature and the local flow inclination) are specified corresponding to the three incoming characteristics (i.e., the vorticity wave, the entropy wave and the right-running acoustic wave). The characteristic variable carried by the outgoing acoustic wave is determined by solving the pertinent decoupled interior characteristic equation. Although this set of boundary conditions is physically reasonable, there is potentially some uncertainty in the specification of the stagnation pressure since, in unsteady flows, it would contain a contribution from the time derivative of the velocity potential. The application of these boundary conditions implies a certain "impedance" condition. Earlier, the characteristics of the current impedance condition were examined by a linearised analysis, and the condition was proven to be of the damping type. Thus, pressure disturbances reaching the inflow boundary will not get amplified.

The above noted uncertainty due to a subsonic inflow can be avoided if the full ramjet configuration as shown in Figure 1b is modeled. For such a realistic ramjet geometry, the inflow is supersonic and all characteristics are incoming. Thus, all conditions can be specified. The supersonic inflow slows to a sonic condition (chokes) at the inlet throat and then becomes supersonic again for a short distance downstream of the throat. Further downstream, the flow becomes subsonic due to the inlet shock that resides under stable conditions in the divergent part of the inlet nozzle. In a practical ramjet device, it has been noted that the flow oscillations downstream of the shock in the inlet diffuser may participate in the flow oscillations in the combustor (Bogar and Sajben, 1979). The shock also undergoes longitudinal oscillations that, under some circumstances, can become large-amplitude oscillations resulting in the engine unstart phenomenon described earlier.

The full ramjet engine is being numerically modeled in a new study. Although a detailed analysis of this study will be presented elsewhere, some preliminary results are shown in Figure 2. Figure 2a shows a time sequence of vorticity contours in the ramjet during cold flow in a full ramjet engine. Figure 2b shows the typical Mach contours in the combustor. For this simulation, the shock undergoes only a small-amplitude oscillation about its stable location in the inlet diffuser. Analysis of the flow field indicates that the boundary layer on the inlet duct wall undergoes unsteady separation downstream of the inlet shock. This separated shear layer rolls up into coherent vortical structures as seen in Figure 2a. The boundary layer sometimes reattaches on the inlet duct wall before finally separating at the dump plane. Downstream of the dump plane, this separated shear layer also undergoes vortex rollup as seen in earlier cold flow studies (Menon and Jou, 1990a). Complex vortex motions and merging processes are observed in the combustor as a consequence of the boundary layer separation in the inlet duct and the shear flow in the combustor. Many of the flow features observed during this simulation (and in other simulations not shown here) are in good qualitative agreement with the observations by Bogar and Sajben (1979). Currently, combustion is being initiated in the full ramjet, and the results will be reported in the future.

2.2 The Combustion Model

To simulate combustion instability, an accurate evaluation of the chemical heat release is required. In particular, the amount of heat release and its time-dependent spatial

distribution must be accurately computed. The flame can be treated as a discontinuity and numerically captured as a smeared discontinuity as long as the important physics, such as the amount of heat release at the flame sheet, can be accurately computed. For LES of premixed combustion, such a thin-flame model is a good approximation, since in LES the large-scale coherent structures are computationally resolvable features and the flame is only thickened by the subgrid turbulent diffusion. This model is also preferable to models in which detailed finite-rate kinetics are considered. In finite-rate kinetics models, the numerical simulations are presumed to compute the local flame speed implicitly and thus the amount of heat release. Since the flame speed depends upon the dissipation mechanism in the flame structure, this implies that the internal structure of the flame must be resolved (Williams, 1985). However, this is not practically achievable, since in LES the number of grid points that can be used is limited by the capacity of the computer, and therefore an adequate resolution of the flame structure is not possible. Furthermore, all numerical schemes have some form of artificial dissipation, either built into the scheme or explicitly provided to stabilise the computations. Thus, the computed flame structure and the local flame speed are contaminated by the numerical dissipation and could in fact be completely overwhelmed by the numerical diffusion.

To circumvent this problem, a model for premixed combustion based on the thin-flame model (Williams, 1985; Kerstein et al., 1988) was incorporated (Menon and Jou, 1990b). In this model, the local turbulent flame speed u_f appears explicitly and is determined as a function of the laminar flame speed u_l and the local subgrid turbulence intensity u' using the renormalisation group (RNG) theory model of Yakhot (1989). The effects of detailed chemical kinetics are contained in the laminar flame speed, and a progress variable G is defined which is governed by the conservation equation

$$\frac{\partial \rho G}{\partial t} + \frac{\partial}{\partial x_i} \rho u_i G = -\rho u_f \left| \nabla G \right| \qquad (1)$$

where u_i are the fluid velocities, $G = 1$ for the fuel mixture, and $G = 0$ for the combustion product.

The turbulent flame speed u_f is given by the RNG model as

$$\frac{u_f}{u_l} = \exp\left[\frac{u'^2}{u_f^2}\right] \qquad (2)$$

Yakhot (1989) found that Equation (2) correlates quite well with various experimental observations. The laminar flame speed contains information on the chemical kinetics and the molecular dissipation; once the local subgrid turbulence intensity is determined, Equation (2) can be used to find u_f for a given fuel mixture.

The chemical heat release is a function of G and the specific chemical energy of the fuel mixture. The chemical energy of the mixture is included in the formulation by specifying the specific enthalpy h of the mixture in the energy equation as $h = C_p T + h_f G$. Here, h_f is the heat of formation of the premixed fuel, C_p is the specific heat of the mixture at constant pressure, and T is the temperature. The heat of formation of the fuel essentially determines the amount of heat released during combustion and thus is a function of the equivalence ratio for a given fuel. The product temperature T_p can be estimated for a given heat of formation for the fuel by the relation $h_f = C_p(T_p - T_{fi})$, where T_{fi} is the fuel temperature at the inlet. In the simulations, the combustion product temperature is initially specified, and the heat of formation is determined from Equation (4).

Due to the explicit appearance of the local flame speed in Equation (1), the amount of heat release does not depend on

2

the computed internal structure of the flame. Even when numerical diffusion broadens the flame, the flame speed is not severely affected. The effect of numerical broadening is shown in Figure 3. In a discontinuous flame model (Figure 3a), the flame propagates at a velocity u_F into the mixture. Therefore, the amount of fuel converted to product is proportional to $u_F \Delta t$, where Δt is the timestep. When the flame is broadened by numerical diffusion, the smeared flame still propagates into the fuel mixture with flame speed u_F, and the amount of fuel mixture converted to product is approximately the same as in the discontinuous flame model, as can be seen in Figure 3b. It was shown earlier (Menon and Jou, 1990) that numerical diffusion does not significantly affect the dynamics of the flame propagation.

2.3 The Subgrid Model

In a practical ramjet device, the Reynolds number of the flow is extremely high. A LES of such a flow would require a validated subgrid model. Subgrid models for compressible flows have just begun to be investigated (e.g., Yoshizawa, 1986; Erlebacher et al., 1987). At present, it is not clear what is an appropriate subgrid model for flows such as those in a ramjet combustor. It is, however, apparent that to close the combustion model described in Section 2.2, the subgrid turbulence intensity must be determined. Therefore, a one-equation model for the subgrid turbulent kinetic energy of the form

$$\frac{\partial \rho k}{\partial t} + \frac{\partial}{\partial x_i} \rho u_i k = P_k - D_k + \frac{\partial}{\partial x_i}(\rho \nu_t \frac{\partial k}{\partial x_i}) \quad (3)$$

is currently being evaluated. This model can be viewed as a simple extension of Schumann's model (e.g., Schmidt and Schumann, 1989) Here, ρ and u_i are, respectively, the filtered large-scale (resolved) density and velocities, and $k = \frac{1}{2}\langle u_i'^2 \rangle$ is the subgrid turbulent kinetic energy. Also, P_k and D_k are, respectively, the production and dissipation of k and are modeled here as

$$P_k = C_k \rho \nu_t (2 S_{ij} S_{ij}) \quad (4)$$

and

$$D_k = C_\epsilon \frac{k^{\frac{3}{2}}}{\Delta_f} \quad (5)$$

Here, $S_{ij} = \frac{1}{2}(\frac{\partial u_i}{\partial x_j} + \frac{\partial u_j}{\partial x_i})$ is the strain tensor in terms of the resolved velocity field and ν_t is the subgrid eddy viscosity, which is related to the subgrid kinetic energy by the relation

$$\nu_t = C_\nu k^{\frac{1}{2}} \Delta_f \quad (6)$$

where Δ_f is the characteristic grid size. Also, C_k, C_ϵ and C_ν are constants that will have to be determined. Some preliminary estimates for these constants can be obtained based on the studies by Schumann. Once k is known, the subgrid turbulence intensity u' appearing in Equation (2) can be easily determined ($u' = \sqrt{2k}$). This k equation model can also be used to determine the turbulent subgrid fluxes appearing in the momentum equations using an approach similar to that described by Schumann (e.g., Schmidt and Schumann, 1989).

At present this model is undergoing evaluation using the full ramjet geometry and using test conditions similar to some past experiments (Crump et al., 1986). However, there are still many issues that need to be resolved, for example, the type of filtering to be used, the effect of variable grid distribution, the near-wall modifications to the eddy viscosity (e.g., Piomelli et al., 1990) and the proper closure for the Leonard and cross terms so that the filtered equations maintain

Galilean invariance (e.g. Speziale, 1985; Germano, 1990).

Since the above model is not yet operational, all simulations carried out so far were for flows in a moderate Reynolds number range. This is considered a first step towards understanding the complex physical processes involved in the ramjet combustor. To model the dissipative effects of the subgrid turbulence, a constant eddy-viscosity model is employed. This eddy-viscosity is chosen to be the laminar dissipative coefficient at the reference temperature and can be viewed as a simple subgrid model, as noted by Ferziger and Leslie (1979). A uniform value of the subgrid turbulent intensity is also used, typically a small percentage of the reference velocity. Some important physical properties, such as the spatial nonuniformity of subgrid turbulence and its effect on the local flame speed and the amount of heat release, are not included at present. However, as shown earlier (Menon and Jou, 1990b), the major qualitative interactions between the large-scale vortex structures and the combustion heat release have been captured by the present simulation model. The effect of nonuniform subgrid turbulence on the turbulent flame speed and on combustion instability will be included once the one-equation subgrid model described above has been fully implemented.

3. SIMULATION OF COMBUSTION INSTABILITY

The details of the simulation of combustion instability in a ramjet combustor are described elsewhere (Menon and Jou, 1990b). The present focus is on active control of the numerically simulated combustion instability. Before describing the control studies, however, some important features of the computed instability are described in this section.

In general, combustion instability in a combustor depends upon various parameters such as the system geometry, the flow parameters, the fuel type, and the equivalence ratio. In the earlier study (Menon and Jou, 1990b), in addition to the flow parameters (e.g., the Mach number M and the Reynolds number Re) and the geometrical parameters (e.g., L_i, L, A_{inlet}/A^* ; see Figure 1a), two important thermochemical parameters were identified. One is $\theta = T_p/T_o$, which is the ratio of the product temperature to the stagnation temperature T_o; the other is $\sigma = u_F/u_{ref}$, which is the ratio of the characteristic flame speed to the characteristic reference velocity u_{ref}. For a fixed fuel mixture, θ can be related to the equivalence ratio ϕ, and σ can be related to the chemical kinetic rate and the level of subgrid turbulence. The effects of varying the geometrical parameters, the ratio between the inlet and throat areas A_{inlet}/A^*, and the thermochemical parameters θ and σ have been studied (Menon and Jou, 1990b). It was determined, that increasing σ with the other parameters held fixed excites the large-amplitude, low-frequency pressure oscillations typical of combustion instability in a ramjet. This instability was also excited when the area ratio A_{inlet}/A^* was increased. The area ratio is increased by reducing the nozzle throat area A^*. This decreases the inlet mass flow rate and reduces the inlet mean flow velocity u_{in}. Thus, the effect of increasing the area ratio can be interpreted as an increase in the effective thermochemical parameter $\sigma^* = u_F/u_{in} = \sigma(u_{ref}/u_{in})$. This appears to indicate that σ^* may be a more general thermochemical parameter than σ.

In this section, two simulations will be described that showed two different types of combustion instability: a small-amplitude, high-frequency combustion instability (Type I) and a large-amplitude, low-frequency combustion instability (Type II). Both types of instability have been observed in various experimental studies (e.g., Smith and Zukoski, 1985; Sterling and Zukoski, 1987; Schadow et al., 1987). The active control of these instabilities will be the focus of this

paper and is described in the next section.

For both the simulations discussed here, the flow parameters such as the reference Reynolds number and the reference Mach number were held fixed at $Re = 10,000$ and $M = 0.32$, respectively, based on the inlet duct diameter and the reference velocity of $u_{ref} = 100$ m/sec. The thermochemical parameters θ and σ were also held fixed at $\theta = 5$ and $\sigma = 0.05$. For $\theta = 5$, the product temperature T_p was 1500 K. All system (geometrical) parameters such as H, L_i, and L were held fixed for both simulations except for the area-ratio parameter A_{inlet}/A^*, which was increased from 1.05 for the Type I instability simulation to 1.20 for the Type II simulation. This results in an increase in the thermochemical parameter σ^* from 0.042 to 0.048. In the following sections, we describe some pertinent features of Type I and Type II combustion instabilities.

3.1 Small-Amplitude, High-Frequency Instability (Type I)

During a Type I combustion instability, the pressure oscillations initially show a large-amplitude, low-frequency oscillation that eventually decays so that only a high-frequency oscillation remains. Spectral analysis of the high-frequency oscillation showed a dominant peak at around 935 Hz. Further analysis showed that this oscillation is a traveling wave in the combustor. The peak-to-peak level of the high-frequency pressure fluctuation is around 15 percent of the mean pressure, as shown in Figure 4a. This was around three times higher than that observed in earlier cold flow studies (Menon and Jou, 1990a). Although the fluctuation level is small, it is by no means insignificant for a realistic ramjet combustor and may be sufficient to expel the inlet shock.

Flow visualization showed that the shear layer separating at the rearward-facing step rolls up into vortices; further downstream, these vortices undergo pairing as observed in earlier cold flow studies. The flame front initially resides along the high shear region in the shear layer, and as the vortex rollup/pairing process occurs, the flame is entrained into the vortical structures. The typical flame structure and vorticity field distribution for this simulation is shown in Figures 4b and 4c. For comparison, a flow visualization by Smith and Zukoski (1985) for premixed "stable" combustion in a two-dimensional combustor is shown in Figure 4d. There is qualitative agreement between the numerical and experimental observations as discussed in Menon and Jou (1990b).

3.2 Large-Amplitude, Low Frequency Instability (Type II)

During a Type II combustion instability, the pressure fluctuations show a large-amplitude, low-frequency oscillation with peak-to-peak levels around 50 percent of the mean pressure, as shown in Figure 5a. The oscillation rapidly reaches a limiting cycle and shows a type of pressure signature that is typical of what is observed during combustion instability. The flame propagation is quite different from that observed during a Type I instability. A large hooked-flame structure propagates through the combustor at a low frequency, and associated with this flame is a large mushroom-shaped vortical structure. The combined vortex/flame structure propagates through the combustor at the same low frequency. Spectral analysis showed that the dominant mode of oscillation is occurring at a frequency of around 166 Hz. The amplitude and phase of the pressure oscillation at various locations in the combustor was nearly the same, indicating that this pressure oscillation is similar to the bulk-mode oscillation observed in some experiments.

The typical flame structure and the vorticity field are shown in Figures 5b and 5c. For comparison, the experimental visualization of Smith and Zukoski (1985) is shown in

Figure 5d. Further analysis was carried out by Menon and Jou (1990b), and it was shown there that many characteristics of this Type II combustion instability, such as the pressure and velocity fluctuation levels, the phase relation between the pressure and velocity fluctuations, and various features of the vortex/flame structure propagation, qualitatively agreed with experimental observations.

4. ACTIVE CONTROL OF COMBUSTION INSTABILITY

Using the stored data for these two simulations, a new study was initiated to investigate techniques for controlling both types of instabilities. Experimentally, there are various approaches being considered. In general, active control strategies fall in three categories: control using acoustic feedback (e.g., Lang et al., 1987; Poinsot et al., 1987; Gutmark et al., 1990; Schadow et al., 1990); control by unsteady modification of the inlet mass flow rate (e.g., Bloxsidge et al., 1988); and control by manipulation of the unsteady heat release in the combustor (e.g., Langhorne and Hooper, 1989). Each of these methods has shown promise in laboratory tests. In this paper, the focus of the numerical experiments is the study of active control using acoustic feedback and secondary fuel injection.

4.1 Acoustic Feedback Control

Active control through acoustic forcing was demonstrated earlier by Lang et al. (1987) and Poinsot et al. (1987). The latter study showed that this technique provided the capability of turning the instability on or off at will, thereby providing a means to study the transient behavior. It was also shown that the power required for control was quite small and that control can be achieved over a wide range of phase differences. This indicates that the control technique is not an anti-sound approach, which would have required a specific phase relation. Recent studies at NWC (e.g., Schadow et al., 1990; Gutmark et al., 1990) have further demonstrated that acoustic feedback control of the combustion instability in a ramjet-type configuration is possible.

A typical acoustic feedback system used in the experiments involves a loudspeaker/microphone system in the active control loop. In this technique, the pressure signal is sensed at some chosen location using a microphone (or a pressure transducer). The signal is analyzed, phase-shifted (or time-delayed), and amplified, and then fed back at some other chosen location using a loudspeaker (see Figure 1a). If the control signal from the loudspeaker destructively interferes with the pressure oscillation in the combustor, then the oscillations will become damped, thereby achieving control of the instability. Here, a similar technique has been studied numerically. To account for the effect of time delay in the control system, a control signal was chosen such that

$$p_{sp}'(t) = Ga \; p_{mic}'(t-\tau) \qquad (7)$$

where $Ga = A_g \dfrac{\bar{p}_{sp}}{\bar{p}_{mic}}$ is an amplification parameter with A_g a constant (typically, $A_g = 0.2$, unless otherwise specified). Here, $\bar{p}$ indicates the time mean value of the pressure and the prime indicates unsteady fluctuation. Also, the subscript sp and mic denote, respectively, the loudspeaker and the microphone. Once the acoustic pressure is determined by Equation (7), the acoustic velocity u_{sp}' generated by this pressure fluctuation at the loudspeaker surface is determined by using the acoustic relation $u_{sp}' = p_{sp}'/\rho c$. Here, ρ and c are the unperturbed mean density and speed of sound, respectively. The loudspeaker is modeled as an adiabatic, non-catalytic surface (i.e. $\dfrac{dT}{dn} = 0$ and $\dfrac{dC}{dn} = 0$, where n is the normal direction). Typically, ten grid points along the base of the

step were used to model the loudspeaker surface. The parameter τ is a specified time delay between the signal recorded by the microphone and the control signal used to drive the loudspeaker. In the simulations, the time delay τ/T where T is the time period of the oscillation ($T \approx 1.07$ msec for a Type I oscillation and $T \approx 6.02$ msec for a Type II oscillation), is specified prior to initiation of the active control. At present, a systematic study of the effect of varying the time delay (or phase) has not been carried out. However, some effects of varying the time delay have been investigated, and the results of these simulations are discussed below.

4.1.1 Active Control of Type I Instability

During a Type I instability, the pressure fluctuation at the base of the step shows a peak-to-peak level of around 15 percent of the mean pressure as shown in Figure 4a. For reference, a short time interval of the pressure fluctuation is shown again in Figure 6a. A control system as shown in Figure 1a and obeying the control law as given by Equation (7) were chosen for the study. Cross-correlation analysis of the uncontrolled pressure fluctuations at the microphone and speaker locations was carried out. The result is shown in Figure 6b. This figure shows that for a $\tau/T \approx 0$ the pressure fluctuations at the two locations are nearly perfectly negatively correlated. This indicates that a time delay close to zero should be effective. Figure 6c shows the pressure fluctuations at the base of the step with active control using $\tau/T = 0.03$. Clearly, the controller is quite effective in reducing the peak-to-peak pressure fluctuation level from 15 percent to less than 4 percent of the mean pressure.

Figure 6d shows the pressure signal at the dump plane with another time delay of $\tau/T = 0.15$ used for the control. In this case also the control is quite effective, with the peak-to-peak pressure fluctuation again decreasing to around 4 percent of the mean pressure. This figure also shows the effect of turning off the control at a later stage. The pressure fluctuation quickly recovers to the levels observed earlier with no control. Note that, for $\tau/T = 0.15$, the correlation coefficient is still negative. This seems to suggest that, for a chosen time delay, if the correlation between the pressure signals from the microphone and loudspeaker locations is negative, then the control may be effective. This would imply that there may be a range of time delays for which control of the instability is possible. A similar observation was made in an experimental study at NWC by Schadow et al. (1990). They showed that, in their test rig, the control was most effective within a specific phase range of 250-330 degrees.

That such an effectiveness range in terms of time delay exists can be ascertained from the simulations by comparing the pressure signal shown in Figure 6e with the earlier simulations (Figures 6c and 6d). Figure 6e shows the pressure signal using active control with $A_y = 1$ and a time delay of $\tau/T = 0.5$. For this chosen time delay, the correlation coefficient is strongly positive as can be seen in Figure 6b. It appears that in this case the control signal has only a small effect on the high-frequency oscillation, and the peak-to-peak fluctuation level is not reduced.

In the experimental studies at NWC, the sensor (microphone) was located approximately one step height downstream of the dump plane due to the restrictions imposed by the test rig configuration. To numerically determine the effect of sensor location on the control effectiveness, simulations were performed with the sensor located one step height downstream of the dump plane as in the experiments (location a, Figure 1a). The results of this study (described earlier in Menon, 1990) also showed that control was effective only

for a certain range of time delays.

Flow visualization of the flame propagation during active control showed that the flame structure does not change in any significant manner from the structure seen in the uncontrolled case (Figure 4b). Spectral analysis of the pressure fluctuation in the combustor showed that as the control becomes effective, the dominant frequency increases from 985 Hz to around 1 kHz. When the control is turned off, the frequency drops back to the original value.

4.1.2 Active Control of Type II Instability

The active control strategy employed for the control of a Type I instability was then applied to the Type II instability. A typical time trace of the uncontrolled pressure fluctuation at the base of the step during this instability is shown in Figure 7a. Cross correlation between the pressure signals from the dump plane and the diffuser location b showed that a peak negative correlation occurs around $\tau/T = 0.5$. This is shown in Figure 7b. Thus, it was expected that the control signal using a time delay of $\tau/T = 0.5$ will be effective. Figure 7c shows the pressure signal with the active control system turned on with $\tau/T = 0.5$ for the same time period as in Figure 7a. It is clear that the control strategy was quite effective in reducing the pressure fluctuation levels. In fact, the peak-to-peak level of oscillation, which was around 50 percent of the mean pressure for the uncontrolled case (Figure 7a), is now reduced to almost 4 percent (Figure 7c), which is about the same level as was achieved for the Type I instability. As seen in the figure, the control does take a certain amount of time (roughly equivalent to two periods of the low-frequency oscillation) to become effective. However, increasing the gain parameter A_y reduces the overall time to achieve control as described in Menon (1990). The effect of turning off the control is shown in Figure 7d, which shows the pressure signal after the control signal was turned off at the end of the simulation shown in Figure 7c. Although it takes a finite amount of time, the Type II instability returns.

Another simulation was carried out with a time delay of $\tau/T = 0.03$ between the sensor and control signal. In this case, cross correlation of the original signals (Figure 7b) indicates a strong positive correlation. Figure 7e shows the pressure signal for this control case. This figure clearly shows that the control is quite poor; however, it is interesting to note that the pressure fluctuation level does decrease slowly. Again, as in the Type I control study, these simulations (and others, described in Menon, 1990) suggest that there may be some time delay range in which optimum control of the instability is possible. Further simulations with different time delays are planned to understand the relationship between phase and control effectiveness.

The propagation of the vortex/flame structure seen in the uncontrolled case (Figure 5b) is also changed drastically, with the flame structure now taking a shape similar to that observed during the Type I instability simulation (Figure 3b). A typical flame structure in the combustor during control of the Type II instability is shown in Figure 8a, corresponding to the time shown in Figure 7c. When the control is turned off, the large-amplitude, low-frequency oscillation reappears (Figure 7d) and the flame structure begins to return to the large hooked shape seen in Figure 5b. This is shown in Figure 8b (corresponding to the time shown in Figure 7d).

Spectral analysis of the pressure fluctuation in the combustor both with and without active control (Figures 7c and 7d, respectively) was carried out. When the control is first turned on, the dominant 166 Hz oscillation frequency increases to 175 Hz, but as the control becomes effective and the pressure fluctuation level drops, only a high-frequency

fluctuation at around 1.2 kHz remains. This increase in fluctuation frequency during active control is similar to that observed during control of the Type I simulation described in Section 4.1.1. When the control is turned off, the dominant frequency begins to decrease and the amplitude increases until finally only the low-frequency, large-amplitude oscillation remains.

It is also instructive to look at the acoustic power used to drive the loudspeaker during the control of the Type II instability. Figures 9a and 9b show the acoustic power as a function of time for the control simulations shown in Figures 7c and 7e, respectively. Here, the acoustic power (in watts) is defined as

$$P = 2\pi \int_{r_1}^{r_2} p_{\omega}' u_{\omega}' \, r \, dr \qquad (8)$$

where r_1 and r_2 are the radial dimensions of the loudspeaker. Note that, for the axisymmetric geometry, the modeled loudspeaker is actually a circular strip of thickness $(r_2 - r_1)$. Figure 9a shows that, initially, the loudspeaker is driven at a high power level, but as the control becomes effective the power levels also drops off. Figure 9b shows that, for the case where the control is less effective, the power level is quite high for a longer period of time. However, it is interesting to note that as the control becomes slowly effective (see Figure 7e) the power level also begins to drop off. These data indicate that for effective control of the Type II instability, a large power level is required only for a short time initially, and as control becomes effective, the overall power required becomes quite low. The acoustic power required to drive the loudspeaker during control of the Type I instability (not shown here) is much lower (by an order of magnitude) when compared to the power requirements for the Type II control. Thus, the power requirement for controlling the Type I instability remains quite low all the time. This computed low-power requirement for achieving control is in qualitative agreement with the experimental results of Poinsot et al. (1987).

4.2 Active Control Using Secondary Fuel Injection

Another technique that has been shown to be quite effective in controlling the low-frequency instability is manipulating the unsteady heat release in the combustor. An approach successfully demonstrated by Langhorne and Hooper (1989) involved introducing secondary (premixed) fuel into the combustor. In this technique, the control system uses additional heat release to modify the acoustic energy balance in the combustor. They showed that both steady and pulsed secondary fuel injection can result in effective control of the instability. They also showed that an increase in the maximum available thrust is possible since the controller allows stable combustion at a higher fuel-air ratio than possible without active control. Fuel modulation is also being studied at NWC (e.g., Schadow et al., 1990) as a means for controlling the instability.

In the following, we describe some results obtained using secondary fuel injection as a control system. Both steady and pulsed (unsteady) fuel injection are being studied, and, so far, two locations have been used as the secondary fuel injector locations. The first location was at the base of the step at approximately the same location where the loudspeaker was located (Figure 1a, location s_1) for the acoustic feedback control study (although only a smaller region with typically five grid points was used to model the injector). Axial fuel injection was modeled at this location. The second location was just upstream of the dump plane in the inlet duct (Figure 1a, location s_2), and normal injection (in the negative r direction) was modeled. Note that, when secondary fuel is

injected axially behind the step, the cold fuel enters the recirculation zone where primarily hot product exists. Thus, the fuel immediately ignites and burns. However, when secondary fuel is introduced upstream of the dump plane, the primary stream is still all (cold) fuel and ignition will not occur. In this case, the effect of secondary fuel addition will be to increase the total mass flow of the fuel entering the combustor.

The injection conditions were determined by first prescribing a reference parameter, $\dot{M} = \dot{m}_{inj}/\dot{m}_{ref}$, where $\dot{m}_{inj}$ is the mass flow rate of the secondary fuel injected, and $\dot{m}_{ref}$ is the reference mass flow rate at the inlet. Systematic variation of $\dot{M}$ has not yet been carried out. All simulations described here were carried out for $\dot{M} = 0.3$. This is higher than the secondary fuel flow rate used by Langhorne and Hooper (1989). However, the current ramjet geometry, the control system and the test conditions are quite different from their experimental setup. Further simulations for different choices of $\dot{M}$ are planned for the future. The secondary fuel temperature was chosen to be the same as the fuel temperature (T_{f_0}) of the primary inflow in the inlet. The flow inclination was specified depending upon whether it is axial injection at the base of the step $(v = 0)$ or normal injection in the inlet $(u = 0)$. The injection pressure was chosen depending upon the type of injection control system used. For steady injection, the injection pressure was the same as the primary inflow reference pressure. For pulsed injection, the injection pressure is a function of time depending upon the control function used (described below). Finally, the injection velocity is determined using the prescribed $\dot{M}$ and the other specified flow conditions.

At present, only a few simulations using both steady and unsteady injection have been carried out. However, the results obtained so far show some interesting effects of secondary fuel injection on the combustion instability mechanism. Some representative results are discussed here.

4.2.1 Active Control of Type I Instability

Two simulations are described here with secondary fuel injection as a control system. The reference uncontrolled fluctuation during the Type I instability was the same as that shown in Figure 6a. The same injection conditions were used for both simulations, and the only difference was the injector location. A pulsed injection strategy was employed whereby injection was turned on only when the condition $p_{mic}' < 0$ was satisfied. Here, the subscript mic indicates the same sensor location b as shown in Figure 1a. This method is somewhat similar to that used by Langhorne and Hooper (1989), although in their case, a time delay was also employed. At present, simulations using pulsed injection with a time delay have not been carried out but will be addressed in the future.

Figure 10a shows the pressure fluctuation at the base of the step with pulsed axial injection at the loudspeaker location (Figure 1a, location s_1). The control appears to be only weakly effective and the fluctuation level does not decrease significantly from the uncontrolled case. A very high frequency oscillation also appears in the pressure signal during this simulation.

Figure 10b shows the same pulsed conditions now used to inject premixed fuel just upstream of the dump plane (Figure 1a, location s_2). In this case, the pressure fluctuation actually begins to show a signature similar to that observed during a Type II instability. The original high-frequency oscillation disappears, and the low-frequency, large-amplitude oscillation similar to a Type II instability appears. The flame structure also starts to show the large structure seen during a Type II

instability. The typical flame structure observed during the low-frequency oscillation is shown in Figures 10c and 10d.

The results described above indicate that the control of a Type I instability using secondary fuel injection has not been successful. However, note that there are other possible control strategies that may succeed. The effect of varying M and the injection locations also needs to be addressed in more detail.

4.2.2 Active Control of Type II Instability

The control of a Type II instability using secondary fuel injection was studied using both steady and pulsed injection. Figure 11a shows the pressure fluctuation at the base of the step with secondary steady fuel injection at location s_1. In this case, the secondary fuel injection is quite successful in reducing the pressure oscillation in the combustor. The peak-to-peak pressure level drops from the original 50 percent level to less than 4 percent of the mean pressure. This is quite similar to that observed during acoustic feedback control. The effect of secondary fuel injection on the flame propagation is shown in a time sequence of the flame in Figures 11b through 11e. These figures (which correspond to the times shown in Figure 11a) show that, initially, the secondary fuel injection into the hot product region at the base of the step causes the formation of a new flame. However, due to flow recirculation behind the base of the step, this flame cannot propagate downstream but eventually merges with the primary flame at the step corner. As the control becomes effective, the flame no longer shows the characteristic hooked-flame shape seen during a Type II instability.

Figures 12a and 12b show, respectively, two simulations with secondary fuel injection upstream in the inlet duct. For the simulation shown in Figure 12a, a steady injection similar to that used for control described in Figure 11 was used. In this case, the control is not very effective; however, the peak-to-peak pressure fluctuation level does decrease from the original 50 percent level to around 30 percent of the mean pressure. A typical flame structure observed during this simulation is shown in Figures 13a and 13b.

Finally, Figure 12b shows the pressure fluctuation occurring during pulsed secondary fuel injection in the inlet duct. The injection strategy was similar to that used for the Type I control study shown in Figure 10b. However, unlike that case, this control system is quite effective in controlling the Type II instability, with the pressure fluctuation level again decreasing to around 5 percent of the mean pressure. A typical flame structure observed during this control is shown in Figure 13c. Figure 12b also shows the effect of switching off the fuel injection. The fluctuation level quickly increases to around 10 percent but then appears to level off. However, the simulation has not been carried out far enough to determine if the Type II instability will reappear. Further study using different injection conditions and time delays are planned to understand the effect of secondary fuel injection on the combustion instability mechanism.

5. CONCLUSIONS

A large-eddy simulation model has been developed that contains the essential physics of combustion instability such as the acoustic wave motion, interactions between large eddies, and combustion and unsteady heat release during premixed fuel combustion in a ramjet. The combustion model used for the simulations explicitly incorporates the local turbulent flame speed and avoids the erroneous numerical heat release that would occur in a finite-rate chemistry model while attempting to resolve the internal structure of the flame. Two types of combustion instability have been

identified from the simulation results: a small-amplitude, high-frequency instability and a large-amplitude, low-frequency instability. Both types of instability have been experimentally observed, and many of the qualitative features of the numerically computed instabilities are in good agreement with the experimental observations.

The data stored during the simulations were then utilized to study active control techniques to control the unstable pressure oscillations. Both acoustic feedback and secondary fuel injection control systems have been studied. The control study using acoustic feedback demonstrated that control of both types of instability can be accomplished successfully. Furthermore, it was shown that the instabilities could be turned on and off. This capability can be used to study and understand the transient process prior to the growth of the instability. Both the control and recovery of the Type II instability take a relatively longer time period compared to the Type I instability. Some effects of varying the time delay between the sensor and the control signal were also studied, and it was shown that control is possible for different choices of the time delays. This is in qualitative agreement with experimental observations.

The effects of both steady and pulsed secondary fuel injection on the instability mechanism were also studied. For the conditions studied so far, the Type I instability could not be successfully controlled. In fact, in one case, the Type I instability shifts to the low-frequency, large-amplitude Type II instability as a result of secondary fuel injection. However, secondary fuel injection, both steady and pulsed, was shown to be quite effective on the Type II instability. Significant reduction in the pressure fluctuation levels was observed during pulsed injection upstream in the inlet duct and during steady injection at the base of the step. Results obtained so far using secondary fuel injection indicate that a more careful parametric study is warranted to determine the mechanism by which the additional heat release affects the instability mechanism.

Further work is planned in addition to these control studies to improve the simulation model by including the subgrid model described earlier. The simulation of combustion instability in the full ramjet will be carried out in the near future, and control strategies will be studied for more realistic flow conditions.

ACKNOWLEDGEMENT

REFERENCES

Bloxridge, G. J., Dowling, A. P., Hooper, N., and Langhorne, P. J. (1988) "Active Control of Reheat Buzz," AIAA J., Vol. 26, pp. 783-790.

Bogar, T. J., and Sajben, M. (1979) "The Role of Convective Perturbations in Supercritical Inlet Oscillations," CPIA Publication No. 412.

Crump, J. E., Schadow, K. C., Yang, V., and Culick, F. E. C. (1986) "Longitudinal Combustion Instabilities in Ramjet Engines: Identification of Acoustic Modes," J. Propulsion and Power, Vol. 2, No. 2, pp. 105-109.

Culick, F. E. C. (1989) "Combustion Instabilities in Liquid-Fueled Propulsion Systems - An Overview," AGARD CP-450, pp. 1.1-1.73.

Erlebacher, G., Hussaini, M. Y., Speziale, C. G., and Zang, T. A. (1987) "Toward the Large-Eddy Simulation of Compressible Turbulent Flows," ICASE Report No. 87-20, NASA Langley Research Center.

Ferziger, J., and Leslie, D. C. (1979) "Large-Eddy Simulations: A Predictive Approach to Turbulent Flow Computations," AIAA-79-1471.

Germano, M. (1990) "Averaging Invarience of the Turbulent Equations and Similar Subgrid Modeling," CTR-116, Center for Turbulence Research, Stanford University.

Gulati, A., and Mani, R. (1990) "Active Control of Unsteady Combustion-Induced Oscillations," AIAA-90-0270.

Gutmark, E., Parr, T. P., Hanson-Parr, D. M., and Schadow, K. C. (1989) "On the Role of Large and Small-Scale Structures in Combustion Control," Combustion Sci. and Tech., Vol. 66, pp. 107-126.

Gutmark, E., Parr, T. P., Parr, D. M., and Schadow, K. C. (1990) "Active Control of a Premixed Flame," AIAA-90-2448.

Hedge, U. G., Reuter, D., Zinn, B. T., and Daniel B. R. (1987) "Fluid Mechanically Coupled Combustion Instabilities in Ramjet Combustors," AIAA-87-0216.

Jou, W.-H., and Menon, S. (1987) "Simulations of Ramjet Combustor Flow Fields, Part II. Origin of Pressure Fluctuations," AIAA-87-1422.

Jou, W.-H., and Menon, S. (1990) "Modes of Oscillations in a Nonreacting Ramjet Combustor Flow," J. Propulsion and Power, Vol. 6, No. 5, pp. 535-543.

Kailasanath, K., Gardner, J. H., Oran, E. S., and Boris, J. P. (1989) "Effects of Energy Release on High Speed Flows in an Axisymmetric Combustor," AIAA-89-0385.

Kerstein, A. R., Ashurst, W. T., and Williams, F. A. (1988) "Field Equation for Interface Propagation in an Unsteady Homogeneous Flow Field," Physical Rev. A., Vol. 37, No. 7, pp. 2728-2731.

Lang, W., Poinsot, T., and Candel, S. (1987) "Active Control of Combustion Instability," Comb. and Flame, Vol. 70, pp. 281-289.

Langhorne, P. J., and Hooper, N. (1989) "Attenuation of Reheat Buzz by Active Control," Presented at the AGARD Meeting on Combustion Instability in Liquid-Fueled Propulsion Systems, AGARD-CP-450, pp. 10.1-10.16.

Menon, S., and Jou, W.-H. (1987) "Simulations of Ramjet Combustor Flow Fields, Part I: Numerical Model, Large-Scale and Mean Motions," AIAA-87-1421.

Menon, S., and Jou, W.-H. (1990a) "Numerical Simulations of Oscillatory Cold Flows in an Axisymmetric Ramjet Combustor," J. Propulsion and Power, Vol. 6, No. 5, pp. 525-534.

Menon, S., and Jou, W.-H. (1990b) "Large-Eddy Simulations of Combustion Instability in an Axisymmetric Ramjet Combustor," AIAA-90-0267, to appear in Combustion Science and Technology.

Menon, S. (1990) "Numerical Simulation and Active Control of Combustion Instability in a Ramjet Combustor," AIAA Paper No. 90-3930, submitted to Combustion and Flame.

Piomelli, U., Ferziger, J. H., and Moin, P. (1987) "Models for Large-Eddy Simulations of Turbulent Channel Flows Including Transpiration," Report TF-32, Dept. of Mechanical Engineering, Stanford University.

Poinsot, T. J., Bourienne, F., Esposito, E., Candel, S., and Lang, W. (1987) "Suppression of Combustion Instability by Active Control," AIAA-87-1876.

Schadow, K. C., Gutmark, E., Parr, T. P., Parr, D. M., Wilson, K. J., and Crump, J. H. (1987) "Large-Scale Coherent Structures as Drivers of Combustion Instability," AIAA-87-1326.

Schadow, K. C., Gutmark, E., and Wilson, K. J. (1990) "Active Combustion Control in a Coaxial Dump Combustor," AIAA-90-2447.

Schmidt, H., and Schumann, U. (1989) "Coherent Structure of the Convective Boundary Layer Derived from Large-Eddy Simulations," J. of Fluid Mechanics, Vol. 200, pp. 511-562.

Smith, D. A., and Zukoski, E. E. (1985) "Combustion Instability Sustained by Unsteady Vortex Combustion," AIAA-85-1248.

Speziale, C. G. (1985) "Galilean Invarience of Subgrid-scale Stress Models in the Large-Eddy Simulation of Turbulence," J. of Fluid Mechanics, Vol. 156, pp. 55-62.

Sterling, J. D., and Zukoski, E. E. (1987) "Longitudinal Mode Combustion Instabilities in a Dump Combustor," AIAA-87-0220.

Williams, F. A. (1985) Combustion Theory, Second Edition, Benjamin/Cummings Publishing Co.

Yakhot, V. (1989) "Propagation Velocity of Premixed Turbulent Flame," Combustion Sci. and Tech., Vol. 60.

Yoshizawa, A. (1986) "Statistical Theory for Compressible Turbulent Shear Flows, with the Application to Subgrid Modeling," Physics of Fluids, Vol. 29, No. 7, pp. 2152-2164.
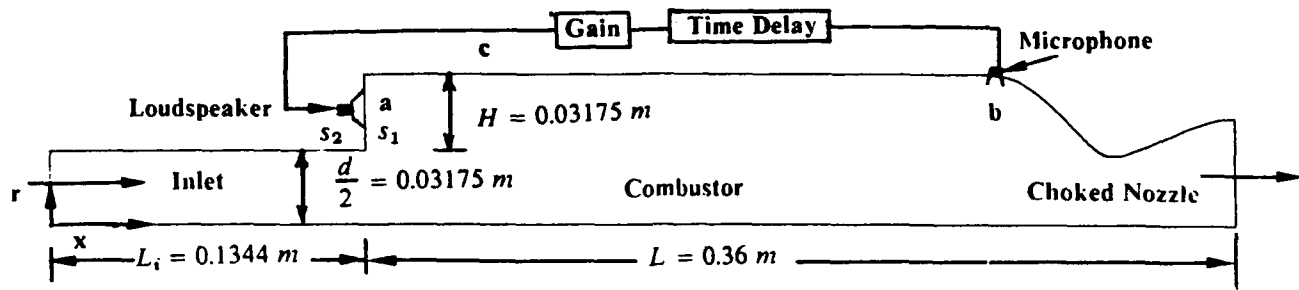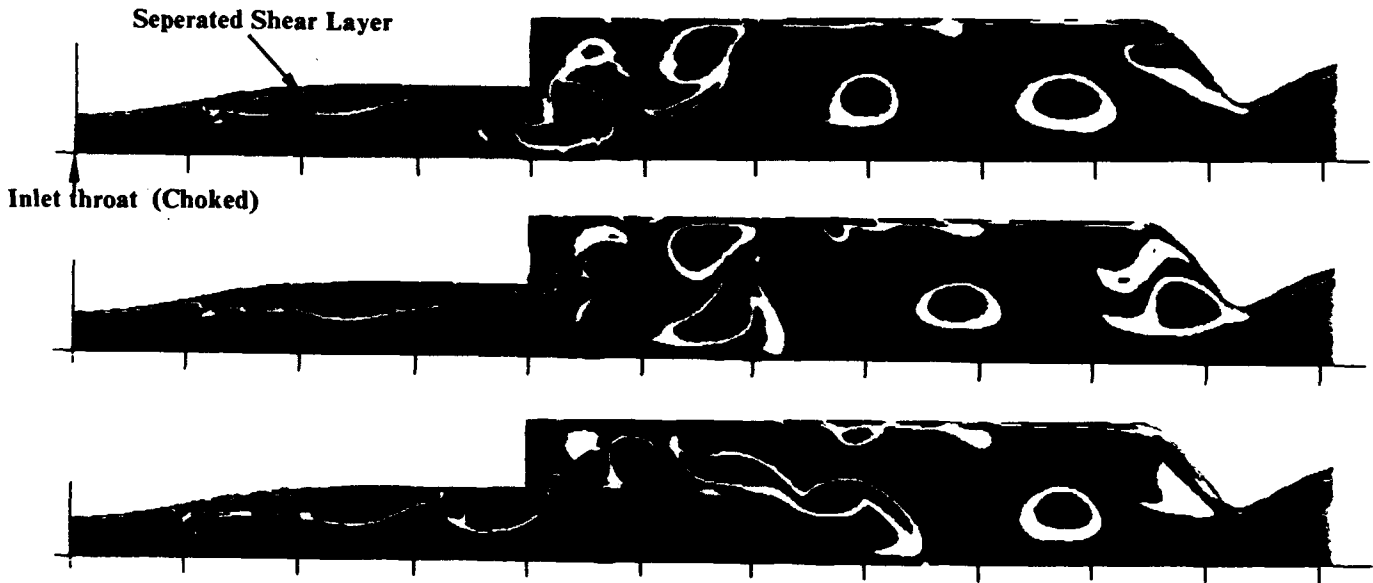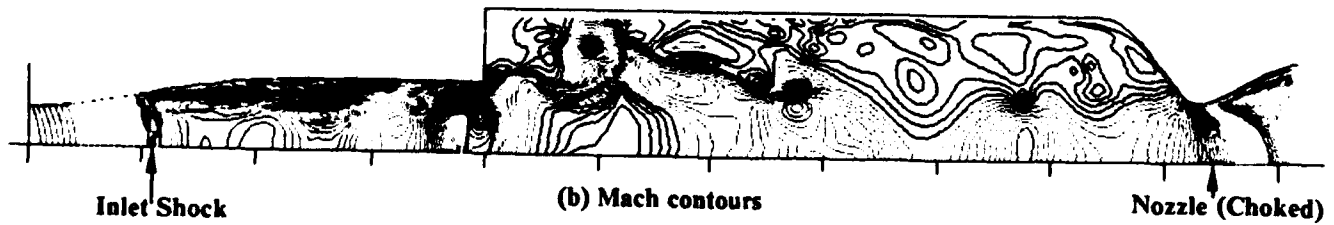
(a) The ramjet geometry without the inlet nozzle
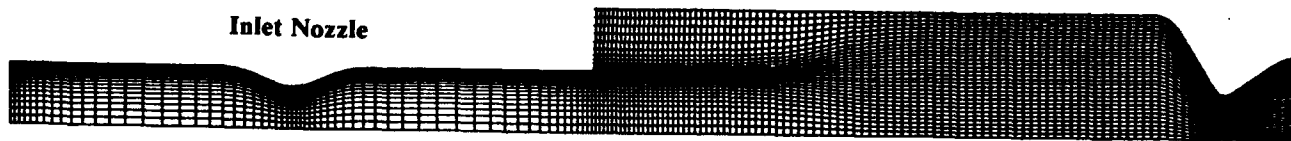
(b) The full ramjet geometry with a 320 x 64 grid distribution

Figure 1. The ramjet engine configuration

(a) Time sequence of vorticity contours

(b) Mach contours

Figure 2. Typical cold flow field in a full ramjet engine
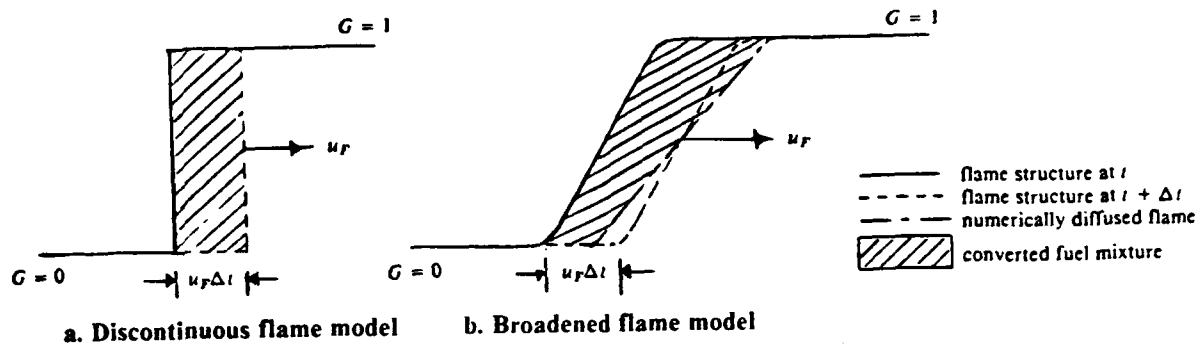
a. Discontinuous flame model   b. Broadened flame model
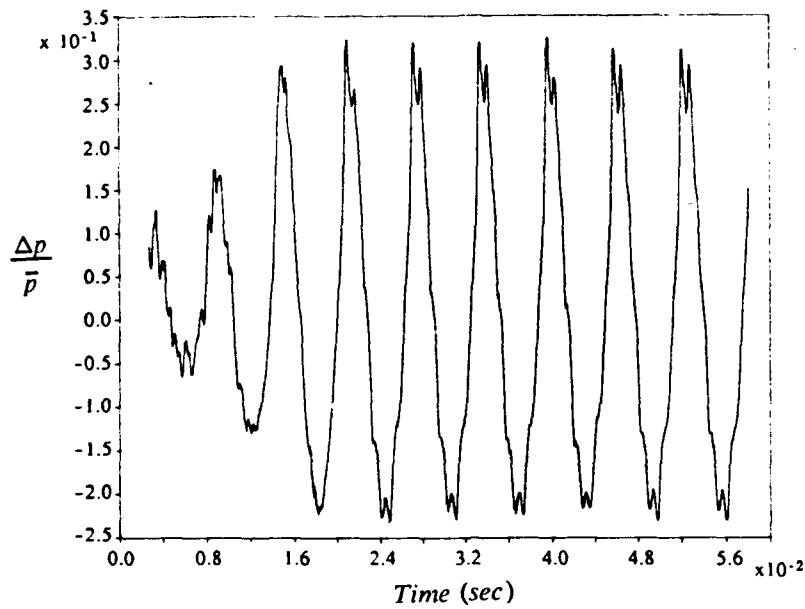
Figure 3. The discontinuous and diffused flame structure

a. Pressure fluctuation at the base of the step

Time (sec)

b. Flame structure

c. Vorticity field

d. Experimental

(Smith and Zukoski, 1985)
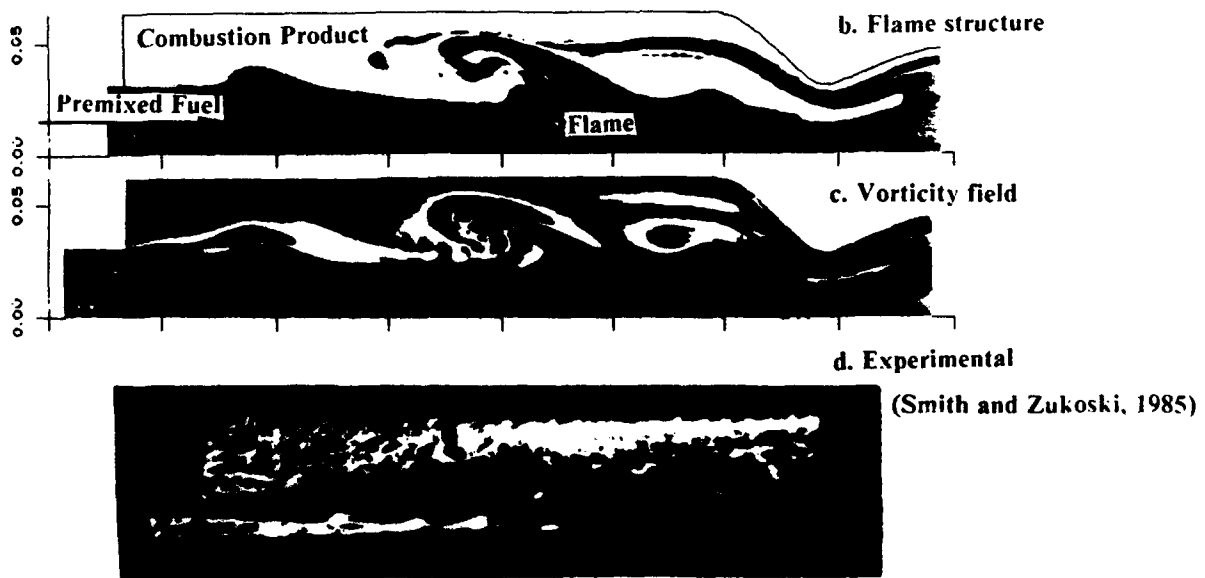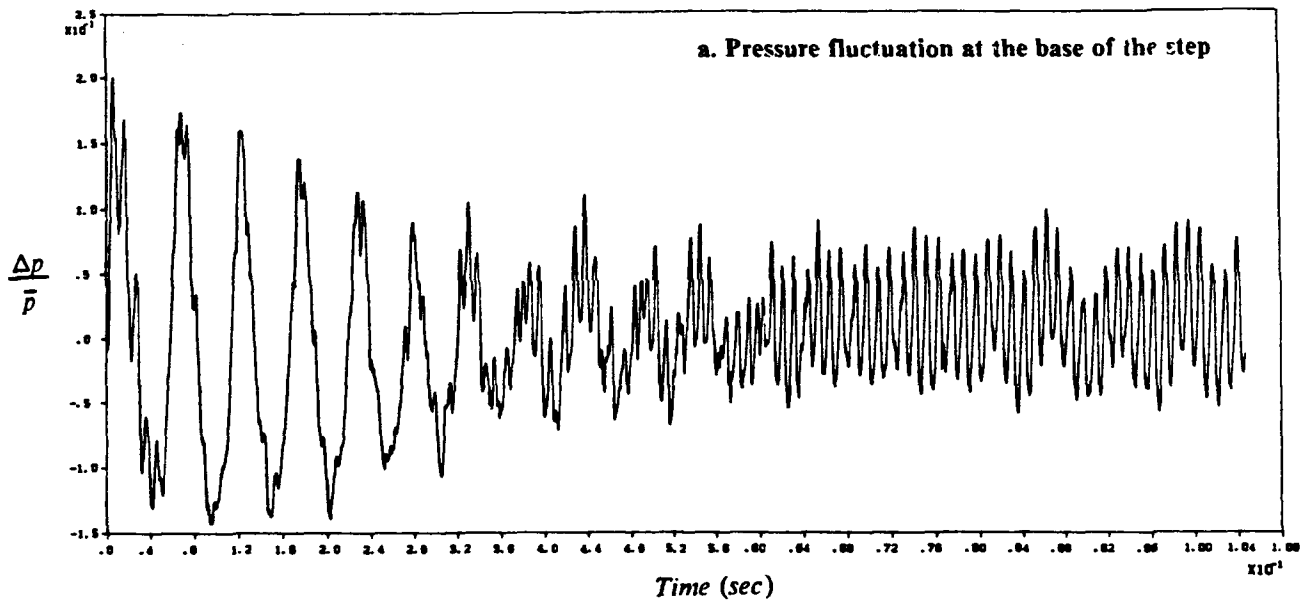
Figure 4. Typical flow features observed during Type I Instability

a. Pressure fluctuation at the base of the step

b. Flame structure

c. Vorticity field

d. Experimental
(Smith and Zukoski, 1985)
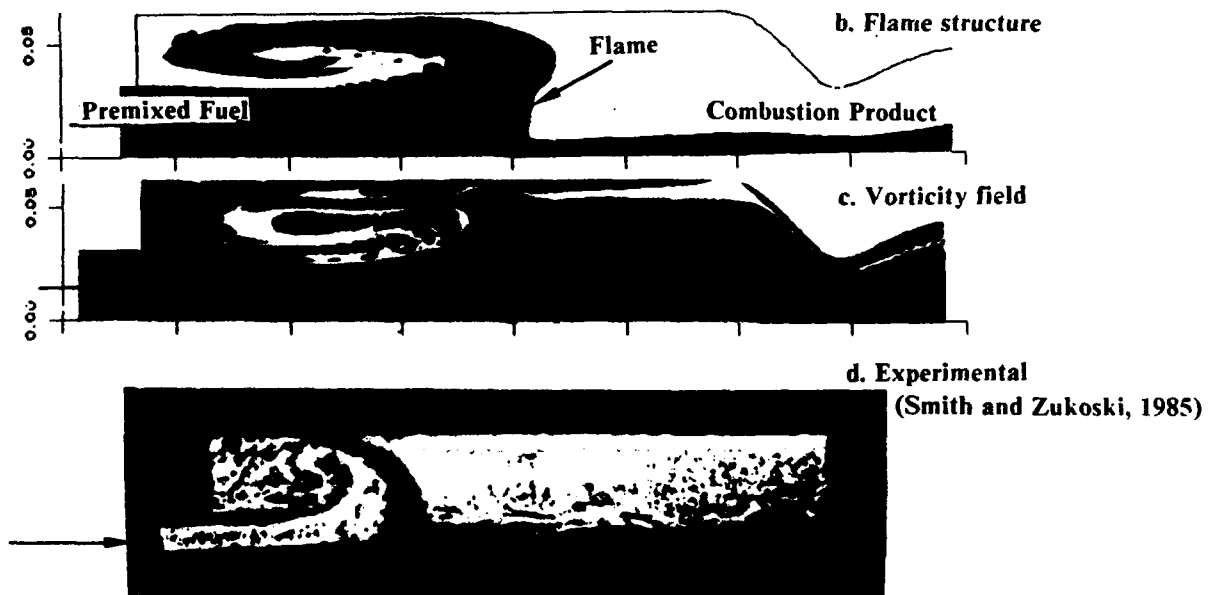
Figure 5. Typical flow features observed during Type II combustion instability.
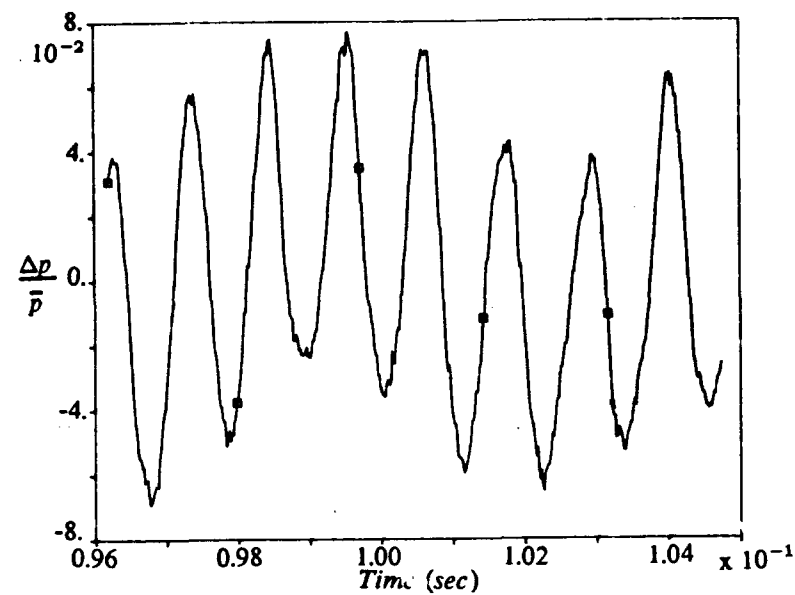
(a) Control OFF; Reference signal
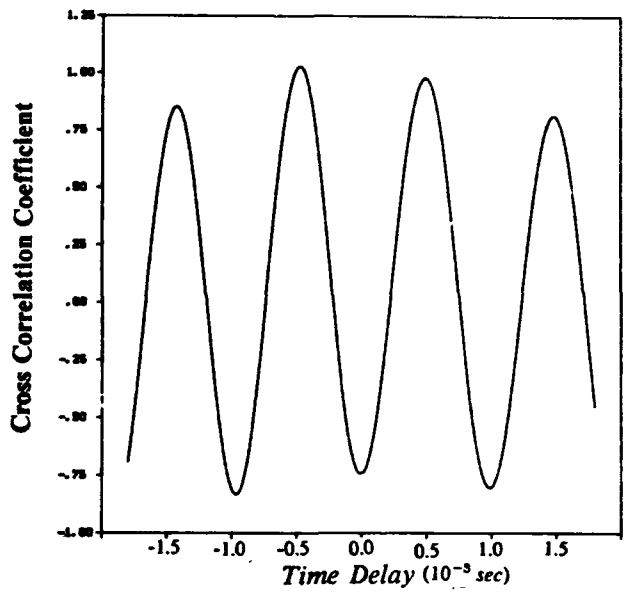
(b) Correlation between the pressure signals at the speaker and microphone locations
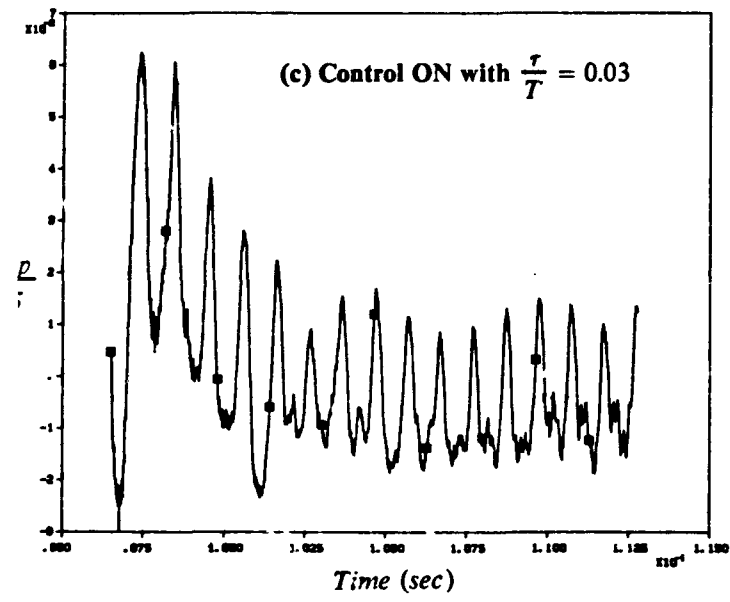
(c) Control ON with $\frac{\tau}{T} = 0.03$
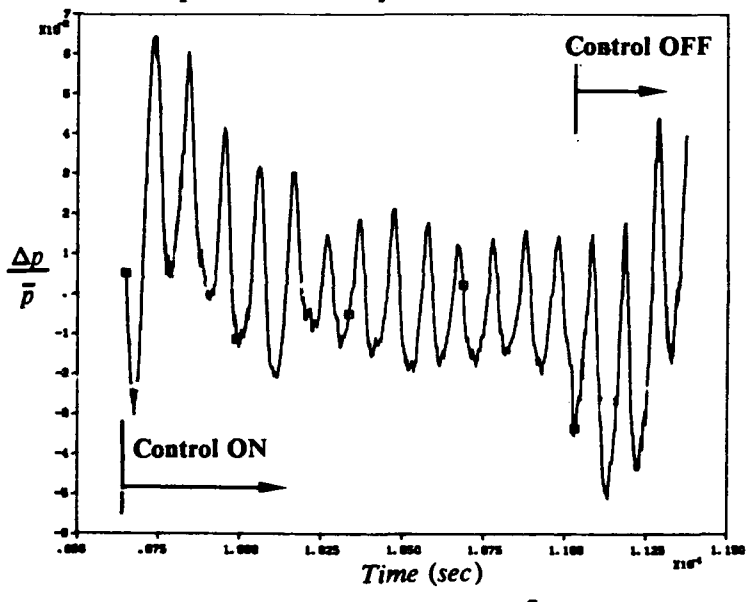
(d) Control ON/OFF with $\frac{\tau}{T} = 0.15$
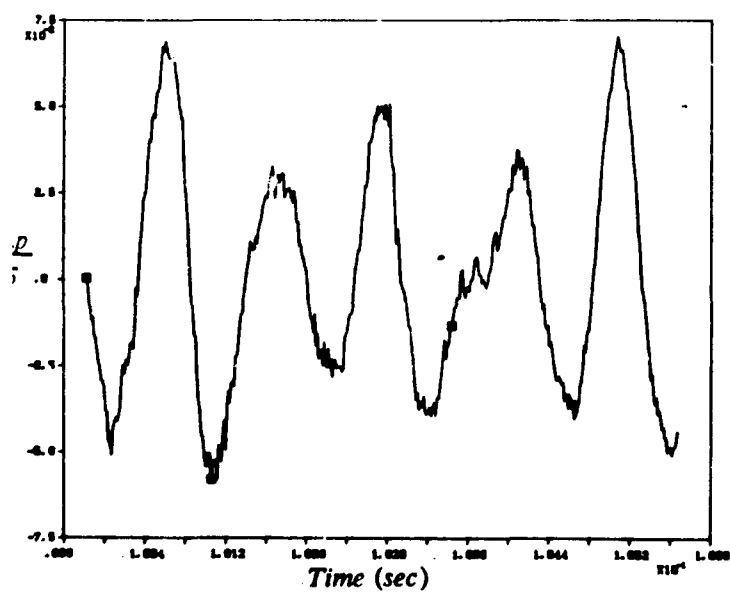
(e) Control ON with $\frac{\tau}{T} = 0.5$

Figure 6. The effect of acoustic feedback control on the Type I instability
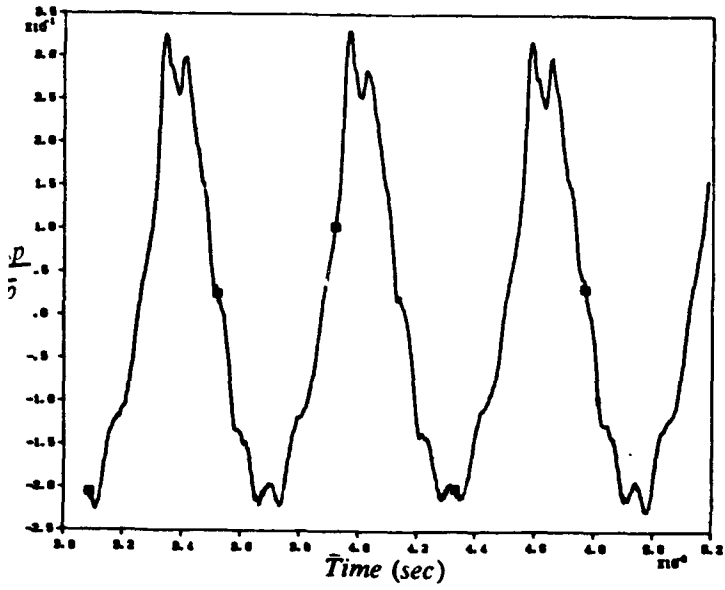
(a) Control OFF; Reference signal
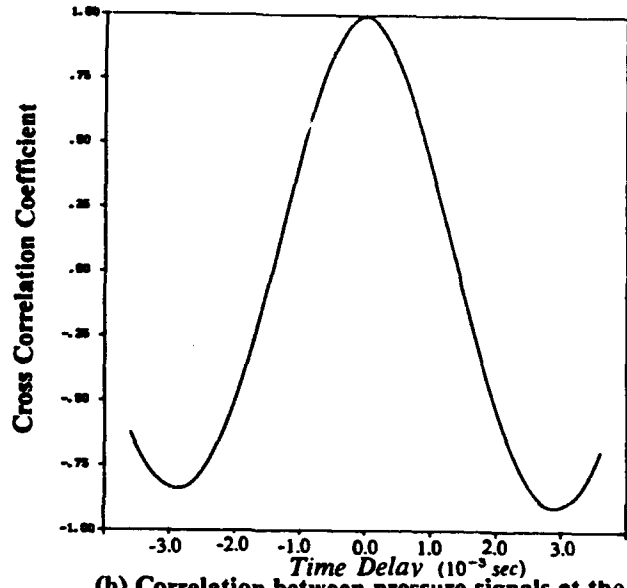
(b) Correlation between pressure signals at the speaker and microphone locations
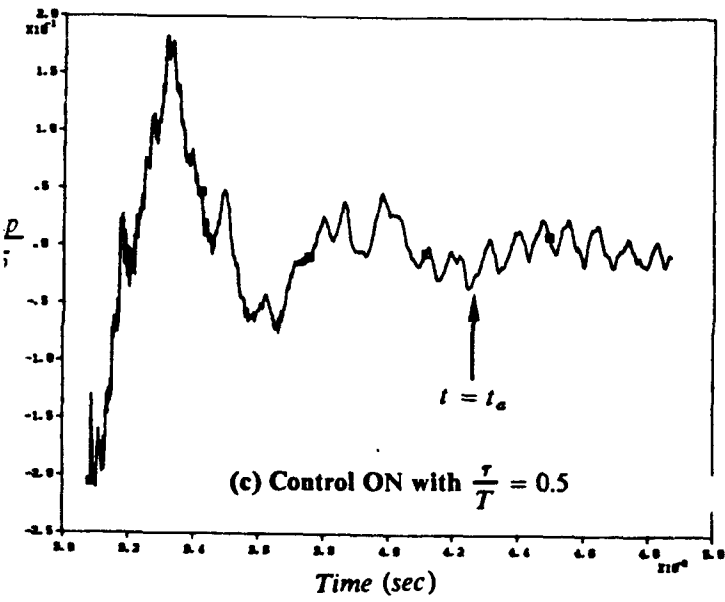
(c) Control ON with $\frac{\tau}{T} = 0.5$
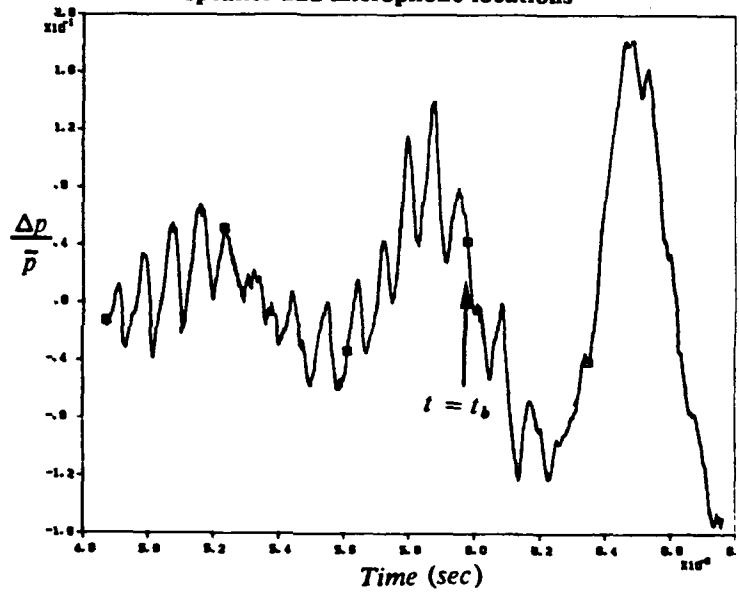
(d) Control OFF, after control ON in Figure 7c
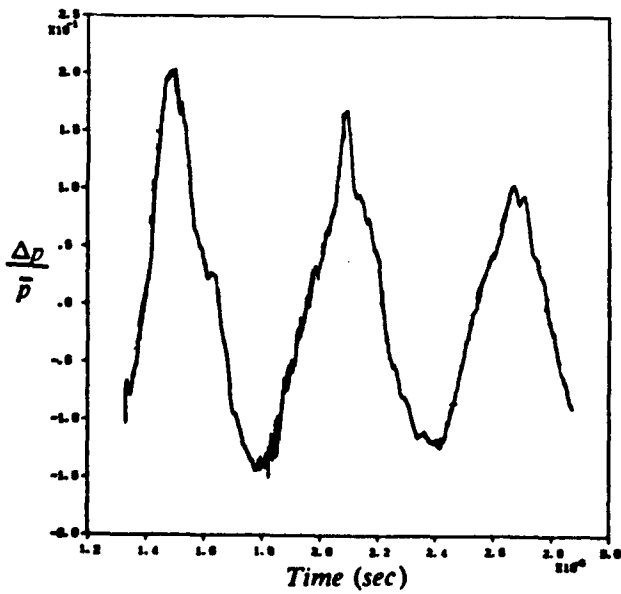
(e) Control ON with $\frac{\tau}{T} = 0.03$

Figure 7. The effect of acoustic feedback control on the Type II instability

(a) Control ON with $\frac{\tau}{T} = 0.5$ ($t = t_a$, Figure 7c)

(b) Control OFF ($t = t_b$, Figure 7d)
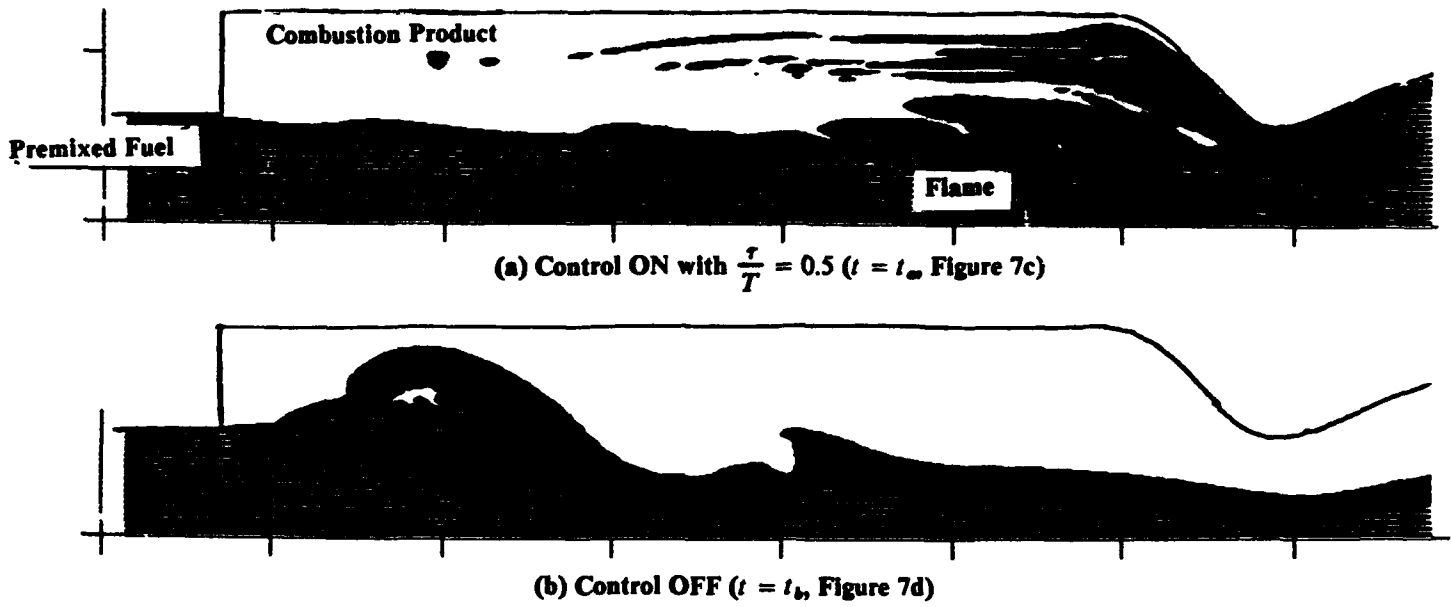
Figure 8. Typical flame structure during acoustic feedback control of Type II instability

(a) Control ON with $\frac{\tau}{T} = 0.5$

(b) Control ON with $\frac{\tau}{T} = 0.03$
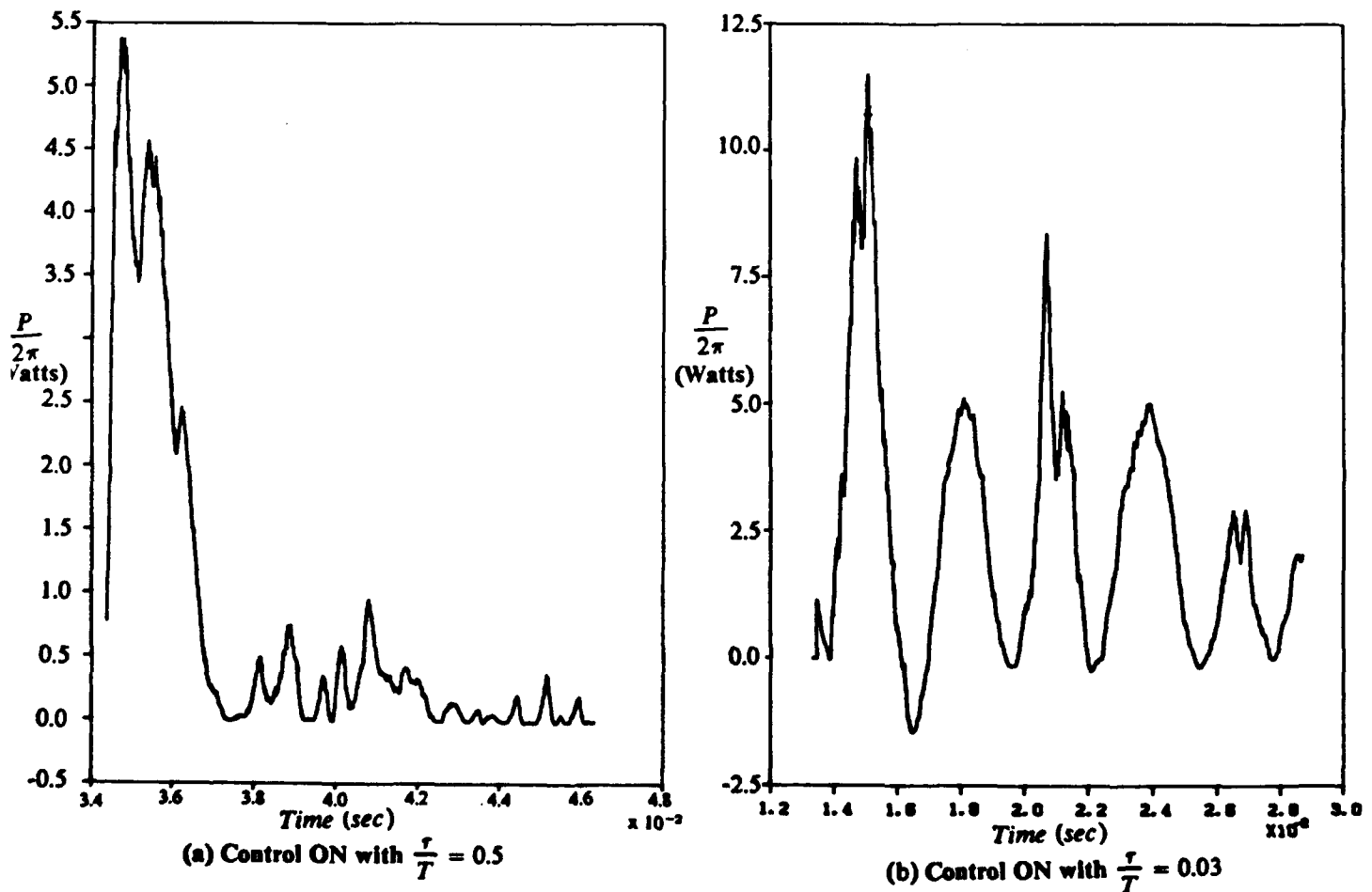
Figure 9. Acoustic power of the loudspeaker during control of Type II instability
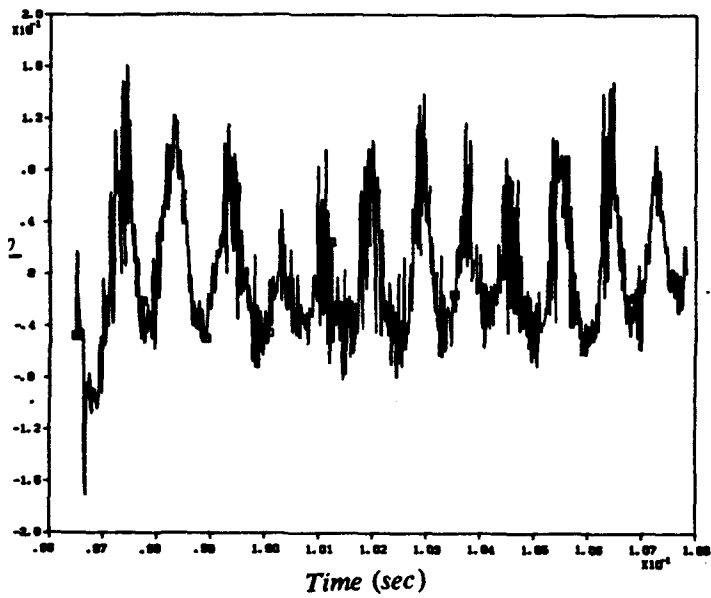
(a) Pulsed injection at the base of the step.
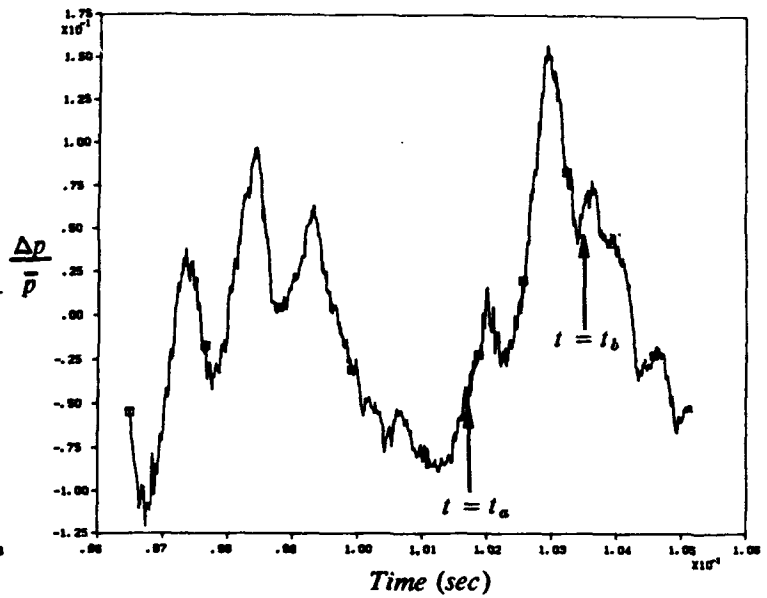
(b) Pulsed injection upstream of the dump plane.
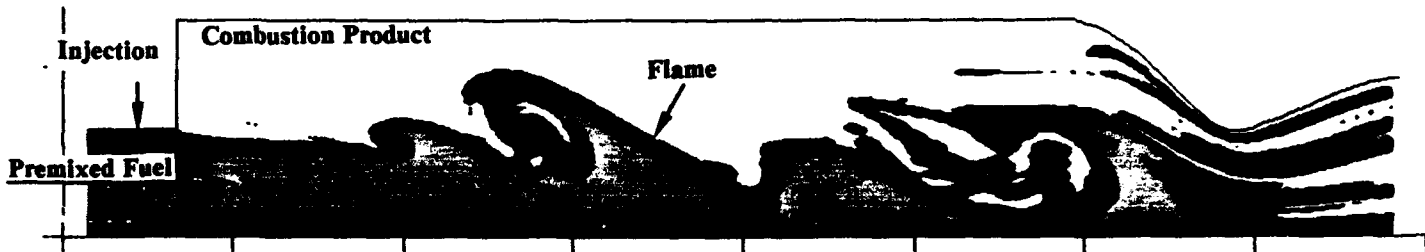
(c) Flame structure at $t = t_a$ (Figure 10b)
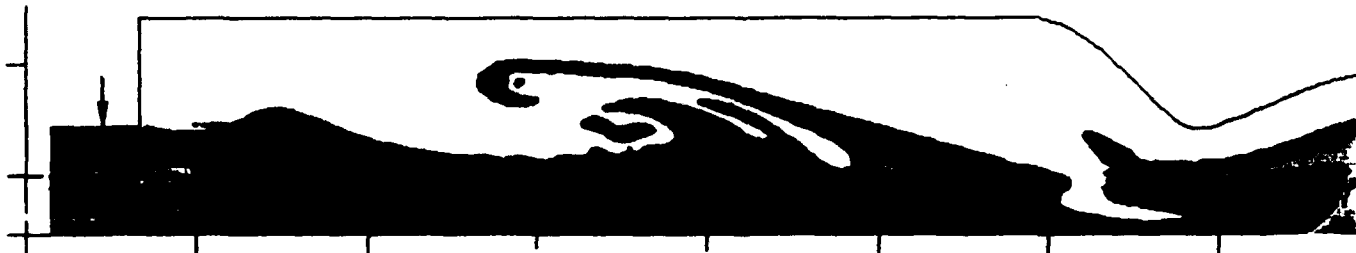
(d) Flame structure at $t = t_b$ (Figure 10b)

Figure 10. The effect of secondary fuel injection control on the Type I instability
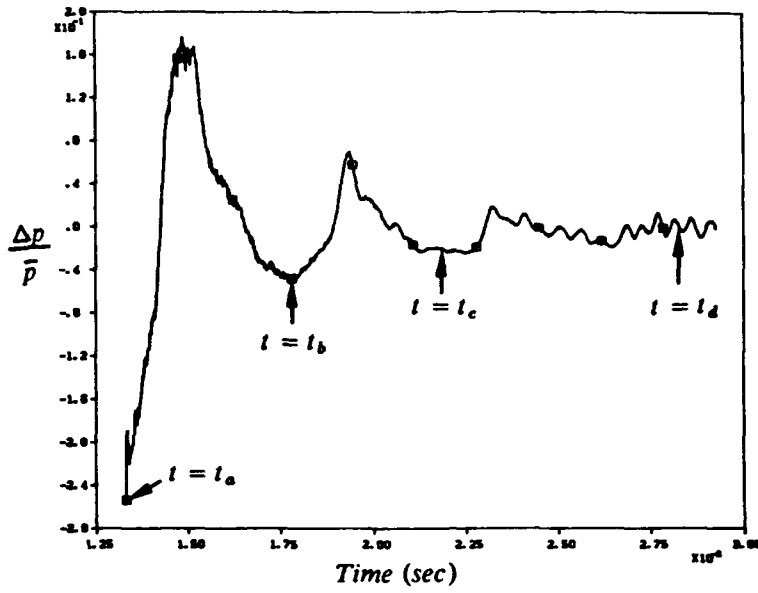
(a) Pressure fluctuation at the base of the step
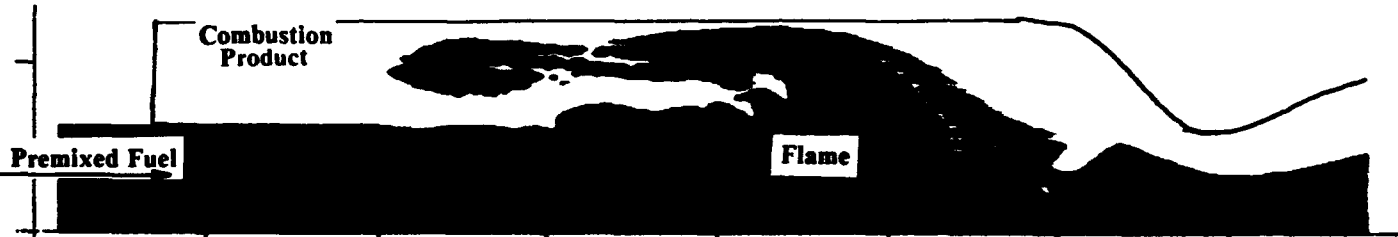
(b) Flame structure at $t = t_a$
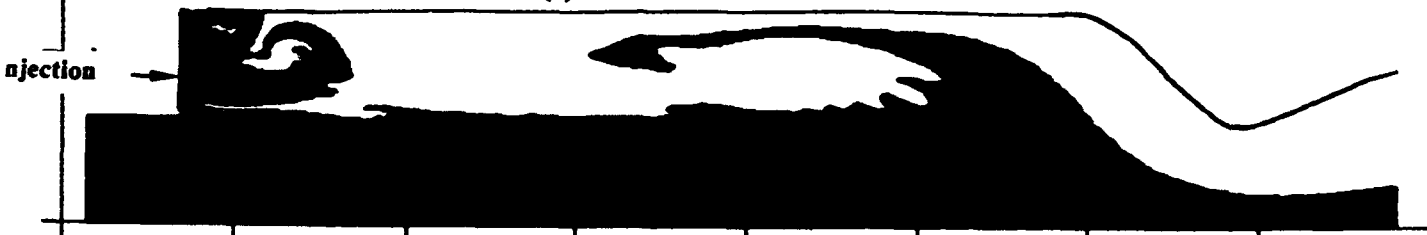
(c) Flame structure at $t = t_b$

(d) Flame structure at $t = t_c$

(e) Flame structure at $t = t_d$

Figure 11. The effect of secondary fuel injection control on Type II instability.
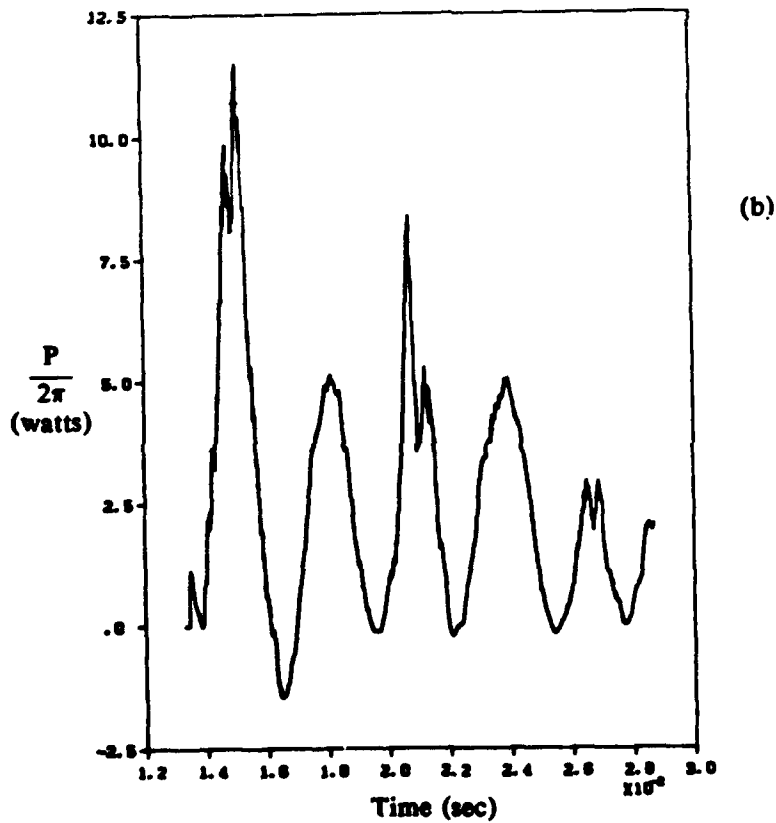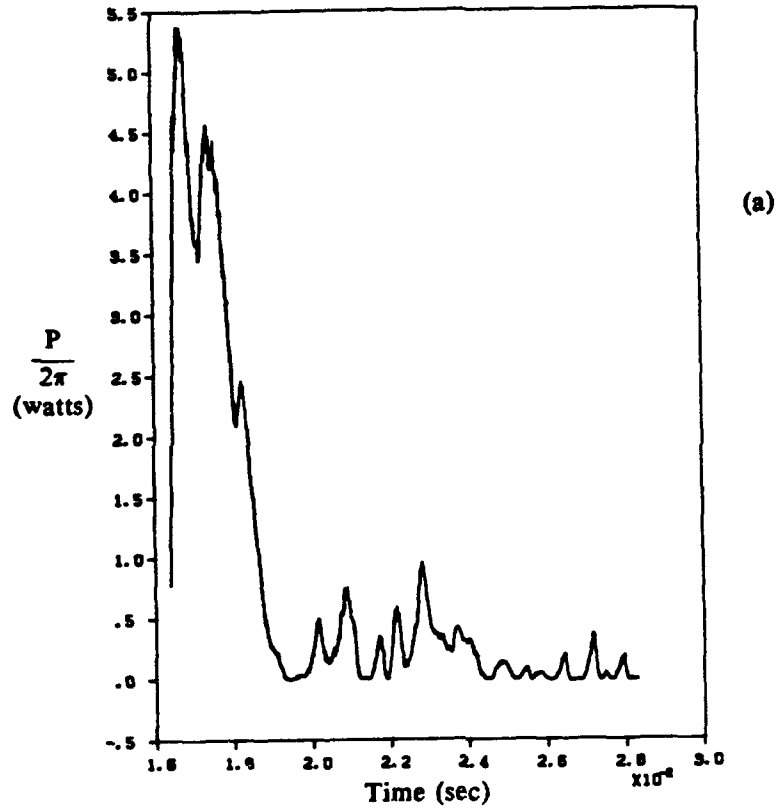Steady injection at the base of the step.

FIGURE 12 Acoustic power of the loudspeaker during active control of Type II instability; (a) control ON with $r/T = 0.5$, (b) control ON with $r/T = 0.03$.

AIAA 90-3930
Numerical Simulation and Active Control of Combustion Instability in a Ramjet Combustor

S. Menon
Quest Integrated, Inc.
(formerly Flow Research, Inc.)
Kent, WA

AIAA 13th Aeroacoustics Conference
October 22-24, 1990 / Tallahassee, FL

NUMERICAL SIMULATION AND ACTIVE CONTROL OF COMBUSTION INSTABILITY IN A RAMJET COMBUSTOR

Suresh Menon*
Quest Integrated, Inc.
(formerly Flow Research, Inc.)
Kent, Washington

ABSTRACT

A large-eddy simulation model has been developed to study combustion instability in a ramjet combustor. A model for premixed combustion is employed in the numerical scheme that explicitly uses the local turbulent flame speed in the governing equation. This not only reduces the computational effort as compared to a model with detailed finite-rate chemical kinetics, but also avoids the potential error in the amount of heat release caused by numerical diffusion. Combustion instability in the ramjet has been numerically simulated. Two types of instability are observed: a small-amplitude, high-frequency instability and a large-amplitude, low-frequency instability. Both such instabilities have been experimentally observed and various computed flow features are in good qualitative agreement with experimental observations. The information obtained from these simulations has been used to develop an active control strategy to suppress the instability. Control of both types of combustion instability was successfully achieved using the acoustic feedback technique, and the control could be used to turn the instability on and off. The pressure fluctuation levels in the combustor are significantly reduced when active control is used.

1. INTRODUCTION

Combustion instability in a ramjet engine is an extremely complex phenomenon involving nonlinear interactions among acoustic waves, vortex motion and unsteady heat release. Typically, the instability manifests itself as a large-amplitude pressure oscillation in the low-frequency range (100-800 Hz). This instability is related to longitudinal acoustic waves and is the most difficult to control. When the amplitude of the pressure oscillation reaches some critical limit, it can result in system failure either by causing structural damage due to fatigue or by causing an engine "unstart," which occurs when the shock in the inlet duct can no longer be stabilised downstream of the choked inlet throat and is expelled to form a bow shock ahead of the inlet. This phenomenon of engine unstart is one of the most serious technical problems encountered in developing an operational ramjet engine. Therefore, in recent years, a major research program was undertaken, both experimentally (e.g., Schadow et al., 1987; Gutmark et al., 1989; Smith and Zukoski, 1985; Sterling and Zukoski, 1987; Hedge et al., 1987) and numerically (e.g., Culick, 1989; Menon and Jou, 1990a, 1990b; Jou and Menon, 1990; Kailasanath et al., 1989), to determine the mechanism of the combustion instability. More recently, methods for controlling this instability using active control techniques are being studied experimentally (e.g., Gulati and Mani, 1990; Langhorne and Hooper, 1989; Schadow et al., 1990; Gutmark et al., 1990). This paper discusses a study of active control techniques using large-eddy simulations.

2. THE SIMULATION MODEL

The simulation model used in this study was developed through a series of numerical experiments starting with cold flow studies (Menon and Jou, 1987, 1990a; Jou and Menon, 1987, 1990) and culminating in the simulation of combustion instability (Menon and Jou, 1990b). The equations solved in this model are the full compressible Navier-Stokes equations formulated in the axisymmetric coordinate system. The ramjet combustor modeled in these studies consists of an axisymmetric inlet duct that is connected to an axisymmetric dump combustor by a sudden expansion. A convergent-divergent nozzle is attached downstream of the combustor. Figure 1 shows the typical ramjet configuration used in these studies.

2.1 The Numerical Model

To simulate the unsteady flow field in a ramjet combustor, the governing equations are solved subject to appropriate boundary conditions. For the flow of a viscous fluid over a solid surface, the no-slip conditions are applied along an adiabatic wall. On the centerline of the device, the symmetry conditions are applied for all variables. The inflow and outflow boundaries are computational boundaries and the number of independent boundary conditions was determined from the local characteristics of the system of hyperbolic equations when viscous effects are neglected locally. On the subsonic inflow boundary, there are three incoming characteristics corresponding to the vorticity wave, the entropy wave and the right-running acoustic wave. Therefore, three conditions were chosen by specifying the stagnation temperature, the stagnation pressure, and the local flow inclination. The characteristic variable carried by the outgoing characteristic is determined by solving the pertinent decoupled interior characteristic equation. Although this set of boundary conditions is physically reasonable, there is potentially an uncertainty in the specification of the stagnation pressure since, in unsteady flows, it would contain a contribution from the time derivative of the velocity potential. The application of these boundary conditions implies certain "impedance" conditions (Chu and Kovasznay, 1958). The characteristics of the current impedance condition were examined by a linearised analysis and the condition was proven to be of the damping type. Therefore, the pressure disturbances that reach the inflow boundary will not be amplified and thus the computed self-sustained oscillations in the combustor are self-generated.

In a practical ramjet device, it has been noted that the flow oscillations downstream of the shock in the inlet diffuser may participate in the flow oscillations in the combustor (Yang and Culick, 1985; Bogar and Sajben, 1979). Thus, a more specific upstream impedance condition for the ramjet configuration would be the acoustic impedance at the inlet shock. To implicitly obtain such a realistic condition, the

inlet nozzle has been incorporated into the computational domain and a new study has begun in which the inlet shock will be captured as a part of the solution. The results of this study will be reported elsewhere.

Implementation of proper outflow boundary conditions is considered important since any nonphysical boundary condition there could generate spurious upstream propagating acoustic waves in the combustor. This is specially true when a subsonic outflow boundary condition is used. In the ramjet model simulated here, a convergent-divergent nozzle is attached downstream of the combustor. This is similar to an operating device configuration. The flow through this nozzle is choked and the outflow is supersonic. Since at supersonic outflow conditions all four characteristics are outgoing, the boundary conditions imposed there will not affect the interior flow field.

The numerical scheme used for these simulations is an explicit finite volume method based on MacCormack's technique. The numerical model and the validation study have been described elsewhere (Menon and Jou, 1987, 1990a). The scheme is second-order accurate in space and time, and no explicit artificial dissipation is used. High-resolution grids, typically 256x64, were used in all the simulations discussed here. The grid lines were clustered in the critical regions such as the inlet duct boundary layer and the separated shear layer where the length scale of the flow features is expected to be small. Structures with length scales of the order of the boundary layer thickness can be resolved by employing the current grid resolution.

In a practical ramjet device, the Reynolds number of the flow is extremely high. A large-eddy simulation (LES) of such a flow would require a validated subgrid model. Subgrid models for compressible flows have just begun to be investigated. However, the validity of these models as applied to complex flows has not yet been proven. Therefore, in the present study, the simulations were performed for flows in a moderate Reynolds number range as the first step towards understanding the physical processes involved. To model the dissipative effects of the subgrid turbulence, a constant eddy-viscosity model is employed. This eddy-viscosity is chosen to be the laminar dissipative coefficient at the reference temperature and can be viewed as a simple subgrid model, as noted by Ferziger and Leslie (1979). Further improvements to the subgrid model are currently being carried out. A subgrid eddy-viscosity model based on renormalization group theory (Yakhot and Orszag, 1986) and a new one-equation subgrid model are currently being evaluated and the results will be reported in the future. The latter model, which solves the subgrid kinetic energy equation, is considered more appropriate for the combustion model used here, as will be shown in the next section.

2.2 The Combustion Model

To simulate combustion instability, an accurate evaluation of the chemical heat release is required. In particular, the amount of heat release and its time-dependent spatial distribution must be computed. In premixed combustion, the amount of heat release per unit length of the flame is determined by the local flame speed and by the specific chemical energy available in the fuel, provided the flame thickness is small compared to the radius of curvature of the flame. The flame can be treated as a discontinuity and numerically captured as a smeared discontinuity as long as the important physics, such as the amount of heat release at the flame sheet, can be accurately computed. This combustion model is a good approximation in LES, since in LES the large-scale coherent structures are computationally resolvable features and the flame is only thickened by the subgrid turbulent

diffusion. This model is also preferable to models in which detailed finite-rate kinetics are considered. In finite-rate kinetics models, the numerical simulations are presumed to compute the local flame speed implicitly and thus the amount of heat release. Since the flame speed depends upon the dissipation mechanism in the flame structure, this implies that the internal structure of the flame must be resolved (Williams, 1985). However, this is not practically achievable, since in LES the number of grid points that can be used is limited by the capacity of the computer and therefore an adequate resolution of the flame structure is not possible. Furthermore, all numerical schemes have some form of artificial dissipation, either built into the scheme or explicitly provided to stabilize the computations. Thus, the computed flame structure and the local flame speed are contaminated by the numerical dissipation and could in fact be completely overwhelmed by the numerical diffusion.

To circumvent this problem, a model for premixed combustion based on the thin-flame model (Williams, 1985; Kerstein et al., 1988) was incorporated (Menon and Jou, 1990b). In this model, the local turbulent flame speed u_F appears explicitly and is determined as a function of the laminar flame speed u_l and the local subgrid turbulence intensity u' using the renormalization group (RNG) theory model of Yakhot (1989). The effects of detailed chemical kinetics are contained in the laminar flame speed, and a progress variable G is defined which is governed by the equation

$$\frac{\partial G}{\partial t} + \vec{u}\cdot\nabla G = -u_F\left|\nabla G\right| \tag{1}$$

where $\vec{u}$ is the fluid velocity, $G = 1$ for the fuel mixture, and $G = 0$ for the combustion product.

The turbulent flame speed u_F is given by the RNG model as

$$\frac{u_F}{u_l} = \exp\left[\frac{u'^2}{u_F^2}\right] \tag{2}$$

Yakhot (1989) found that Equation (2) correlates quite well with various experimental observations. The laminar flame speed contains information on the chemical kinetics and the molecular dissipation; once the local subgrid turbulence intensity is determined, Equation (2) can be used to find u_F for a given fuel mixture.

The chemical heat release is a function of G and the specific chemical energy of the fuel mixture. The chemical energy of the mixture is included in the formulation by specifying the specific enthalpy h of the mixture in the energy equation as

$$h = C_pT + h_fG \tag{3}$$

Here, h_f is the heat of formation of the premixed fuel, C_p is the specific heat of the mixture at constant pressure, and T is the temperature. The heat of formation of the fuel essentially determines the amount of heat released during combustion and thus is a function of the equivalence ratio for a given fuel. The product temperature T_p can be estimated for a given heat of formation for the fuel by the relation

$$h_f = C_p(T_p - T_{fu}) \tag{4}$$

where T_{fu} is the fuel temperature at the inlet. In the simulations, the combustion product temperature is initially specified, and the heat of formation determined from Equation (4).

Due to the explicit appearance of the local flame speed in Equation (1), the amount of heat release does not depend on the computed internal structure of the flame. Even when numerical diffusion broadens the flame, the flame speed is not severely affected. The effect of numerical broadening is

2

shown in Figure 2. In a discontinuous flame model (Figure 2a), the flame propagates at a velocity u_F into the mixture. Therefore, the amount of fuel converted to product is proportional to $u_F \Delta t$, where Δt is the timestep. When the flame is broadened by numerical diffusion, the smeared flame still propagates into the fuel mixture with flame speed u_F, and the amount of fuel mixture converted to product is approximately the same as in the discontinuous flame model, as can be seen in Figure 2b. The fact that the numerical flame broadening has only a small effect on the amount of converted fuel mixture, and thus on the heat release, was demonstrated in an earlier paper (Menon and Jou, 1990b).

To complete the combustion model described above the subgrid turbulence intensity must be specified. As noted above, this can be determined if a subgrid model for the turbulent kinetic energy is solved. Such a model is currently under evaluation. For the present application, a uniform value of the subgrid turbulent intensity is used, typically a few percent of the reference velocity. Some important physical properties, such as the spatial nonuniformity of subgrid turbulence and its effect on the local flame speed and the amount of heat release, are not included in the present model. However, as shown earlier (Menon and Jou, 1990b), the major qualitative interactions between the large-scale vortex structures and the combustion heat release have been captured by the present simulation model. The effect of nonuniform subgrid turbulence on combustion instability will be discussed elsewhere (Menon, 1991).

3. SIMULATION OF COMBUSTION INSTABILITY

The details of the simulation of combustion instability in a ramjet combustor are described elsewhere (Menon and Jou, 1990b). The present focus is on active control of the numerically simulated combustion instability. Before describing the control studies, however, some important features of the computed instability are described in this section.

In general, combustion instability in a combustor depends upon various parameters such as the system geometry, the flow parameters, the fuel type, and the equivalence ratio. In the earlier study (Menon and Jou, 1990b), in addition to the flow parameters (e.g., the Mach number M and the Reynolds number Re) and the geometrical parameters (e.g., L_i, L, A_{inlet}/A^*; see Figure 1), two important thermochemical parameters were identified. One is $\theta = T_p/T_o$, which is the ratio of the product temperature to the stagnation temperature T_o; the other is $\sigma = u_F/u_{ref}$, which is the ratio of the characteristic flame speed to the characteristic reference velocity u_{ref}. For a fixed fuel mixture, θ can be related to the equivalence ratio ϕ, and σ can be related to the chemical kinetic rate and the level of subgrid turbulence. The effect of varying the geometrical parameter, the ratio between the inlet and throat areas A_{inlet}/A^* and the thermochemical parameters θ and σ have been studied (Menon and Jou, 1990b). In this section, two simulations will be described that showed two different types of combustion instability: a small-amplitude, high-frequency combustion instability (Type I) and a large-amplitude, low-frequency combustion instability (Type II). Both types of instability have been observed in various experimental studies (e.g., Smith and Zukoski, 1985; Sterling and Zukoski, 1987; Schadow et al., 1987). The active control of these instabilities will be the focus of this paper and is described in the next section.

For both the simulations discussed here, the flow parameters such as the reference Reynolds number and the reference Mach number were held fixed at Re = 10,000 and M = 0.32, respectively, based on the inlet duct diameter and the reference velocity of u_{ref} = 100 m/sec. The thermochemical parameters θ and σ were also held fixed at $\theta = 5$ and

$\sigma = 0.05$. For $\theta = 5$, the product temperature T_p was 1500 K, which corresponds approximately to the product temperature of a methane-air mixture at an equivalence ratio of around 0.65 (Malte et al., 1977). Alternatively, this could be interpreted as a type of premixed fuel that has a product temperature of 1500 K at some mixture ratio. All system (geometrical) parameters such as H, L_i, and L were held fixed for both simulations except for the area-ratio parameter A_{inlet}/A^*, which was increased from 1.05 for the Type I instability simulation to 1.20 for the Type II simulation. This was accomplished by reducing the nozzle throat area A^*. This results in a decrease in the inlet mass flow rate and reduces the inlet mean flow velocity u_{in} by approximately 14 percent. At present, the reason for the shift in the instability mechanism from Type I to Type II instability when the mean velocity is reduced is not entirely clear. A plausible explanation is that the effective thermochemical parameter $\sigma^* = u_F/u_{in} = \sigma(u_{ref}/u_{in})$ increases when the mean inlet velocity decreases. In the earlier study (Menon and Jou, 1990b) it was shown that when σ was increased for fixed mean flow velocity, the Type II instability is excited. A similar behavior is observed here when σ^* is increased from around 0.042 for the Type I instability to around 0.048 for the Type II instability. This appears to indicate that σ^* may be a more general thermochemical parameter than σ. Further study is required to determine if this hypothesis is valid. In the following sections, we describe some pertinent features of Type I and Type II combustion instabilities.

3.1 Small-Amplitude, High-Frequency Instability (Type I)

In Type I combustion instability, the pressure oscillations initially show a large-amplitude, low-frequency oscillation that eventually decays so that only a high-frequency oscillation remains. The peak-to-peak level of the high-frequency pressure fluctuation is around 15 percent of the mean pressure, as shown in Figure 3a. This was around three times higher than that observed in earlier cold flow studies (Menon and Jou, 1990a). Although the fluctuation level is small, it is by no means insignificant for a realistic ramjet combustor and may be sufficient to expel the inlet shock.

Flow visualization showed that the shear layer separating at the rearward-facing step rolls up into vortices; further downstream, these vortices undergo pairing as observed in earlier cold flow studies. The flame front initially resides along the high shear region in the shear layer, and as the vortex rollup/pairing process occurs, the flame is entrained into the vortical structures. The typical flame structure and vorticity field distribution for this simulation is shown in Figures 3b and 3c. For comparison, a flow visualization by Smith and Zukoski (1985) for premixed "stable" combustion in a two-dimensional combustor is shown in Figure 3d. There is qualitative agreement between the numerical and experimental observations as discussed in Menon and Jou (1990b).

Classical considerations using the Rayleigh criteria have been used in past studies (e.g., Sterling and Zukoski, 1987; Hedge et al., 1987) to demonstrate that, for instability to occur, the unsteady fluctuations in heat release should be in-phase locally with the pressure fluctuations. A local Rayleigh parameter $R(\vec{s}, t)$ is defined such that

$$R(\vec{s}) = \frac{1}{T} \int_T q'(\vec{s}, t) p'(\vec{s}, t) dt \qquad (5)$$

where T is the time period and $q'(\vec{s}, t)$ and $p'(\vec{s}, t)$ are the unsteady heat release term and the pressure fluctuation, respectively. When $R(\vec{s})$ is positive, then local amplification occurs. When $R(\vec{s})$ is integrated radially, one obtains $R(z)$, which is the axial variation of the Rayleigh parameter. Alternatively, if $R(\vec{s}, t)$ is integrated in both the axial and

3

radial directions, a volume-averaged parameter $\bar{R}(t)$ is obtained, which represents the time-dependent state of the combustion process in the combustor. If $\bar{R}(t)$ is further integrated in time, a global Rayleigh parameter R^* is obtained.

Both $R(z)$ and $\bar{R}(t)$ in the combustor were evaluated for this simulation. Figure 4a shows the time-dependent variation of the volume-averaged Rayleigh parameter $\bar{R}(t)$ normalized by R^* for two cycles of the high-frequency pressure fluctuation. Also shown is the normalized pressure fluctuation $(\Delta p/\bar{p})$ at the base of the step for this simulation period. Note that the curve for $\bar{R}(t)/R^*$ has been rescaled by a factor to simplify comparison. This figure shows that during the high-frequency oscillations there are periods of time when the combustion process is stable. If we assume that the pressure fluctuation shown in this figure is representative of the volume-averaged unsteady pressure field (an assumption that is strictly not valid since the amplitude of the high-frequency oscillation is not a constant in the combustor), then to obtain the observed variation in the Rayleigh parameter, the unsteady heat release term should have a variation as sketched in Figure 4a. This indicates that the unsteady heat release fluctuations occur at a much higher frequency than the pressure fluctuation during the Type I instability. Figure 4b shows the axial variation of the Rayleigh parameter $R(z)/R^*$ for the time period shown in Figure 4a. Although the combustion process is globally unstable, there are regions in the combustor where it is locally stable. The combustion process is highly unstable in the diffuser region where the vortices in the shear layer impinge on the wall.

3.2 Large-Amplitude, Low-Frequency Instability (Type II)

In Type II combustion instability, the pressure fluctuations show a large-amplitude, low-frequency oscillation with peak-to-peak levels around 50 percent of the mean pressure, as shown in Figure 5a. The oscillation rapidly reaches a limiting cycle and shows a type of pressure signature that is typical of what is observed during combustion instability. The flame propagation is quite different from that observed during Type I instability. A large hooked-flame structure propagates through the combustor at a low frequency, and associated with this flame is a large mushroom-shaped vortical structure. The combined vortex/flame structure propagates through the combustor at the same low frequency. Spectral analysis showed that the dominant mode of oscillation is occurring at a frequency of around 166 Hz. The amplitude and phase of the pressure oscillation at various locations in the combustor was nearly the same, indicating that this pressure oscillation is similar to the bulk-mode oscillation observed in some experiments.

The typical flame structure and the vorticity field are shown in Figures 5b and 5c. For comparison, the experimental visualization of Smith and Zukoski (1985) is shown in Figure 5d. Further analysis was carried out by Menon and Jou (1990b), and it was shown there that many characteristics of this Type II combustion instability, such as the pressure and velocity fluctuation levels, the phase relation between the pressure and velocity fluctuations, and various features of the vortex/flame structure propagation, qualitatively agreed with experimental observations.

The Rayleigh criteria for this instability was also computed. Figure 6a shows the variation of $\bar{R}(t)/R^*$ and the pressure fluctuation at the dump plane for a period of the low-frequency oscillation. During the Type II instability, the pressure amplitude is nearly the same throughout the combustor and thus the pressure fluctuation shown in Figure 6a can be considered to represent the volume-averaged pressure

field in the combustor. Figure 6a shows that there are two time periods during which the combustion process is stable. Again, this is due to a phase difference between the pressure fluctuations and the unsteady heat release term as shown in Figure 6a. However, unlike the Type I instability case (Figure 4a), the fluctuation in the heat release term appears to be occurring at the same low frequency as the pressure fluctuation. The spatial variation of the Rayleigh parameter, $R(z)/R^*$, is shown in Figure 6b. As seen during the Type I instability (Figure 4b), the combustion process is highly unstable near the vortex impingement region in the diffuser. Figure 6b also shows that there is a region near the dump plane where the combustion process is locally stable. This is different from the case seen during Type I instability (Figure 4b) during which multiple regions with locally stable combustion are present in the combustor.

4. ACTIVE CONTROL OF COMBUSTION INSTABILITY

Using the stored data for these two simulations, a new study was initiated to investigate techniques for controlling the instability. Experimentally, there are various approaches being considered. In general, active control strategies fall in three categories: control using acoustic feedback (e.g., Lang et al., 1987; Poinsot et al., 1987; Gutmark et al., 1990; Schadow et al., 1990); control by unsteady modification of the inlet mass flow rate (e.g., Bloxsidge et al., 1988); and control by manipulation of the unsteady heat release in the combustor (e.g., Langhorne and Hooper, 1989). Each of these methods has shown promise in laboratory tests. In this paper, the focus of the numerical experiments is the study of active control using acoustic feedback.

Active control through acoustic forcing was demonstrated earlier by Lang et al. (1987) and Poinsot et al. (1987). The latter study showed that this technique provided the capability of turning the instability on or off at will, thereby providing a means to study the transient behavior. It was also shown that the power required for control was quite small and that control can be achieved over a wide range of phase differences. This indicates that the control technique is not an anti-sound approach, which would have required a specific phase relation. Recent studies at the Naval Weapons Center (NWC), China Lake (e.g., Schadow et al., 1990; Gutmark et al., 1990) have further demonstrated that acoustic feedback control of the combustion instability in a ramjet-type configuration is possible. The present numerical research is aimed at modeling a flow field similar to that being experimentally studied at NWC.

A typical acoustic feedback system used in the experiments involves a loudspeaker/microphone system in the active control loop. In this technique, the pressure signal is sensed at some chosen location using a microphone (or a pressure transducer). The signal is analyzed, phase-shifted, and amplified, and then fed back at some other chosen location using a loudspeaker (see Figure 1). If the control signal from the loudspeaker destructively interferes with the pressure oscillation in the combustor, then the oscillations will become damped, thereby achieving control of the instability. Here, a similar technique has been studied numerically.

4.1 Active Control of Type I Instability

Before implementing the active control method, the effect of direct acoustic forcing was studied. Spectral analysis showed that the high-frequency pressure oscillation for the Type I instability occurred at a frequency of 935 Hz. Using this information, the simulation was restarted at an earlier time and a small region at the base of the step was modeled as a loudspeaker (see Figure 1). This loudspeaker was then forced at a fixed frequency of 935 Hz so that the

4

acoustic pressure generated by the speaker could be modeled as

$$p_{sp}' = A \sin(\omega t) \qquad (6)$$

where A is the amplitude and ω is the frequency. The amplitude was chosen to be 5 percent of the mean pressure. The acoustic velocity generated by this fluctuation was determined by the relation $u' = p'/\rho c$, where ρ is the unperturbed density and c is the speed of sound. The results of this study (not shown here) showed that the oscillation level was not reduced; in fact, the forcing resulted in a small increase in the peak-to-peak fluctuation levels. Thus, it appeared that this open-loop control approach was not effective for this type of instability.

For the closed-loop control study, a location near the downstream diffuser wall was chosen as the microphone (sensor) location (location b, Figure 1). The unsteady pressure signal at this location, p_{mic}', was used to force the loudspeaker using the relation

$$p_{sp}' = -Ga\, p_{mic}' \qquad (7)$$

where the gain Ga was defined as $Ga = A_g \dfrac{\bar{p}_{sp}}{\bar{p}_{mic}}$ and A_g is a constant. Also, $\bar{p}$ is the mean pressure and the subscript sp and mic indicate the loudspeaker and the microphone, respectively. If the sensor signal is of the form given by Equation (6), then Equation (7) implies that $p_{sp}' = Ga \sin(\omega t + \phi)$, where ϕ is 180 degrees.

Figure 7a shows the original pressure signal near the base of the step, and Figure 7b shows the pressure signal using active control with $A_g = 1$. It appears that the 180-degree phase shift control signal has only a small effect on the high-frequency oscillation. This was not very surprising since cross-correlation analysis of the pressure signals from the dump plane and the diffuser location showed that the pressure field was not in-phase in the combustor and that the time-delay for peak positive correlation was around $\tau/T = 0.475$, where T is the time period for the dominant oscillation frequency. The 180-degree phase-shifted signal corresponds to a time-delay of $\tau/T = 0.5$, which is close to the time-delay for peak correlation. To explicitly account for the effect of time-delay in the control system, a new control signal was chosen so that

$$p_{sp}'(t) = Ga\, p_{mic}'(t-\tau) \qquad (8)$$

where τ is the specified time-delay between the signal recorded by the microphone and the control signal used to drive the loudspeaker. In the simulations, the time-delay τ/T is specified prior to initiation of the active control. At present, a systematic study of the effect of varying the time-delay (or phase) has not been carried out. However, some effects of varying the time delay have been investigated, and the results of these simulations are discussed below.

Figure 7c shows the pressure signal at the dump plane with a time-delay $\tau/T = 0.15$ used for the active control. In this case, the control is quite effective, with peak-to-peak pressure fluctuation dropping from 15 percent of the mean pressure for the uncontrolled case to around 4 percent of the mean pressure. This figure also shows the effect of turning off the control at a later stage. The pressure fluctuation quickly recovers to the levels observed earlier with no control. Cross correlation of the uncontrolled (original) pressure signatures from the diffuser and the dump plane locations showed that peak negative correlation occurs around $\tau/T = 0.05$. For the time delay used here $\tau/T = 0.15$, the correlation coefficient is still negative. This suggests that, for a chosen time-delay, if the correlation coefficient is negative, then the control may be effective. This would imply that

there may be a range of time delays for which control of the instability is possible. A similar observation was made in an experimental study at NWC by Schadow et al. (1990). They showed that, in their test rig, the control was most effective within a specific phase range of 260-330 degrees. In the present study, more simulations are necessary to determine if a similar phase range exists for control effectiveness.

In the experimental studies at NWC, the sensor (microphone) was located approximately one step height downstream of the dump plane due to the restrictions imposed by the test rig configuration. To numerically determine the effect of sensor location on the control effectiveness, another simulation was performed with the sensor located one step height downstream of the dump plane as in the experiments (location c, Figure 1). Figure 7d shows the pressure signal at the dump plane for this simulation. The time-delay used for this simulation was the same as in the simulation shown in Figure 7c. Although the pressure fluctuation level drops from the 15 percent uncontrolled level to around 5 percent of the mean pressure, comparison between Figures 7c and 7d shows that for the chosen time-delay, the control with the sensor close to the loudspeaker was less effective than when the sensor was located in the diffuser. Cross correlation between the original pressure signals from the dump plane and a step height downstream showed that the peak positive correlation occurs around $\tau/T = 0.03$ and, for the time-delay chosen for this simulation, the correlation coefficient was still positive. The relatively weaker control of the pressure fluctuation shown in Figure 7d appears to indicate that negative correlation maybe required for effective control.

To further evaluate this hypothesis, another simulation with a new time-delay of around $\tau/T = 0.3$ was performed. For this time-delay, the correlation coefficient is negative. Figure 7e shows the pressure signal for this case. Comparison with Figure 7d shows that, for this time-delay, a better control of the high-frequency pressure fluctuation is achieved, with the peak-to-peak level dropping to less than 5 percent of the mean pressure, as was seen in Figure 7c.

Flow visualization of the flame propagation during active control showed that the flame structure does not change in any significant manner from the structure seen in the uncontrolled case (Figure 3b). Spectral analysis of the pressure fluctuation in the combustor showed that as the control becomes effective, the dominant frequency increases from 935 Hz to around 1 kHz. When the control is turned off, the frequency drops back to the original value.

4.2 Active Control of Type II Instability

The active control strategy employed for the control of Type I instability was then applied to the Type II instability. Cross-correlation between the pressure signals from the dump plane and the diffuser location b showed that there is negligible time-delay between the two signals. Further analysis also showed that the pressure field is nearly in-phase everywhere in the combustor. Thus, it was expected that the control signal as defined by Equation (7) should be effective. Figure 8a shows the pressure signal with no control, and Figure 8b shows the corresponding pressure signal with the active control system turned on. The constant A_g for this simulation was 0.2. It is clear that the control used for this case was quite effective in reducing the pressure fluctuation levels. In fact, the peak-to-peak level of oscillation, which was around 50 percent of the mean pressure for the uncontrolled case (Figure 8a), is now reduced to almost 4 percent (Figure 8b), which is about the same level as was achieved for the Type I instability. As seen in the figure, the control does take a certain amount of time to become effective. The effect of turning off the control is demonstrated in Figure 8c, which shows

the pressure signal after the control signal was turned off at the end of the simulation shown in Figure 8b. Although it takes a finite amount of time, the Type II instability returns.

The propagation of the vortex/flame structure seen in the uncontrolled case (Figure 5b) is also changed drastically, with the flame structure now taking a shape similar to that observed during the Type I instability simulation (Figure 3b). A typical flame structure in the combustor during control of the Type II instability is shown in Figure 8d.

Spectral analysis of the pressure fluctuation in the combustor both with and without active control (Figures 8b and 8c, respectively) was carried out. When the control is first turned on, the dominant 166 Hz oscillation frequency increases to 175 Hz, but as the control becomes effective and the pressure fluctuation level drops, only a high-frequency fluctuation at around 1.2 kHz remains. This increase in fluctuation frequency during active control was also observed during control of the Type I simulation described in Section 4.1. When the control is turned off, the dominant frequency begins to decrease and the amplitude increases until finally only the low-frequency, high-amplitude oscillation remains.

To determine if the finite time required for the control to become effective can be reduced, the control of Type II instability was initiated at nearly the beginning of the growth of the Type II instability (see Figure 5a). Figure 9a shows the result of this simulation. Although the peak pressure level that is reached in the first cycle is lower than what was observed in the earlier simulation (Figure 8b), the control still takes nearly the same amount of time to become effective. Also shown in this figure are two other (partial) simulations with increasing value of the gain parameter A_f. Increase in A_f essentially translates to an increase in the power used to drive the loudspeaker. The simulations show that when A_f is increased the peak pressure that is reached in the first oscillation decreases and the control becomes more effective.

The time variation of the Rayleigh parameter and the pressure fluctuation at the dump plane is shown in Figure 9b for a portion of the active control simulation described in Figure 9a (with $A_f = 0.2$). The Rayleigh parameter indicates that the oscillation is very unstable during the early period of the control but that as the control becomes effective, the Rayleigh parameter becomes very small and the combustion process approaches stable operation.

Another simulation was carried out with a very different time-delay between the sensor and control signal. Figure 9c shows the pressure signal for the control case with a time-delay of $\tau/T = 0.03$. Since the pressure field was nearly in-phase everywhere in the combustor, this time-delay implies a situation close to peak positive correlation. Therefore, this control approach was not supposed to be effective. Figure 9c clearly shows that the control is quite poor; however, it is interesting to note that the pressure fluctuation level does decrease slowly. Also shown in this figure is the computed Rayleigh parameter, $\bar{R}(t)/R^s$, and the projected variation of the unsteady heat release term. The Rayleigh parameter also slowly decreases indicating that although the control is poor, it has a stabilizing effect in the pressure oscillation. This indicates that control of the Type II instability is also possible for different phases between the recorded and control signals, but that there may again be some optimum range in which the control effectiveness is at a maximum. Further simulations with different phases are planned to understand the relationship between phase and control effectiveness.

5. CONCLUSIONS

A large-eddy simulation model has been developed that contains the essential physics of combustion instability such as the acoustic wave motion, interaction between the large eddies, and combustion and unsteady heat release during premixed fuel combustion in a ramjet. The combustion model used for the simulations explicitly incorporates the local turbulent flame speed and avoids the erroneous numerical heat release that would occur in a finite-rate chemistry model, while attempting to resolve the internal structure of the flame. Two types of combustion instability have been identified from the simulation results: a small-amplitude, high-frequency instability and a large-amplitude, low-frequency instability. Both types of instability have been experimentally observed and many of the qualitative features of the numerically computed instabilities are in good agreement with the experimental observations.

The data stored during the simulations was then utilized to study active control techniques to control the unstable pressure oscillations. The first phase of this study involved the application of acoustic feedback control techniques. It has been demonstrated here that active control of both types of instability can be accomplished by such a technique. Furthermore, it was shown that the instabilities could be turned on and off. This capability can be used to study and understand the transient process prior to the growth of the instability. Both the control and recovery of the Type II instability take relatively a much longer time period as compared to the Type I instability. Some effects of varying the time-delay between the sensor and control signal was also studied and it was shown that control is possible for different choices of the time delays. This is in qualitative agreement with experimental observations.

Further work is planned to study the effect of time delay on acoustic feedback control and to explore another approach to actively control the instability by using unsteady, secondary fuel injection. Also, as mentioned earlier, the local turbulent flame speed in the present combustion model used only a constant value for the subgrid turbulence intensity. To study more realistic cases, a subgrid model based on the solution of the subgrid turbulent kinetic energy has been incorporated. This model will be used to take into account the nonuniformity of the turbulent fluctuations in the subgrid scales, and then used to determine the local turbulent flame speed.

REFERENCES

Bloxsidge, G. J., Dowling, A. P., Hooper, N., and Langhorne, P. J. (1988) "Active Control of Reheat Buzz," *AIAA J.*, Vol. 26, pp. 783-790.

Bogar, T. J., and Sajben, M. (1979) "The Role of Convective Perturbations in Supercritical Inlet Oscillations," CPIA Publication No. 412.

Chu, B.-T., and Kovasznay, L. S. G. (1958) "Nonlinear Interactions in a Viscous Heat-Conducting Compressible Gas," *J. Fluid Mech.*, Vol. 3, pp. 494-514.

Culick, F. E. C. (1989) "Combustion Instabilities in Liquid-Fueled Propulsion Systems - An Overview," AGARD CP-450, pp. 1.1-1.73.

Ferziger, J., and Leslie, D. C. (1979) "Large-Eddy Simulations: A Predictive Approach to Turbulent Flow Computations," AIAA-79-1471.

Gulati, A., and Mani, R. (1990) "Active Control of Unsteady Combustion-Induced Oscillations," AIAA-90-0270.

Gutmark, E., Parr, T. P., Hanson-Parr, D. M., and Schadow, K. C. (1989) "On the Role of Large and Small-Scale Structures in Combustion Control," *Combustion Sci. and Tech.*, Vol. 66, pp. 107-126.

Gutmark, E., Parr, T. P., Parr, D. M., and Schadow, K. C. (1990) "Active Control of a Premixed Flame," AIAA-90-2448.

Hedge, U. G., Reuter, D., Zinn, B. T., and Daniel B. R. (1987) "Fluid Mechanically Coupled Combustion Instabilities in Ramjet Combustors," AIAA-87-0216.

Jou, W.-H., and Menon, S. (1987) "Simulations of Ramjet Combustor Flow Fields, Part II. Origin of Pressure Fluctuations," AIAA-87-1422.

Jou, W.-H., and Menon, S. (1990) "Modes of Oscillations in a Nonreacting Ramjet Combustor Flow," to appear in *J. Propulsion and Power*, Vol. 6, No. 5.

Kailasanath, K., Gardner, J. H., Oran, E. S., and Boris, J. P. (1989) "Effects of Energy Release on High Speed Flows in an Axisymmetric Combustor," AIAA-89-0385.

Kerstein, A. R., Ashurst, W. T., and Williams, F. A. (1988) "Field Equation for Interface Propagation in an Unsteady Homogeneous Flow Field," *Physical Rev. A.*, Vol. 37, No. 7, pp. 2728-2731.

Lang, W., Poinsot, T., and Candel, S. (1987) "Active Control of Combustion Instability," *Comb. and Flame*, Vol. 70, pp. 281-289.

Langhorne, P. J., and Hooper, N. (1989) "Attenuation of Reheat Buzz by Active Control," Presented at the AGARD Meeting on Combustion Instability in Liquid-Fueled Propulsion Systems, AGARD-CP-450, pp. 10.1-10.16.

Malte, P. C., Schmidt, S. C., and Pratt, D. T. (1977) "Hydroxyl Radical and Atomic Oxygen Concentrations in High-Intensity Turbulent Combustion," *Proc. 16th Symposium (Intn.) on Combustion*, pp. 145-155.

Menon, S., and Jou, W.-H. (1987) "Simulations of Ramjet Combustor Flow Fields, Part I: Numerical Model, Large-Scale and Mean Motions," AIAA-87-1421.

Menon, S., and Jou, W.-H. (1990a) "Numerical Simulations of Oscillatory Cold Flows in an Axisymmetric Ramjet Combustor," to appear in *J. Propulsion and Power*, Vol. 6, No. 5.

Menon, S., and Jou, W.-H. (1990b) "Large-Eddy Simulations of Combustion Instability in an Axisymmetric Ramjet Combustor," AIAA-90-0267, to appear in *Combustion Science and Technology*.

Menon, S. (1991) "Active Control of Combustion Instability in a Ramjet using Large-Eddy Simulations," AIAA Paper No. 91-0411, to be presented at the 29th Aerospace Sciences Meeting, Reno, NV, January 7-11.

Poinsot, T. J., Bourienne, F., Esposito, E., Candel, S., and Lang, W. (1987) "Suppression of Combustion Instability by Active Control," AIAA-87-1876.

Schadow, K. C., Gutmark, E., Parr, T. P., Parr, D. M., Wilson, K. J., and Crump, J. H. (1987) "Large-Scale Coherent Structures as Drivers of Combustion Instability," AIAA-87-1326.

Schadow, K. C., Gutmark, E., and Wilson, K. J. (1990) "Active Combustion Control in a Coaxial Dump Combustor," AIAA-90-2447.

Smith, D. A., and Zukoski, E. E. (1985) "Combustion Instability Sustained by Unsteady Vortex Combustion," AIAA-85-1248.

Sterling, J. D., and Zukoski, E. E. (1987) "Longitudinal Mode Combustion Instabilities in a Dump Combustor," AIAA-87-0220.

Williams, F. A. (1985) *Combustion Theory*, Second Edition, Benjamin/Cummings Publishing Co.

Yakhot, V. (1989) "Propagation Velocity of Premixed Turbulent Flame," *Combustion Sci. and Tech.*, Vol. 60.

Yakhot, V., and Orszag, S. A. (1986) "Renormalization Group Analysis of Turbulence, I: Basic Theory, *J. Sci. Comp.*, Vol. 1, No. 3.

Yang, V., and Culick, F. E. C. (1985) "Analysis of Unsteady Inviscid Diffuser Flow with a Shock Wave," *J. Propulsion and Power*, Vol. 1, No. 3, pp. 222-228.
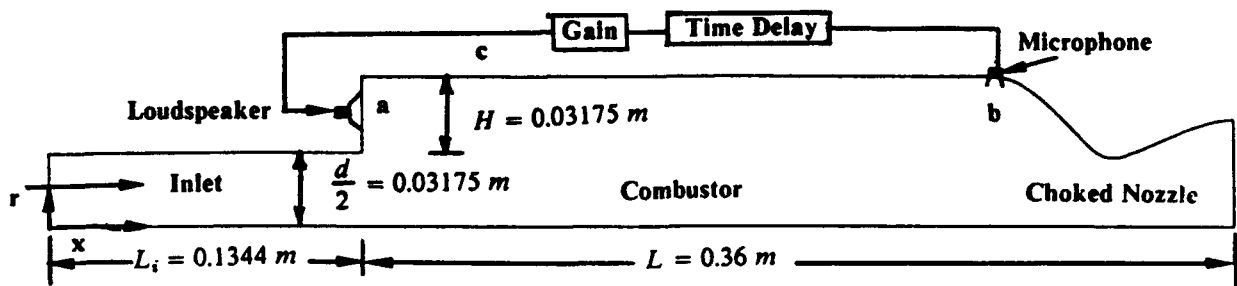
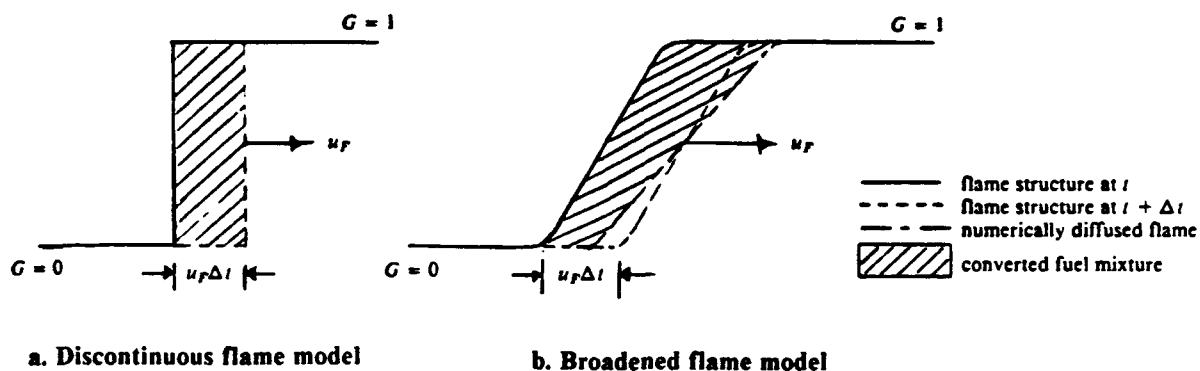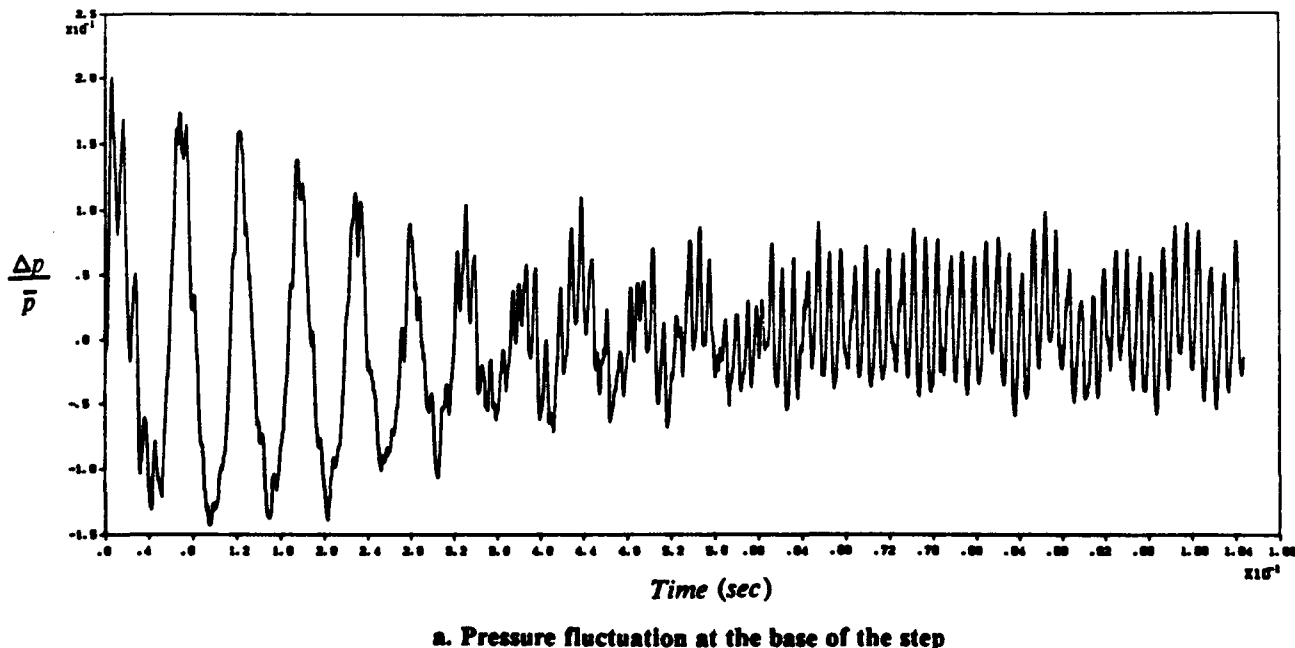Figure 1. The axisymmetric ramjet configuration

a. Discontinuous flame model   b. Broadened flame model

Figure 2. The discontinuous and diffused flame structure

a. Pressure fluctuation at the base of the step

Figure 3. Typical flow features observed during Type I combustion instability

b. Flame structure

Combustion Product

Premixed Fuel

Flame

c. Vorticity field

d. Experimental

(Smith and Zukoski, 1985)

Figure 3. Typical flow features observed during Type I combustion instability (cont.)

$\dfrac{\bar{R}(t)}{R^*} \times 0.004$

$\dfrac{\Delta p}{\bar{p}}$

Δq (no scale)

Time (sec)

a. Temporal variation of $\bar{R}(t)$

$\dfrac{R(x)}{R^*}$

x (meters)

Dump Plane   Choked Throat

b. Spatial variation of $R(x)$
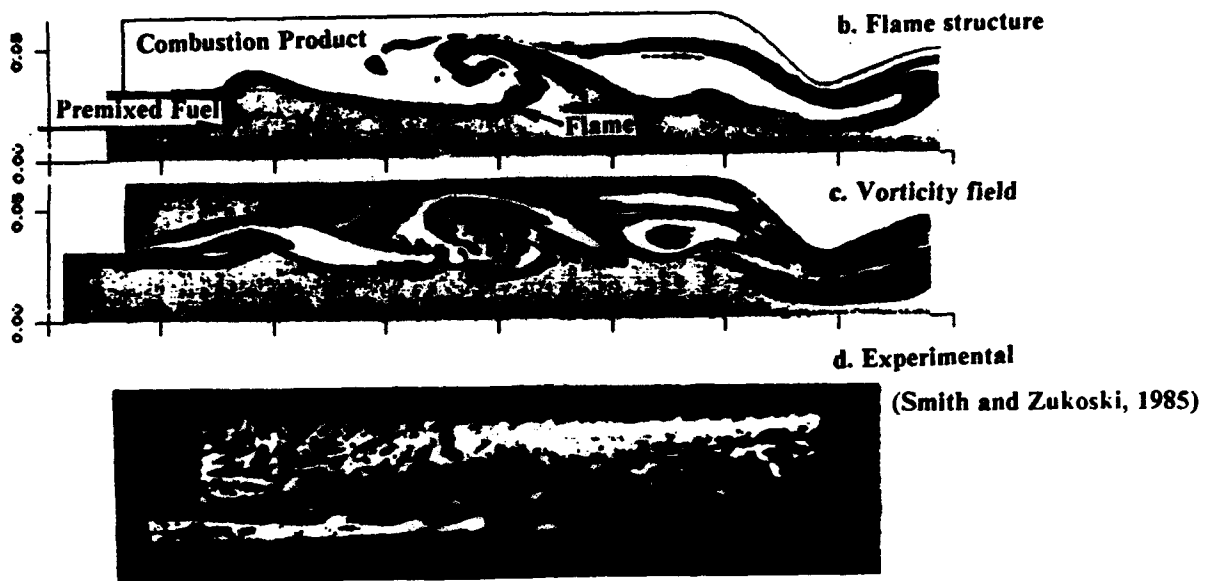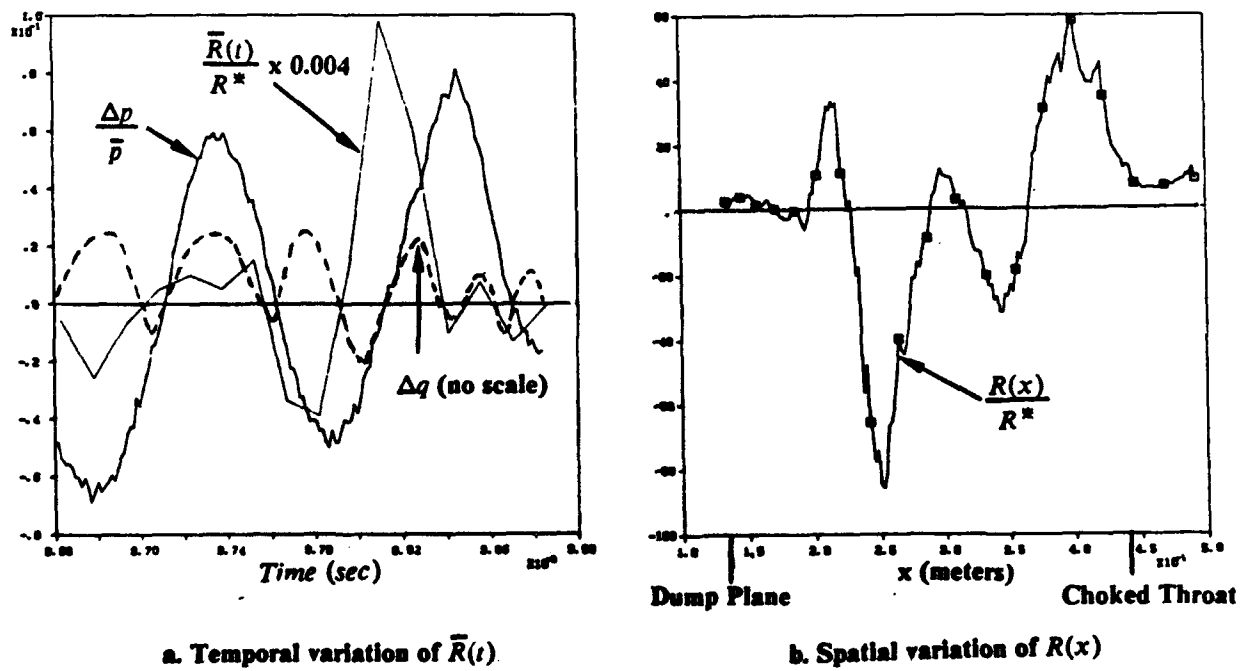
Figure 4. Rayleigh criteria in the combustor for Type I instability
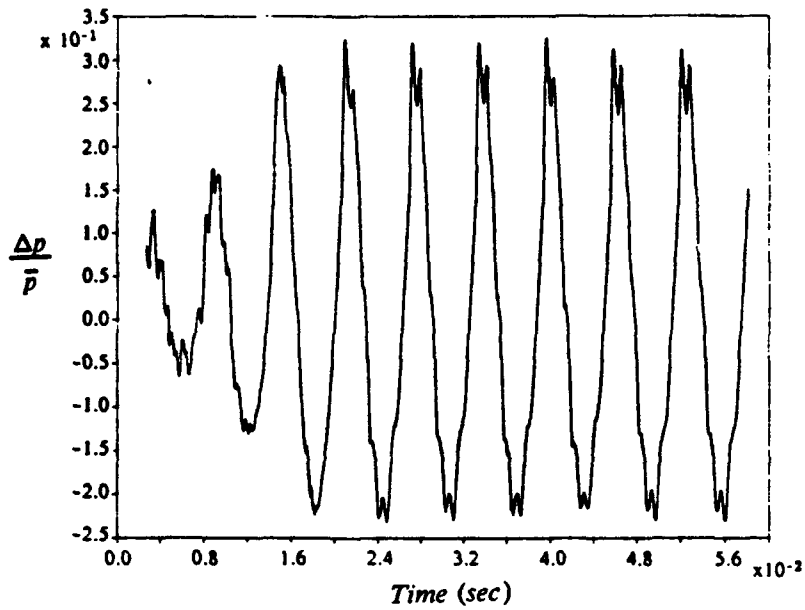
a. Pressure fluctuation at the base of the step

b. Flame structure

c. Vorticity field

d. Experimental
(Smith and Zukoski, 1985)
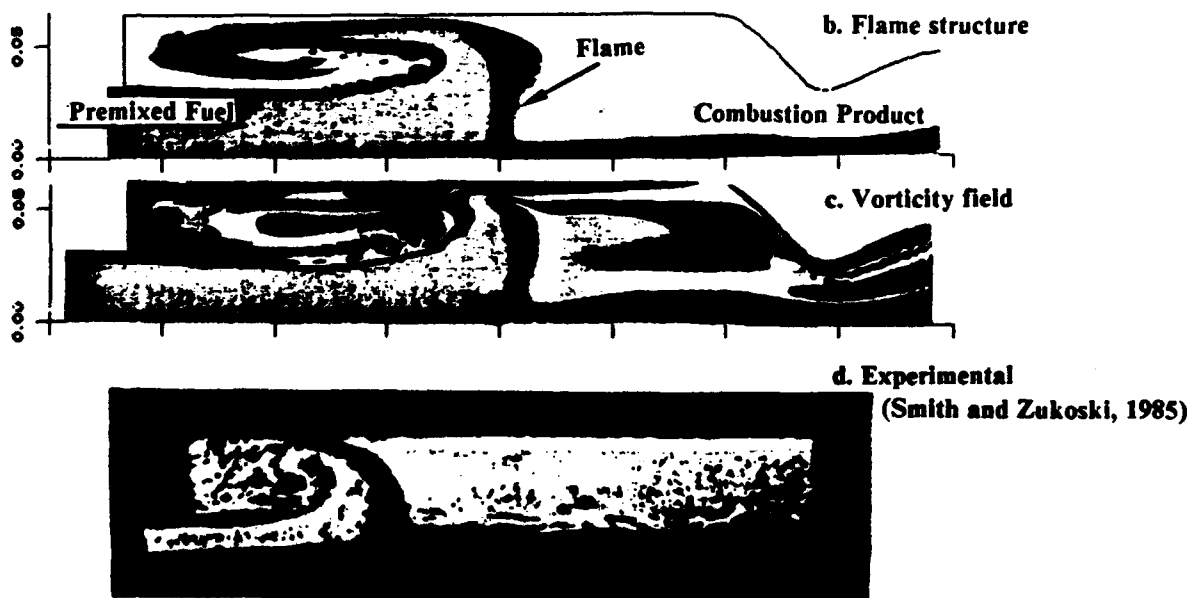
Figure 5. Typical flow features observed during Type II combustion instability.
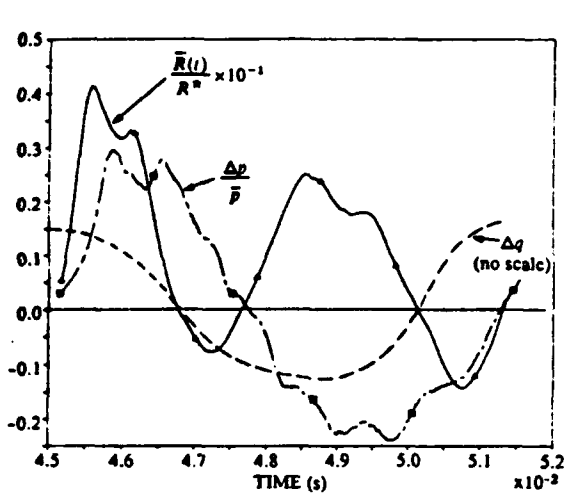
a. Temporal variation of $\bar{R}(t)$
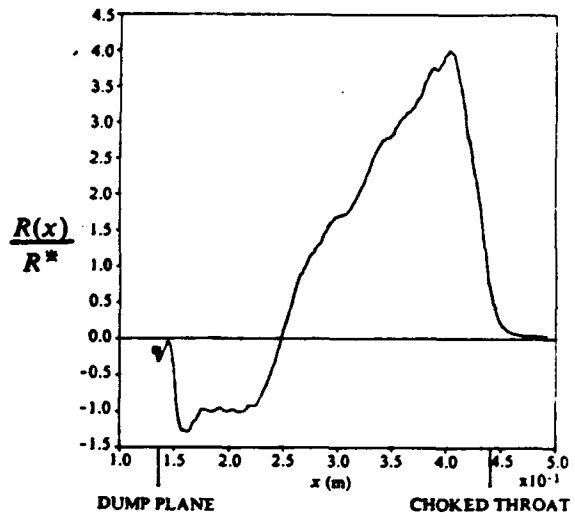
b. Spatial variation of $R(x)$

Figure 6. Rayleigh criteria in the combustor for Type II instability
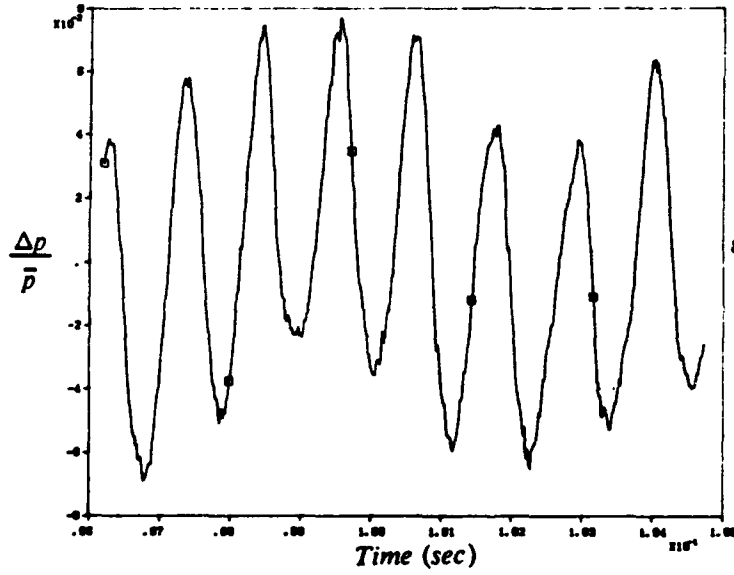
a. Control OFF; Reference signal.
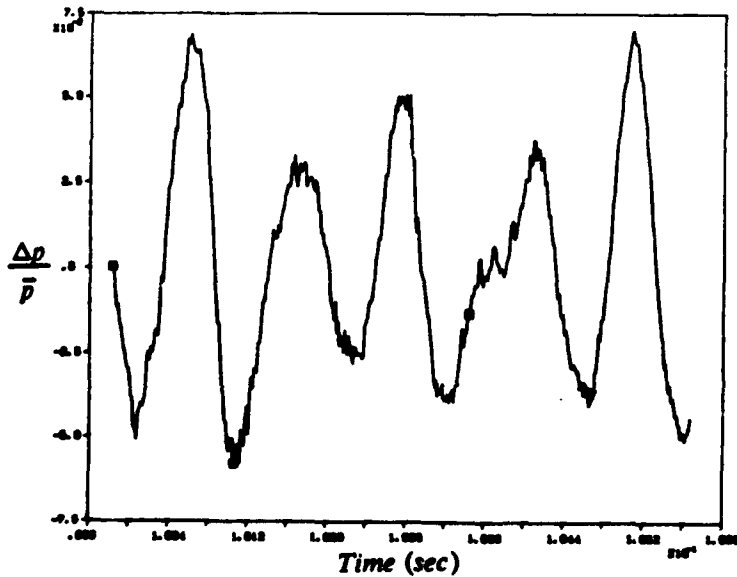
b. Control ON with $\dfrac{\tau}{T} = 0.5$;
Sensor at location b.

Figure 7. The effect of acoustic feedback control on the Type I pressure fluctuations
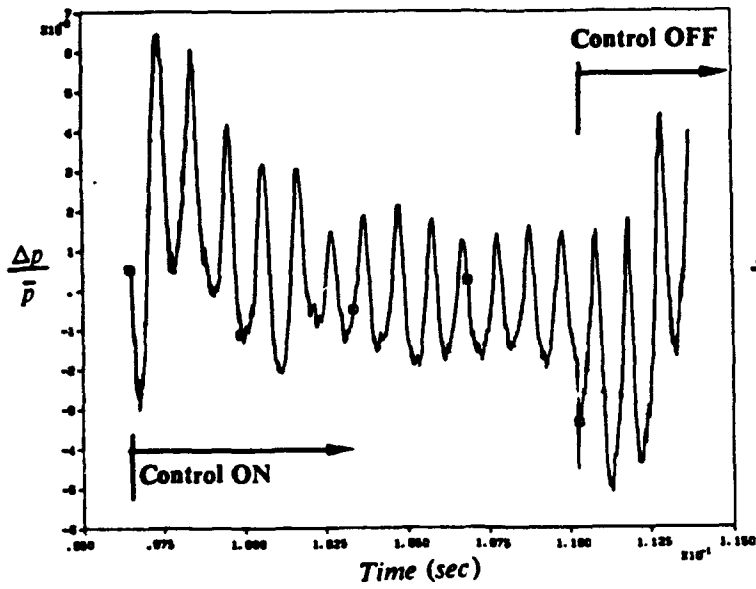
c. Control ON/OFF with $\frac{\tau}{T} = 0.15$;
Sensor at location b.
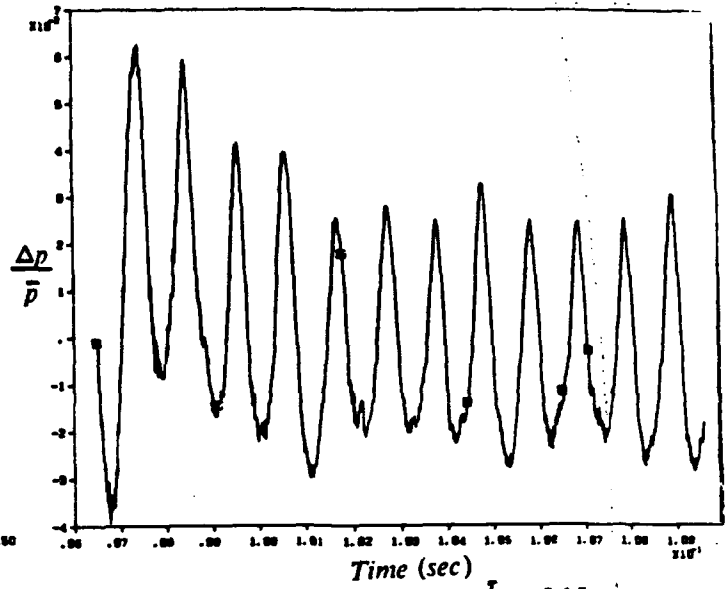
d. Control ON with $\frac{\tau}{T} = 0.15$;
Sensor at location c.
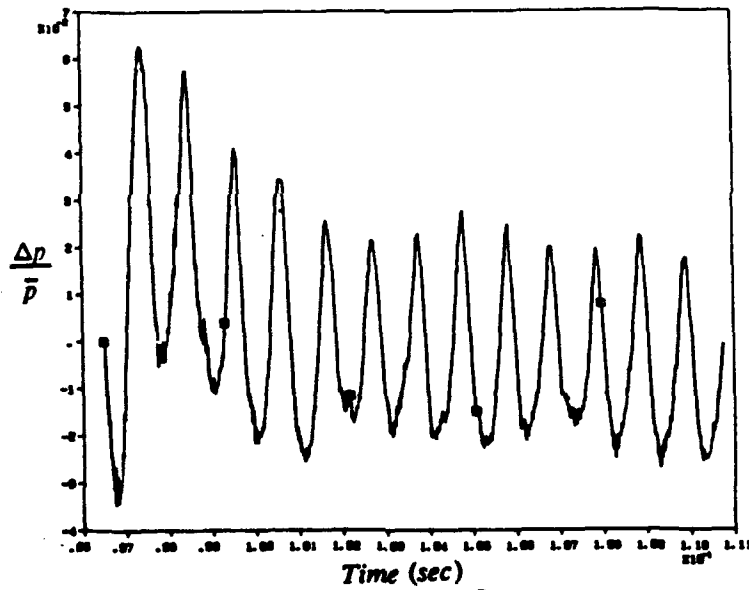
e. Control ON with $\frac{\tau}{T} = 0.30$;
Sensor at location c.

Figure 7. The effect of acoustic feedback control on the Type I pressure fluctuations (cont.)
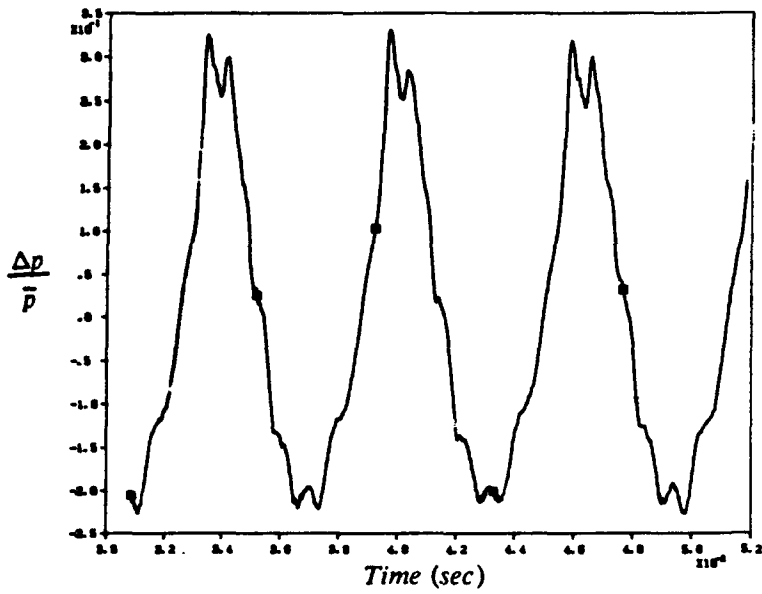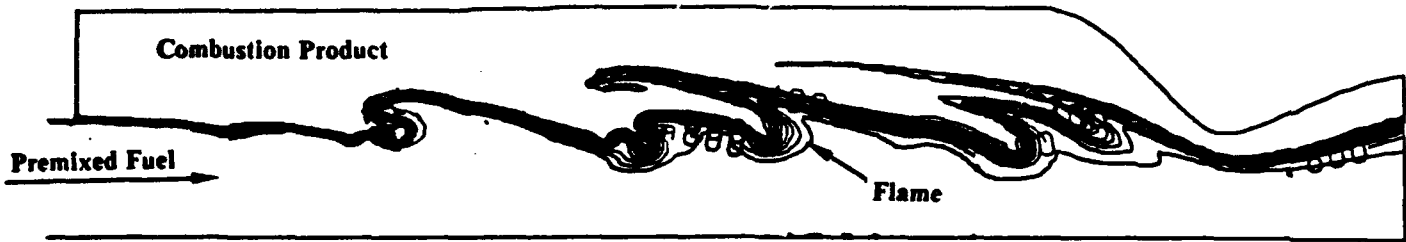
a. Control OFF, reference signal.
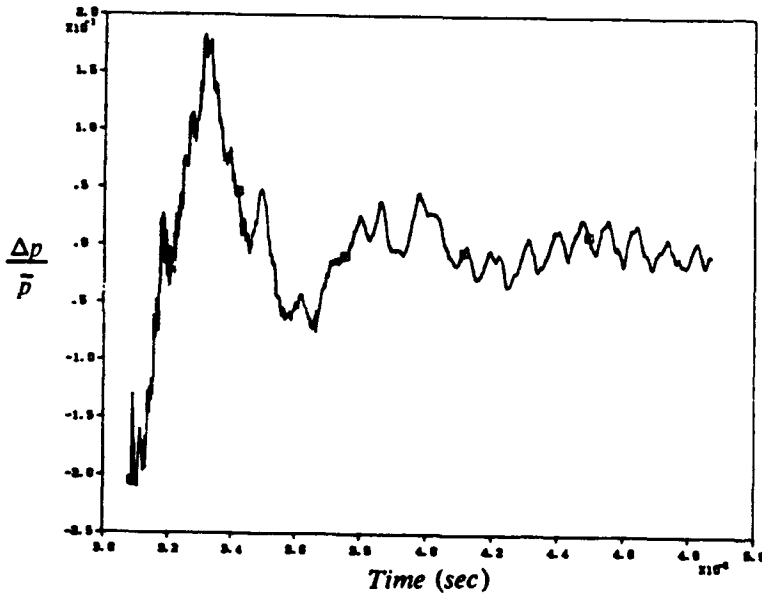
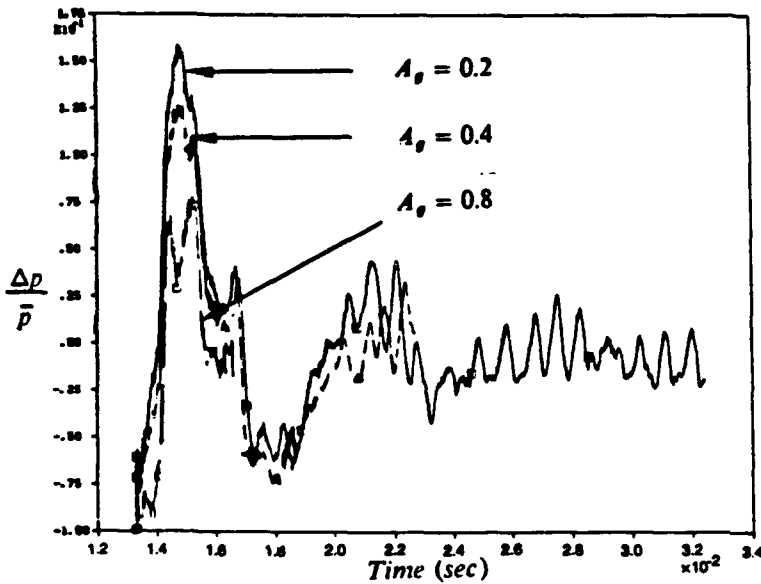b. Control ON with $\frac{\tau}{T} = 0.5$; Sensor at location b.
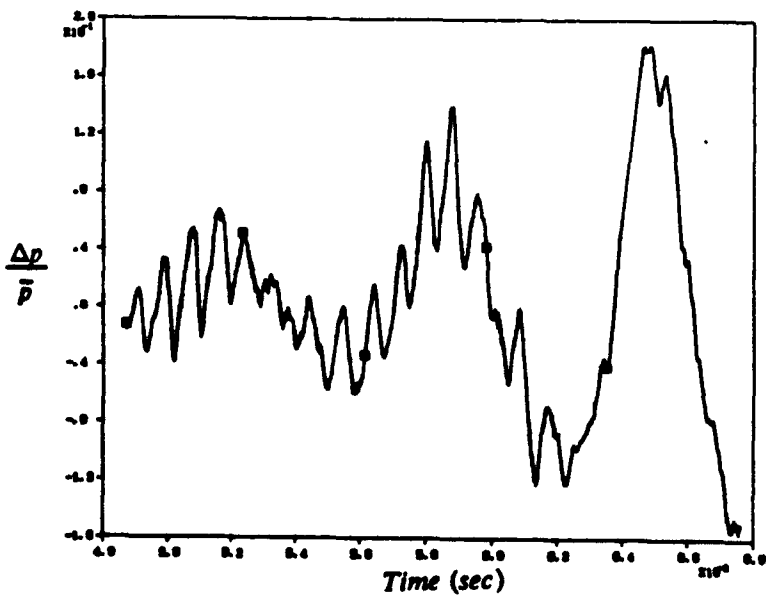
c. Control OFF, after control ON in Figure 8b.

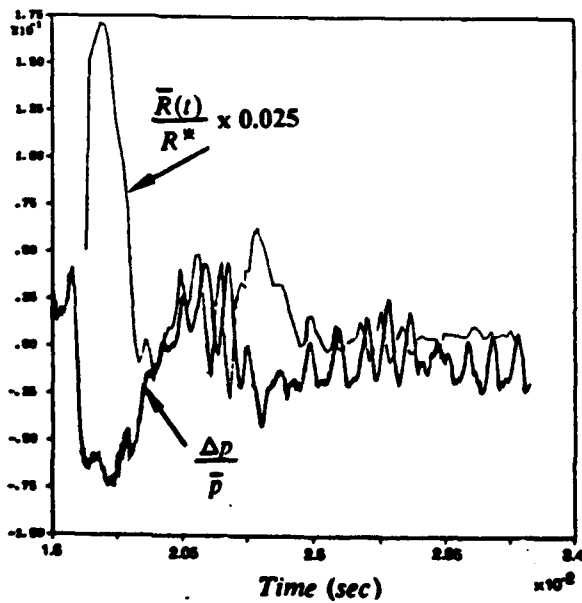**Figure 8. The effect of acoustic feedback control on the Type II pressure fluctuation**

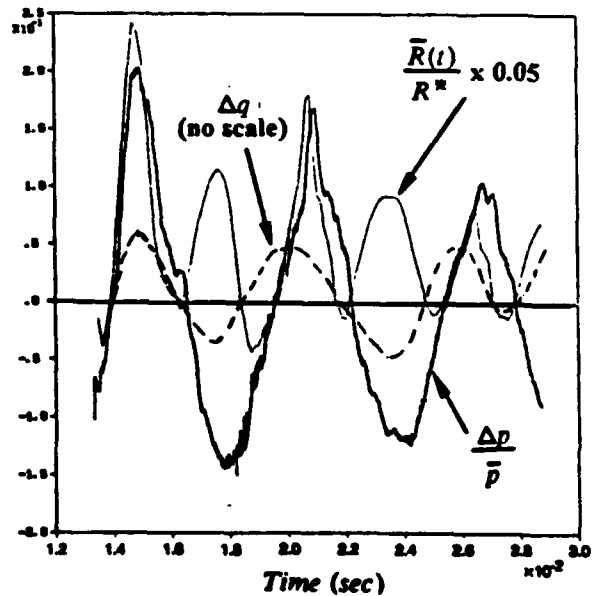d. Typical flame structure with control ON with $\frac{\tau}{T} = 0.5$

Figure 8. The effect of acoustic feedback control on the Type II pressure fluctuation (cont.)

a. Effect of increasing gain on the pressure fluctuation

b. Rayleigh Criteria, $\overline{R}(t)$ and pressure fluctuation for control ON with $\frac{\tau}{T} = 0.5$ and $A_g = 0.2$

c. Rayleigh Criteria, $\overline{R}(t)$ and pressure fluctuation for control ON with $\frac{\tau}{T} = 0.03$ and $A_g = 0.2$

Figure 9. The effect of gain and time delay on the Type II instability